Forschungszentrum Karlsruhe

in der Helmholtz-Gemeinschaft

Wissenschaftliche Berichte

FZKA 6869

Experimental Investigation of Non-linear Constitutive Behavior of PZT Piezoceramics

Dayu Zhou

Institut für Materialforschung

Von der Fakultät für Maschinenbau der Universität Karlsruhe (TH)
genehmigte Dissertation

Forschungszentrum Karlsruhe GmbH, Karlsruhe

2003

Impressum der Print-Ausgabe:

Als Manuskript gedruckt

Forschungszentrum Karlsruhe GmbH
Postfach 3640, 76021 Karlsruhe

Mitglied der Hermann von Helmholtz-Gemeinschaft
Deutscher Forschungszentren (HGF)

ISSN 0947-8620

Experimental Investigation of Non-linear Constitutive Behavior of PZT Piezoceramics

Zur Erlangung des akademischen Grades eines

DOKTOR-INGENIEURS

der Fakultät für Maschinenbau
der Universität Karlsruhe (TH)

genehmigte

DISSERTATION

von
Master of Engineering, Dayu Zhou
aus Jilin, V. R. China

Tag der mündlichen Prüfung: 11. Feb. 2003

Hauptreferent: Prof. Dr. rer. nat. Dietrich Munz
Korreferent: Prof. Dr. rer. nat. Michael. J. Hoffmann

Abstract

Experimental Investigation of Non-linear Constitutive Behavior of PZT Piezoceramics

The uni-axial non-linear large signal behavior of PIC 151 soft PZT ceramics was experimentally investigated under a pure electric field, a pure compressive stress and combined electromechanical loading conditions, respectively.

Polarisation and strain *vs.* E field hysteresis loops were observed under a pure cyclic electric field load. The corresponding strain *vs*. polarisation (S – P) curves also exhibited a significant hysteresis. The material response was found to depend on the loading rate and amplitude of the applied E field. A higher loading rate resulted in a smaller coercive field. Ageing effects caused the remnant polarisation and strain to decrease with time after removing the E field load.

As subjected to a pure compressive stress load, the material exhibited non-linear stress-strain behavior. In addition, a non-linear depolarisation curve was observed for the pre-poled specimen. Permanent changes of polarisation and strain induced by the mechanical load could be brought back to their initial values by a subsequent application of an electric field to repolarise the material. Loading rate dependence was also found in the non-linear stress - strain behavior.

When being subjected to a constant load, this material exhibited significant time-dependent effects. Polarisation and strain exhibited creep-like behavior with the passage of the external load hold time. Most pronounced time-dependent effects were observed as the load was close to the coercive field or the coercive stress.

Polarisation and strain versus electric field hysteresis loops were measured under various levels of a preload compressive stress. It turned out that the superimposed compression load reduced the remnant polarisation, decreased the coercive field and also had a significant impact on the dielectric and piezoelectric properties.

High field dielectric permittivity and piezoelectric coefficients were found to be enhanced by the compressive preload within a small range. The improved performance was accompanied by an unfavorable larger hysteresis, which was attributed to larger extrinsic contribution due to more non-180° domain switching induced by the prestress.

The effects of a bias electric field on the non-linear stress – strain and stress – depolarisation response were also studied. The non-linear curves were effectively closed upon application of an electric field parallel to the pre-poling direction. Larger stresses were needed to initiate and forward the ferroelastic domain switching. The inverse of this trend occurred when the specimen was subjected to a bias electric field anti-parallel to the pre-poling direction.

Zusammenfassung

Experimentelle Untersuchung des nichtlinearen konstitutiven Verhaltens von PZT Piezokeramiken

Das uniaxiale nichtlineare Großsignalverhalten der weichen PZT Keramik PIC 151 wurde unter Belastung mit einem elektrischen Feld, unter Druckspannungsbelastung und unter kombinierter elektromechanischer Belastung experimentell untersucht.
Unter zyklischer Belastung mit einem elektrischen Feld wurden bei der Polarisation und der Dehnung in Abhängigkeit von der elektrischen Feldstärke Hystereseschleifen beobachtet. Ebenso trat bei der Dehnung in Abhängigkeit von der Polarisation (S – P) eine deutliche Hysterese auf. Es hat sich herausgestellt, dass das Materialverhalten sowohl von der Belastungsgeschwindigkeit als auch von der Amplitude des elektrischen Feldes abhängt. Eine höhere Belastungsgeschwindigkeit führte zu einer kleineren Koerzitivfeldstärke. Alterungseffekte führten mit der Zeit zu einer Abnahme der remanenten Polarisation und der Dehnung nach der Belastung mit einem elektrischen Feld.
Unter reiner Druckspannungsbelastung zeigte das Material ein nichtlineares Spannungs-Dehnungsverhalten. Außerdem wurde bei vorpolarisierten Proben eine nichtlineare Depolarisationskurve beobachtet. Permanente Änderungen in der Polarisation und Dehnung, die durch die mechanische Belastung verursacht wurden, konnten durch ein nachfolgendes Anlegen eines elektrischen Feldes, mit dem das Material wieder polarisiert wurde, rückgängig gemacht werden. Beim nichtlinearen Spannungs-Dehnungverhalten stellte sich auch eine Abhängigkeit von der Belastungsgeschwindigkeit heraus.
War das Material einer konstanten Belastung unterworfen, traten zeitabhängige Effekte deutlich in Erscheinung. Solange die äußere Belastung aufrechterhalten war, trat bei der Polarisation und der Dehnung ein Kriechverhalten auf. Am ausgeprägtesten waren diese zeitabhängigen Effekte bei einer Belastung nahe der Koerzitivfeldstärke und der Koerzitivspannung.
Für unterschiedliche Druckvorspannungen wurden Hystereseschleifen für die Polarisation und die Dehnung in Abhängigkeit von der elektrischen Feldstärke gemessen. Es stellte sich heraus, dass die überlagerte Druckbelastung sowohl die remanente Polarisation als auch die Koerzitivfeldstärke verminderte und einen deutlichen Einfluss auf die dielektrischen und piezoelektrischen Eigenschaften des Materials ausübte.
Es wurde festgestellt, dass bei hohen Feldstärken die dielektrische Permittivität und die piezoelektrischen Koeffizienten durch die Druckvorspannung in einem kleinen Bereich erhöht werden. Diese vorteilhaften Eigenschaften waren allerdings begleitet von unerwünscht großen Hysteresen, die einem größeren extrinsischen Beitrag von nicht 180° Umklappprozessen der Domänen aufgrund der Vorspannung zugeschrieben wurden.
Der Einfluss einer anliegenden konstanten elektrischen Feldstärke auf das nichtlineare Spannungs-Dehnungsverhalten bzw. Spannungs-Depolarisationsveralten wurde ebenso untersucht. Durch Anlegen eines elektrischen Feldes in Richtung der Vorpolarisation konnten die nichtlinearen Kurven praktisch geschlossen werden. Größere Spannungen waren notwendig, um das ferroelastische Umklappen der Domänen auszulösen und voranzutreiben. Das umgekehrte Verhalten trat in Erscheinung, wenn an die Probe eine ansteigende elektrische Feldstärke entgegen zur Vorpolarisation angelegt wurde.

Table of Contents

Preface

Since the discovery of lead zirconate titanate (PZT) ceramic material about 5 decades ago, due to the high efficiency of electromechanical energy conversion and the ease of fabricating the material into a wide variety of sizes and shapes, PZT ceramics and related modified families have become the most widely used piezoelectric materials with a great deal of technological applications [Haertling, 1999].

The prospect of piezoelectric ceramics is very promising. According to the BCC (Business Communications Co., U.S.A.) market statistics, the U.S. market for piezoelectric ceramics in 2000 was about 200 million U.S. dollars, and the annual average growth rate was about 8% [Abraham, 2000].

Sets of linear equations are used to describe the electromechanical coupling effects of poled piezoelectric ceramics under small signal electric field or stress load. However, nowadays practical devices normally have complicated structures and work under severe loading conditions such that the assumption of small signal linear responses is no longer justified in general. Rather, domain switching related non-linear behavior becomes dominant and must be taken into account for the electromechanical coupling calculation, devices design and service life / reliability evaluation.

At this time, the literature on experimental investigation of piezoceramics under large signal electromechanical loading conditions is still too rare. Therefore, the experimental data are not sufficient to serve as a basis for the development of constitutive laws for the complete response of piezoceramics in general.

This thesis is focused on the experimental investigation of the large signal non-linear behavior of a typical commercially available soft PZT ceramic material (PIC 151, PI Ceramic, Lederhose, Germany). To start with, the fundamental definitions related to piezoelectric ceramics, research motivation and a summary of state of the art are given in Chapter 1.

Chapter 2 is devoted to the introduction of measurement principles and experimental set-up. A special specimen preparation method, which can ensure secure and correct strains measurement under combined electromechanical loading conditions, will also be presented in this chapter.

The basic non-linear behavior of piezoceramics under a pure cyclic electric field and a pure compressive stress loading will be described in Chapter 3 and Chapter 4, respectively. In

particular, experimental results and discussions of the time-dependent effects of polarisation and strain response under a constant external load can be found in these two chapters.

The response of a piezoceramic material under combined electromechanical loading is the focus of this thesis. In this experimental work, the coupled electromechanical tests are performed under a uni-axial compressive stress load together with a coaxial electric field application at the same time. In Chapter 5, the experimental results of polarisation and strain versus full cycles of electric field hysteresis loops under various compressive stress preloads will be presented at first. The influence of prestress on the remnant polarisation, coercive field, and dielectric and piezoelectric coefficients will be clarified. Thereafter, the effects of compressive prestress on the high field dielectric and piezoelectric performance of piezoceramics will be shown. Such a kind of investigations is more important for the practical actuator applications. Finally, measurements of the compressive ferroelastic switching behavior with different bias electric field preloads will be presented in this chapter.

A brief summary of this experimental work is given in Chapter 6.

The systematic experimental data presented in this thesis can serve the purpose of calibrating the existing models and developing a more suitable constitutive law for the non-linear behavior of piezoceramics.

Chapter 1 Introduction and Motivation

1.1 Smart materials and structures

Material science has undergone a distinct evolution: from the use of inert structure materials to materials built for a particular function, and finally to smart materials with more acute recognition, discrimination and reaction capabilities [Akhras, 2000].

The sensing and actuating functions of smart materials are explored to develop smart structures. Passive smart structures respond to external changes in a useful manner without assistance, whereas active smart structures have a feedback loop, which is composed of sensors and actuators together with external macroscale control and logic circuits [Newnham and Ruschau, 1991].

In our days, more and more engineering problems from very different fields are solved by the so-called smart systems. Smart systems are defined as "systems that incorporate particular functions of sensing and actuation to perform smart actions in an ingenious way". The basic five components of a smart system are: data acquisition, data transmission, command and control unit, data instructions, and action devices. Smart materials and structures have already been applied in both civil and military areas, for example, vibration reduction in sporting goods, noise reduction in vehicles, smart skin, smart aircraft, smart systems for bridges and highways, and stealth applications [Akhras, 2000].

Figure 1.1.1. Approach for classification of active materials [After www.intellimat.com].

As seen in Fig. 1.1.1, smart or active materials can exchange a kind of input stimulus into a kind of output response. Consequently, the materials can be classified according to the type of input driving force. Piezoelectric materials, shape-memory alloys, electrostrictive materials, magnetostrictive materials, and electrorheological liquids are some examples of currently available smart materials. The most notable features of three main kinds of smart materials are compared in Table.1.1.1. Related data are from Intellmat [www.intellimat.com] and the thesis of Trease [Trease, 2002].

Table1.1.1. Qualitative comparison of different smart materials

Active Materials	Shape-Memory Alloys	Magnetostrictive Materials	Piezoelectric Materials
Driving Force	Thermal field	Magnetic field	Electric field
Materials	TiNi, TiPd	TbFe, (TbDy)Fe, SmFe	PZT, $BaTiO_3$, Quartz
Advantages	• Large strain range (4-6%) • Large forces • High energy density • High material strength • High elasticity	• Contact-less control via magnetic field • High operating frequencies, up to 30 kHz • High temperature range • Good linearity and moderate level of hysteresis at 2%	• High bandwidth, operation frequency up to GHz. • Low thermal coefficient • Relative good linearity • Electrically driven, directly integrated with operating electronics
Limitations	• Low frequency bandwidth (0.5 – 5 Hz) • High hysteresis • Limited temperature range • Thermally activated	• Delivery of controlled magnetic field to actuator • Limited strains (0.1-0.6%) • Low material tensile strength • Typically brittle materials • More power requirement than piezo-actuators	• Limited strains (0.1-0.2%) • Hysteresis and creep • Low material tensile strength • Typically brittle materials • Limited temperature range • High voltage requirements

Besides the advantages summarized in Table 1.1.1, piezoelectric materials also possess the capabilities of an ultramicroscopic displacement control and a high rate of electromechanical energy conversion ($K \leq 0.7$). Therefore, small scale and stackable actuators made of piezoelectric materials are the most commercialised and understood technologies in the current smart actuator market.

1.2 Fundamentals of electromechanical coupling phenomena

Applications of piezoelectric materials are based on the electromechanical coupling effects, e.g. mechanical deformation can be induced by an application of an electric field loading. Piezoelectricity and electrostriction are two kinds of electromechanical coupling effects. However, their microscopic mechanisms are quite different.

1. *Electrostrictivity*

Electrostriction is a general property of all dielectric materials, whether they are crystalline, amorphous, polar, or centro-symmetric. For a dielectric material, as a consequence of an electric field, the centres of positive and negative charges will be separated, leading to the occurrence of a polarisation (defined as the value of electric dipole moment per unit volume) in the direction of the electric field. An accordingly opposite direction polarisation will be caused by an application of a reverse direction electric field loading. The crucial point is that in both situations, if those two electric fields with opposite directions have the same magnitude, the centres of charges will be separated by the same distance only leading to an elongation of the unit cells of equal amount. The electrically induced deformation effect in this case is called electrostriction. In electrostriction, the sign of the strain (S) is independent of the polarity of the field and the magnitude is proportional to the square of the polarisation (P). Consequently, electrostriction is a higher order effect originating from ionic shift from their equilibrium positions. The corresponding equation is

$$S = QP^2 \tag{1.2.1}$$

Here Q is the electrostrictive coefficient. Fig. 1.2.1 schematically shows the electrostrictive effect.

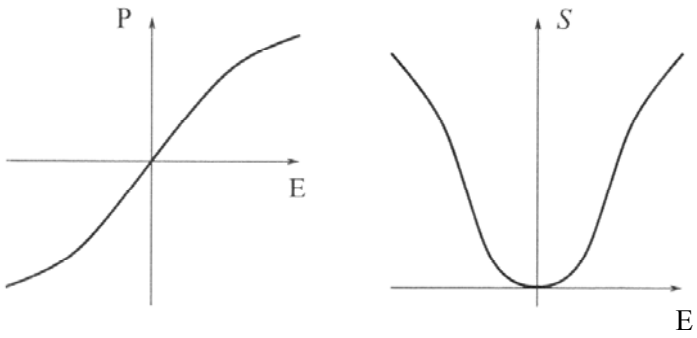

Figure 1.2.1. Schematic illustration of electrostrictive effect, left: change of polarisation with application of electric field; right: change of strain with electric field.

In some ferroelectric relaxor materials, such as $Pb(Mg_{1/3}Nb_{2/3})O_3$ (PMN) and $Pb(Zn_{1/3}Nb_{2/3})O_3$ (PZN), the electrostriction strain can be very large (≈ 0.1%) when the working temperature is higher than their curie temperature. However, the disadvantage of relatively poor temperature stability limits their applications [Cross, 1987; Haertling, 1999].

2. *Piezoelectricity*

Piezoelectricity is a linear effect with respect to the applied field and changes sign when the field is reversed. This particular phenomenon can only be found in some special materials.

As defined by Cady, piezoelectricity is: "electric polarisation produced by mechanical strain in crystals belonging to certain classes, the polarisation being proportional to the strain and changing sign with it." [Cady, 1946]. This is the *direct piezoelectric effect* (see Fig. 1.2.2, right), it is linear and the magnitude of polarisation is dependent on the magnitude of stress and the sign of the charge produced is dependent on the type of stress (tensile or compressive). The direct piezoelectric effect is always accompanied by the *inverse piezoelectric effect* (see Fig. 1.2.2, left) where a solid becomes strained when placed in an electric field [Jaffe *et al.*, 1971].

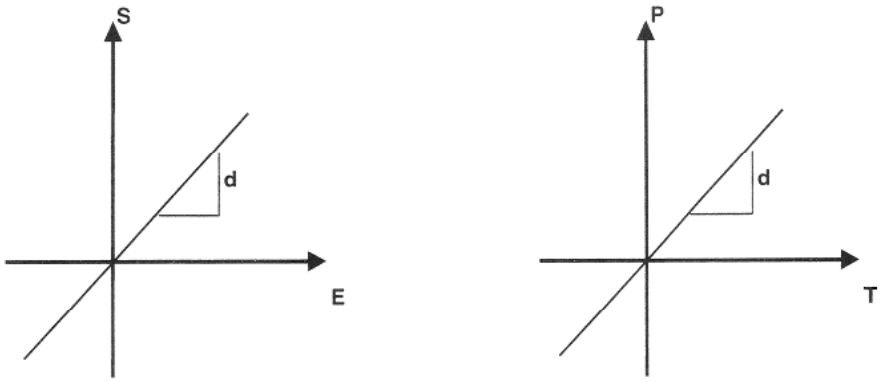

Figure 1.2.2. Left: inverse piezoelectric effect; right: direct piezoelectric effect.

The basic equations that describe these two effects in regard to electric and elastic properties are

$$\begin{aligned} D_i &= \varepsilon_{ij}^T E_j + d_{ijk} T_{jk} \\ S_{ij} &= d_{ijk} E_k + s_{ijkl}^E T_{kl} \end{aligned} \tag{1.2.2}$$

Here D is the dielectric displacement, E is the electric field, T is the mechanical stress, S is the mechanical strain, d is the charge constants, ε is the dielectric constants (superscript T means under constant stress, i.e. mechanically free condition), s is the mechanical compliance (superscript E means under constant E field, i.e. short-circuit condition) [Lines and Glass, 1977].

Since all the experiments for this thesis were performed under uni-axial electric field and/or compressive stress loading, Equation 1.2.2 can be simplified for the calculation of electromechanical coupling effects. The external load direction is defined as the 3-axis, which

is also the poling direction of a pre-poled specimen. Then, the resultant dielectric displacement and the strain along the poling direction can be expressed as

$$\begin{aligned} D_3 &= \varepsilon_{33}^T E_3 + d_{33} T_3 \\ S_3 &= d_{33} E_3 + s_{33}^E T_3 \end{aligned} \tag{1.2.3}$$

In the direction perpendicular to the poling, the material is transversely isotropic. Thus, the transverse strain is given by

$$S_1 = S_2 = s_{13}^E T_3 + d_{31} E_3 \tag{1.2.4}$$

The direct effect is suitable for sensor applications, and the inverse effect can be exploited for actuator applications (see Fig. 1.2.3). This makes piezoelectric materials one of the prime choices of current smart material and structure technologies.

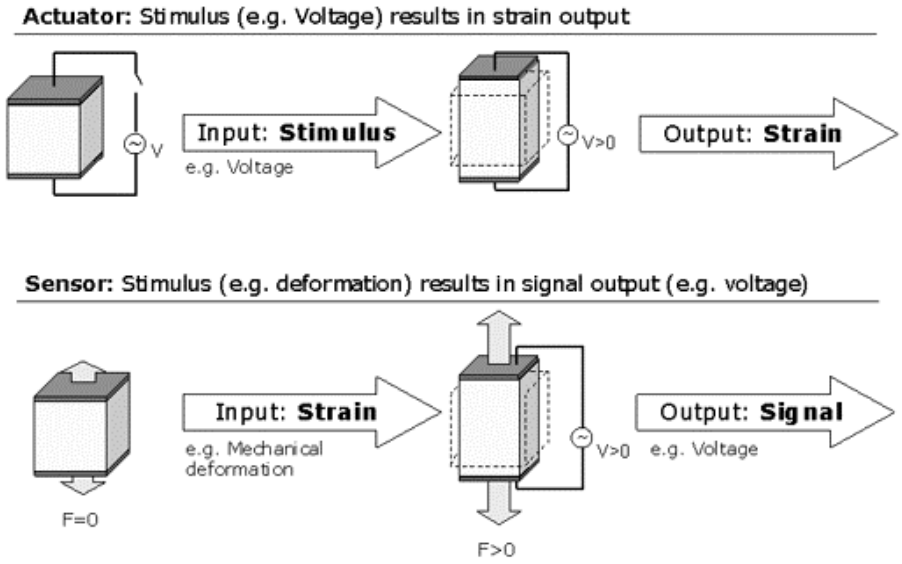

Figure 1.2.3. Piezoelectric materials used as actuator (top) and sensor (bottom) [After Intellmat: www.intellimat.com].

3. *Microstructure reason of piezoelectricity*

All crystals can be divided into 32 classes or point groups (from 7 basic crystal systems). The 32 point groups can be further classified into (a) 11 point groups having a centre of symmetry and (b) 21 point groups that do not possess a centre of symmetry. A lack of a centre of symmetry is all-important for the presence of piezoelectricity. As shown in Fig. 1.2.4, the lack of a centre of symmetry means that a net movement of the positive and negative ions with respect to each other as a result of stress produces an electric dipole, whereas, for the centro-symmetric crystals, the centres of charges of different polarity will still coincide even after the stress inducing a deformation.

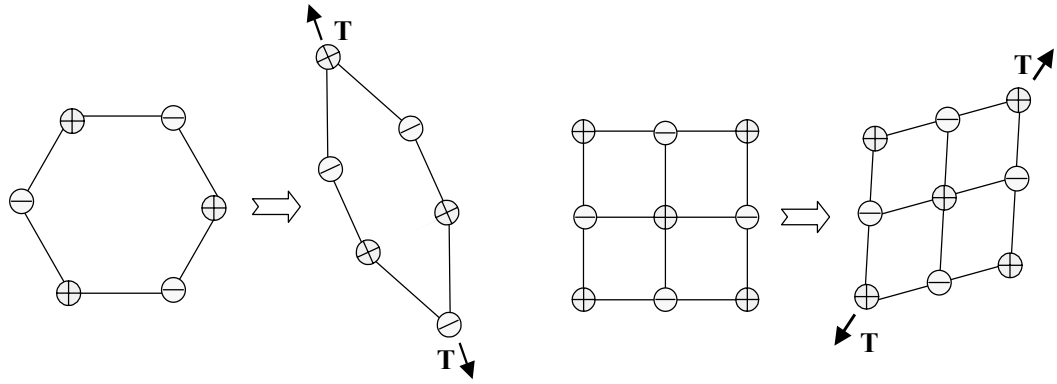

(a) noncentrosymmetric crystal strucrure with piezoeffect

(b) centrosymmetric crystal strucrure no piezoeffect

Figure 1.2.4. Microstructural origin of piezoelectric effect.

Of the 21 non-centrosymmetric point groups, 20 are piezoelectric (one class, although lacking a centre of symmetry, is not piezoelectric because of the combination of other symmetry elements) [Haertling, 1999].

4. *Pyroelectricity*

Out of the 20 point groups which show the piezoelectric effect, 10 point groups have only a unique polar axis. In absence of any load, they develop a polarisation spontaneously and form a permanent dipole within the unit cell. Such kinds of crystals are called polar crystals. The spontaneous polarisation (P_{spon}) is defined as the value of dipole moment per unit volume or the value of charge per unit area on the surface perpendicular to the axis of spontaneous polarisation. The value of spontaneous polarisation depends on the temperature (Θ), this phenomenon is called pyroelectric effect and the crystals with this effect are called pyroelectrics [Damjanovic, 1998]. The pyroelectric effect can be described in terms of pyroelectric coefficient p as shown in

$$\Delta P_{spon} = p\Delta\Theta \tag{1.2.5}$$

5. *Ferroelectricity*

A subgroup of the spontaneously polarized pyroelectrics is a very special category of materials known as ferroelectrics. By definition, ferroelectrics are polar materials that possess at least two equilibrium orientations of the spontaneous polarisation vector in the absence of an external electric field, and in which the spontaneous polarisation vector may be switched between those orientations by an electric field.

Materials in this group possess spontaneous dipoles, and these dipoles are reversible by an electric field loading of some magnitude less than the dielectric breakdown strength of the material itself. Thus, the two conditions necessary in a material to classify it as a ferroelectric are (1) the existence of spontaneous polarisation and (2) a demonstrated reorienting of the polarisation [Haertling, 1999].

The interrelationship of piezoelectrics and subgroups can be seen in Fig. 1.2.5. All ferroelectrics are piezoelectrics, but not all piezoelectrics are ferroelectrics.

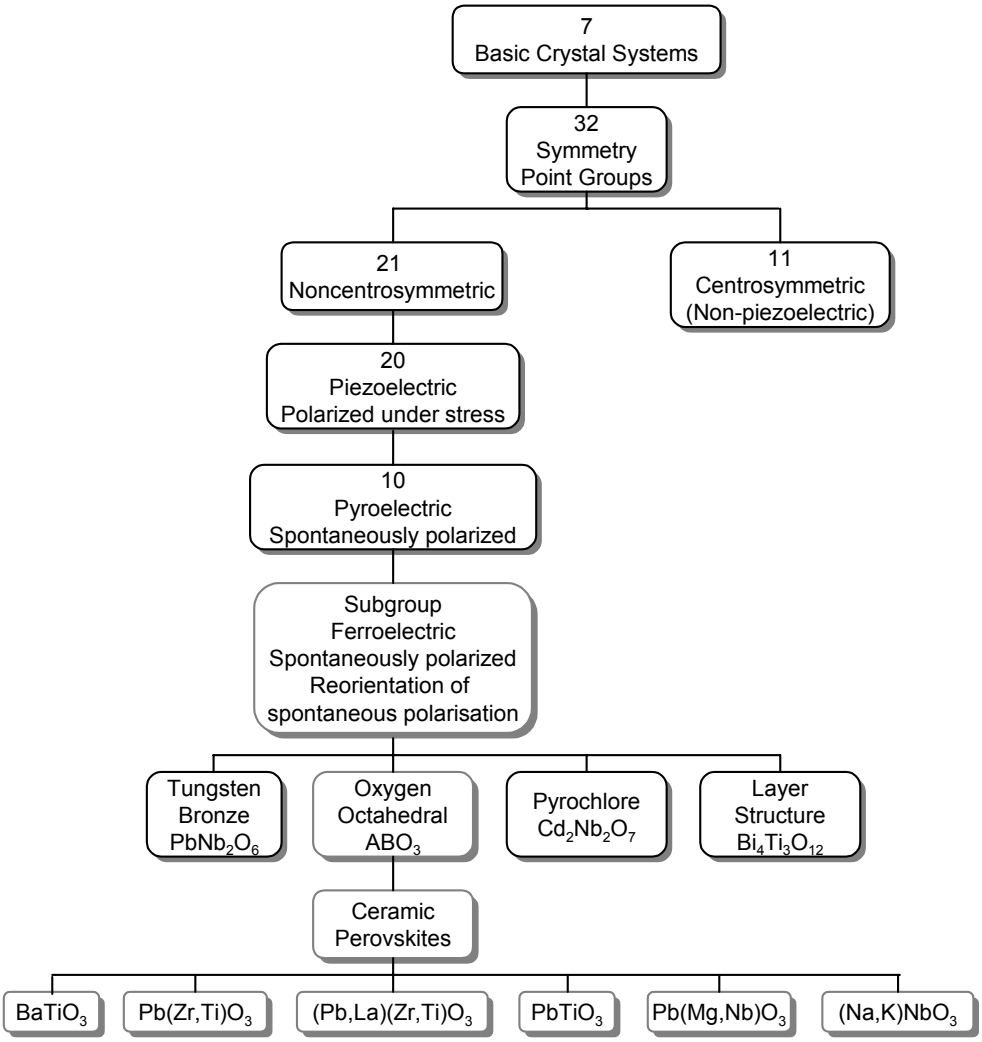

Figure 1.2.5. Interrelationship of piezoelectrics and subgroups on the basis of symmetry [After Haertling, 1999].

Piezoelectricity was observed first by the brothers Jacques and Pierre Currie in 1880. A historical overview of the development of piezoelectric phenomena research and applications is summarized in Table 1.2.1. Related reference treatises can be found in the book of Jaffe *et*

al. [Jaffe *et al.*, 1971], the review article of Haertling [Haertling, 1999] and the website at www.intellimat.com.

Table 1.2.1. A chronological list of the specific events in the history of piezoelectric materials.

Time	Events
1880	Piezoelectricity was discovered in Rochelle Salt by brothers Jacques and Pierre Currie.
1881	The term "piezoelectricity" was first suggested by W. Hankel, and the inverse effect was deduced by Lipmann from thermodynamic principle.
1910	"Lehrbuch der Kristallphysik" by Voigt was published, and it became a standard reference work detailing the complex electromechanical relationships in piezoelectric crystals.
World War I	Piezoelectric ultrasonic transducer was developed by Langevin; piezoelectric materials began to be used as microphones, accelerometers, underwater transducers, etc..(Limited material performance inhibitted commercialisation.)
1935	Piezoelectricity was discovered in KDP by Busch and Sherrer, which became the second type of piezoelectric crystals discovered until 1940.
World War II	$BaTiO_3$ was discovered as high dielectric constant material in USA, UK, USSR, and Japan, independently. Gray discovered poling process, which makes ceramic materials act as a single crystal possessing both ferroelectric and piezoelectric properties.
1950s	In 1952, PZT was reported as ferroelectric solid-solution system, and the phase diagram was established by Shirane, et al.. PZT was reported as useful piezoelectric transducer material by B. Jaffe et al. in 1954. Piezoelectric ceramics applications became commercialised, e.g., phonograph pick-ups, microphones, underwater transducers (sonar), ignition systems, discrete actuators, etc..
1960s-1980s	Discovery and research of transparent electroopic $(Pb,La)(Zr,Ti)O_3$ (PLZT) ceramics; Development of $Pb(Mg_{1/3}Nb_{2/3})O_3$ (PMN) and other relaxor ferroelectric ceramics and devices. Development of multi-layer stack actuators.
1980s-now	Piezoelectric actuators were used for smart structures, e.g., distributed actuator systems, prototype smart beam, active airfoil, etc.. Development of flexible actuators based on piezoelectric fibers embedded in polymer matrix (active fiber composites), with applications for active vibration reduction and noise control system (e.g., active helicopter rotor blade).

1.3 Piezoelectric ceramic materials

Most of the current commercially available piezoelectric materials are ferroelectric polycrystalline ceramics, such as $BaTiO_3$ and lead zirconate titanate (PZT). These ceramic materials are easier to fabricate than single crystals and also exhibit high piezoelectric and dielectric properties, which make them to be widely exploited for practical actuator and sensor applications.

Consider e.g. $BaTiO_3$ or PZT, the microstructure of these materials is of the so-called ABO_3 type perovskite structure. The perovskite structure is shown in Fig. 1.3.1, in which $BaTiO_3$ is used as an example. Above a certain temperature (which is called Curie temperature Θ_C) of 120°C, the prototype crystal structure is cubic. The larger Ba^{2+} cations are situated at the 8 corners (A site) of a cube, O^{2-} anions are located at the face centres and form an oxygen octahedral, the smaller Ti^{4+} cation is at the body centre (B site). Below the Curie temperature, the structure is slightly deformed, with Ba^{2+} and Ti^{4+} ions displaced relatively to the O^{2-} ions. As a result, an electric dipole is formed due to the separation of positive and negative charge centres, and the value of dipole moment per unit volume is the spontaneous polarisation (P_{spon}) [Xu, 1991].

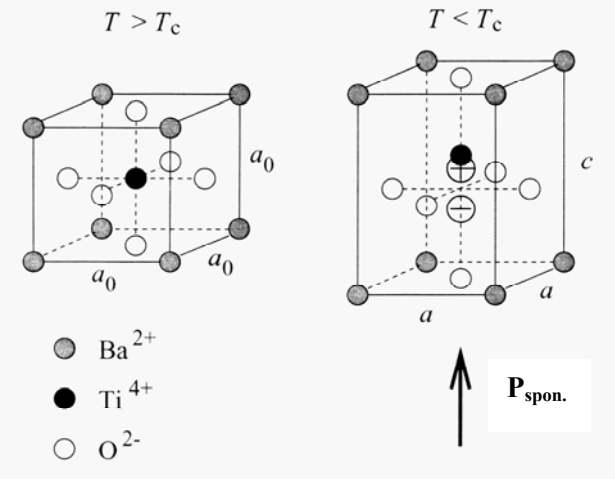

Figure 1.3.1. The crystal structure of perovskite barium titanate. Left: above the Curie temperature the unit cell is cubic; right: below the Curie temperature the unit cell structure is tetragonal with Ba^{2+} and Ti^{4+} ions displaced relatively to the O^{2-} ions, spontaneous polarisation is in the direction of displaced Ti^{4+} ion [After Kamlah, 2001].

The cubic state, which exhibits no spontaneous polarisation, is called paraelectric phase and has no piezoelectricity. Below Θ_C, a phase transition happens from the cubic structure to the tetragonal structure. The new phase is called ferroelectric phase, which possesses a spontaneous polarisation along the *c*-axis and shows piezoelectricity. In comparison with the cubic state, the unit cell of the ferroelectric tetragonal structure elongates along the *c*-axis and contracts along the perpendicular *a*-axis. The relative deformation is called spontaneous strain (S_{spon}). For $BaTiO_3$, the spontaneous strain is

$$\frac{c-a}{a} \approx 1\% \tag{1.3.1}$$

After the sintering processing, during cooling phase transition from the paraelectric cubic state to the ferroelectric tetragonal state has to be passed. There are six different possibilities

for each unit cell to displace the central ion along the axes of the original cube, as a result, the spontaneous polarisation has six different directions to develop (see Fig. 1.3.2).

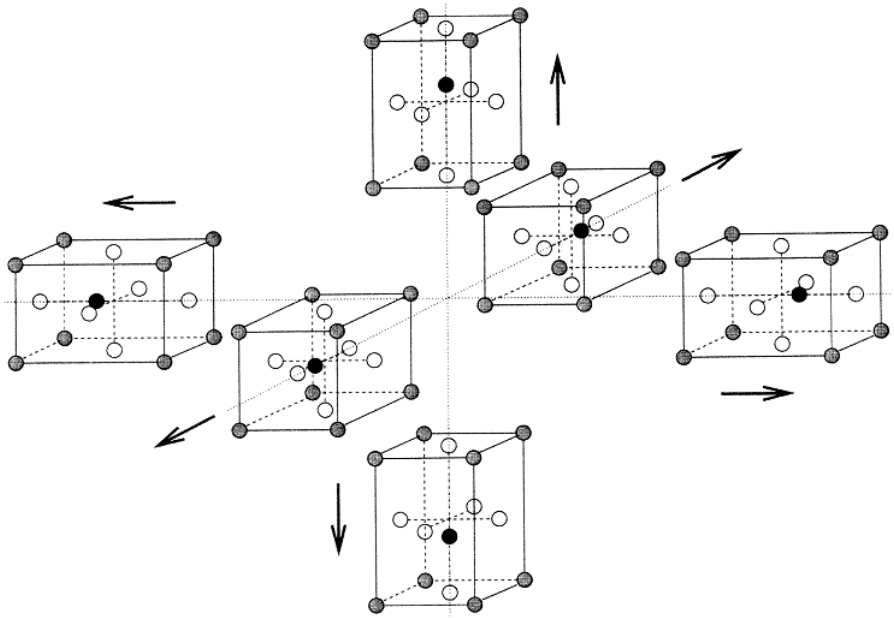

Figure 1.3.2. At the paraelectric ferroelectric phase transition, there are six different directions for the central Ti ion to be displaced, resulting in six different spontaneous polarisation vector [After Kamlah, 2001].

1. *Domains and domain walls*

Within a ferroelectric single crystal, the homogenous areas with the same spontaneous polarisation orientation are referred to as domains, with domain walls existing between areas of unlike polarisation orientation. Due to the six equivalent spontaneous polarisation development directions (see Fig. 1.3.2), only 180° and 90° domain walls can exist in the tetragonal structure ferroelectrics. 180° domain walls separate adjacent domains with oppositely orientated polarisation, whereas 90° domain walls separate domains with mutually perpendicular polarisation [Haertling, 1999].

The reason of domain walls formation is still not exactly clear. The generally acknowledged explanation is: both 180° and 90° domain walls are formed to minimize the electrostatic energy of depolarising fields arising from spontaneous polarisation, and the formation of 90° domain walls may also reduce the elastic energy associated with spontaneous strain of the unit cells [Damjanovic, 1998].

The types of domain walls that can occur in a ferroelectric crystal depend on the symmetry of both the paraelectric and ferroelectric phases of the crystal. For a ferroelectric phase with rhombohedral structure, the direction of spontaneous polarisation develops along the body

diagonals (direction [111]) of the paraelectric cubic unit cell. This gives eight possible directions of the spontaneous polarisation with 180°, 71° and 109° domain walls [Haertling, 1999].

2. *Poling of ferroelectric ceramics*

After sintering, the ferroelectric ceramics are polycrystalline, and consist of grains and grain boundaries. Each grain can be considered as a ferroelectric single crystal, which is split into many domains below the Curie temperature (see Fig. 1.3.3, left). Every domain has a certain spontaneous polarisation and strain. Since the spontaneous polarisation is randomly distributed throughout the material, the contributions of piezoelectricity and ferroelectricity from the domains cancel each other out in the macroscopic mean. For this reason, there is no residual macroscopic polarisation and, therefore, no discernable piezoelectricity is present in this "virgin" state of the material.

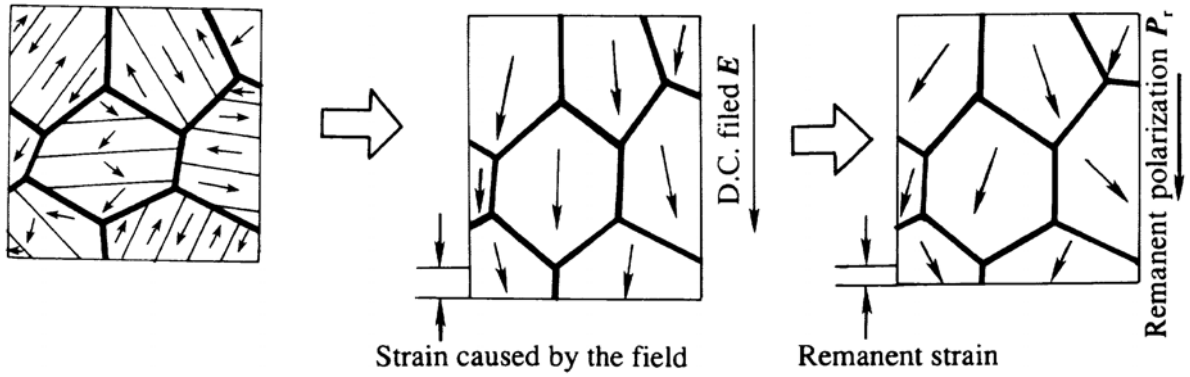

Figure 1.3.3. Schematic illustration of the domain structure and poling process [After Xu, 1991].

The polycrystalline ferroelectric ceramics may be brought to a polar state by applying a strong electric field with a magnitude above the coercive field E_c. This process, called poling, can't orient grains, but can reorient domains within individual grains in the direction of the field (see Fig. 1.3.3, middle). During poling, the material elongates along the field and contracts in the directions perpendicular to the field. The polarisation after removal of the field is called remnant polarisation (P_r) (see Fig. 1.3.3, right). The actual remnant polarisation of a ferroelectric ceramic material is always lower than the spontaneous polarisation within a single domain. This is due to the fact that domains can only be oriented to some certain crystalline axes and because some domains will switch back to their initial states after the poling field is removed (driven by internal stresses) [Damjanovic, 1998].

The poling process produces a ceramic material that acts very similar to a single domain crystal possessing both ferroelectric and piezoelectric properties. In 1945, Gray discovered

this method, which was considered as one of the most startling discoveries during the research history of piezoelectricity, since the "poling" process is a key to turn an inert ceramic material into an electromechanically active material with a multitude of industrial and commercial uses [Haertling, 1999].

3. *PZT ceramics*

PZT is the abbreviation for solid solution of $xPbZrO_3$-$(1-x)PbTiO_3$ ($0<x<1$) binary system. Its chemical formula is $Pb(Zr_xTi_{1-x})O_3$. PZT was first reported as ferroelectric material in 1952, and Shirane established the phase diagram. In 1954, PZT was reported as a useful piezoelectric material by Jaffe et al.. Since then, PZT and its modified families become the most economically important category for civil and military piezoelectric applications [Haertling, 1999].

The phase diagram of the PZT solid solution is shown in Fig. 1.3.4, where the T_c-line is the boundary between the cubic paraelectric phase and the ferroelectric phases. A morphotropic phase boundary (MPB) divides the regions of ferroelectric phase into two parts: a tetragonal phase region on the Ti-rich side and a rhombohedral phase region on the Zr-rich side. At room temperature, this boundary is at the point of Zr/Ti ≈ 52/48. In the region where Zr/Ti lies between 100/0 and 94/6, the solid solution is an antiferroelectric orthorhombic phase exhibiting no observable piezoelectric effect.

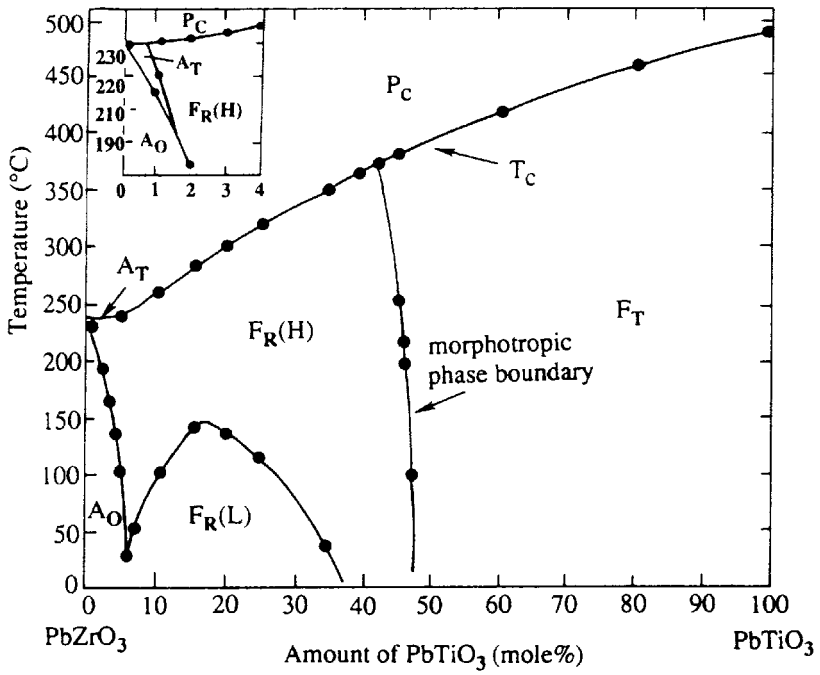

Figure 1.3.4. Phase diagram of the $PbTiO_3$-$PbZrO_3$ solid solution [After Jaffe *et al.*, 1971].

The lattice parameters of PZT also change abruptly near the composition corresponding to the MPB (see Fig. 1.3.5). Most PZT materials of technological importance have compositions near the morphotropic phase boundary, and PZT ceramics usually exhibit their maximum values of relative dielectric permittivity and electromechanical coupling coefficient close to this MPB (see Fig. 1.3.6).

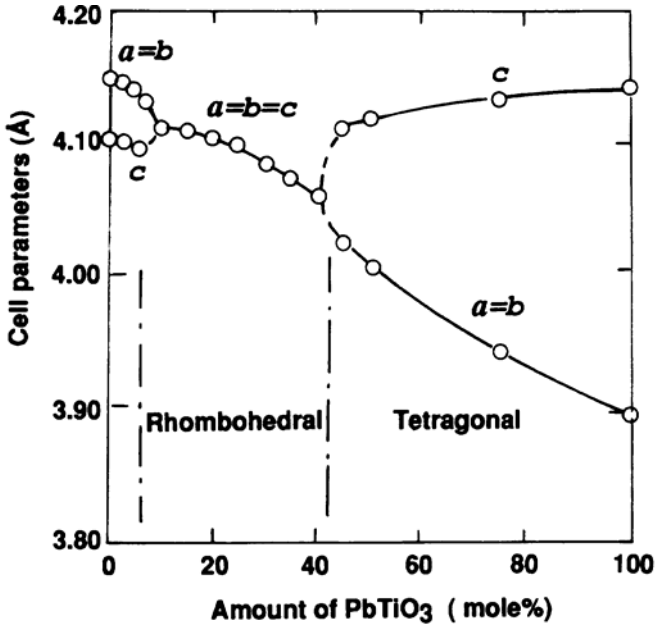

Figure 1.3.5. Lattice parameter change at room temperature for the $PbTiO_3$-$PbZrO_3$ solid solution [After Shirane *et al.*, 1952].

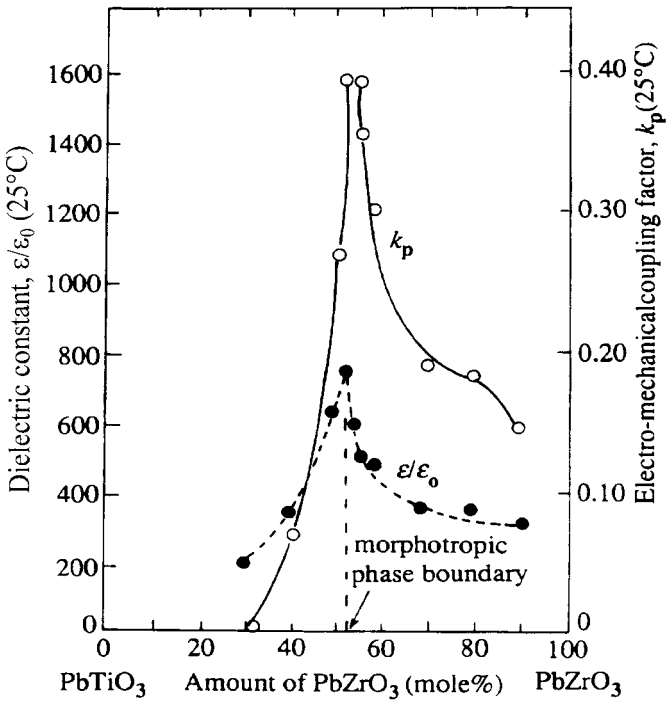

Figure 1.3.6. Dielectric and piezoelectric properties of the $PbTiO_3$-$PbZrO_3$ solid solution [After Jaffe *et al.*, 1971].

The maximum piezoelectric properties of PZT near MPB are due to more domain switching possibilities than in a single ferroelectric phase material [Cross, 1993]. Investigations have demonstrated that there can be a co-existence of the tetragonal and rhombohedral phases over a certain composition interval around the MPB. The tetragonal phase possesses 6 domain states along the equivalent [100] direction, and the rhombohedral phase possesses 8 domain states along the equivalent [111] direction. There are totally 14 possible poling directions near the MPB over a very wide temperature range, which may in part explain the extremely pronounced piezoelectric effects of PZT ceramics with composition near this boundary (see Fig. 1.3.7).

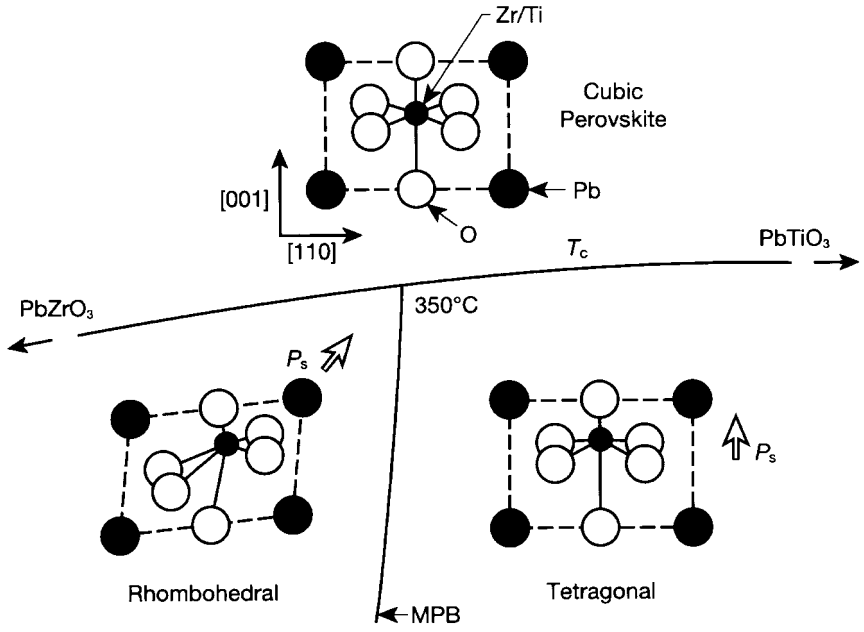

Figure 1.3.7. A portion of the $PbTiO_3$-$PbZrO_3$ phase diagram showing the structure changes at the Curie temperature (Θ_c) and the morphotropic phase boundary. Titanium-rich compositions in the PZT system favour a tetragonal modification with sizeable elongation along [001] and a large spontaneous polarisation in the same direction. There are six equivalent polar axes in the tetragonal phase corresponding to [100], [$\bar{1}$00], [010], [0$\bar{1}$0], [001], and [00$\bar{1}$] directions of the cubic paraelectric state. A rhombohedral ferroelectric state is favoured for zirconium-rich compositions. Here the distortion and polarisation are along [111] directions, giving rise to eight possible domain states: [111], [$\bar{1}$11], [1$\bar{1}$1], [11$\bar{1}$], [1$\bar{1}\,\bar{1}$], [$\bar{1}\,\bar{1}$1], [$\bar{1}$1$\bar{1}$], and [$\bar{1}\,\bar{1}\,\bar{1}$]. There are fourteen possible poling directions near the MPB over a very wide temperature range, which may in part explain the ceramic piezoelectric behavior near this boundary [After Newnham, 1997].

Though the maximum piezoelectric effect was found in the composition of pure PZT at the MPB of Zr/Ti ≈ 52/48, in practice, PZT ceramics are often modified to meet the stringent requirements for various applications. Basically, three types of additives have been employed in the compositional modification of PZT. These typical additives and their effects on the piezoelectric properties are summarised in Table 1.3.1.

Table 13.1. Typical additives to PZT and their major effects on piezoelectric properties. Ionic radii, in nanometre, are given in parentheses [After Berlincourt, 1992 and Xu, 1991].

Additives	Major Effects
Isovalent additives Ba^{2+} (0.134) or Sr^{2+} (0.112) for Pb^{2+} (0.132) Sn^{4+} (0.071) for Zr^{4+} (0.079) or Ti^{4+} (0.068)	Lower Curie point Higher permittivity
Soft dopants (donors) La^{3+} (0.122), Nd^{3+} (0.115), Sb^{3+} (0.090), Bi^{3+} (0.114) Or Th^{4+} (0.110) for Pb^{2+} (0.132) Nb^{5+} (0.069), Ta^{5+} (0.068), Sb^{5+} (0.063) Or W^{6+} (0.065) for Ti^{4+} (0.068) or Zr^{4+} (0.079)	Make the material "soft": Higher permittivity Higher K_p Much lower Q_m Resistivity about 10^3 higher
Hard dopants (acceptors) K^+ (0.133) or Na^+ (0.094) for Pb^{2+} (0.132) Fe^{3+} (0.067), Al^{3+} (0.057), Sc^{3+} (0.083), In^{3+} (0.092) Or Cr^{3+} (0.064) for Ti^{4+} (0.068) or Zr^{4+} (0.079)	Make the material "hard": Lower permittivity Lower dielectric loss Lower K_p Much higher Q_m

1.4 Domain switching related non-linear behavior of piezoelectric ceramics

As mentioned before, the domains in ferroelectric polycrystalline ceramics can be reoriented by an electric field or by a mechanical stress loading of sufficient magnitude. The consequences of domain switching in ferroelectric materials are the occurrence of non-linear responses.

1. *Ferroelectric domain switching*

Domain reorientation induced by an electric field loading is called ferroelectric domain switching. As seen in Fig. 1.4.1, both 180° and non-180° (here use 90° switching as a representation) domain switching can occur in this case.

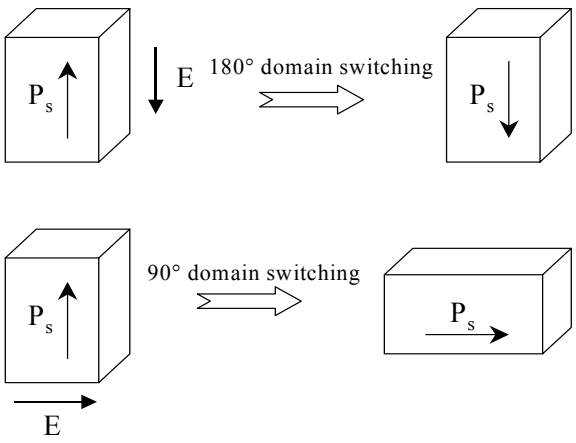

Figure 1.4.1. 90° or 180° domain switching induced by an electric field above the coercive strength ($E \geq E_c$) [After Kamlah, 2001].

Applying a large alternating electric field causes the polarisation to reverse, and this gives rise to the ferroelectric hysteretic loop, relating the polarisation P to the applied electric field. Generally, the existence of the P-E loop is considered as an evidence towards establishing that a material is ferroelectric. A typical field-polarisation loop of an initially thermally depoled PIC151 soft PZT material is illustrated in Fig. 1.4.2 (left-top). At large signals, both the dielectric displacement D and the polarisation P depend non-linearly on the field E. They are related to each other through the linear equation below

$$D_i = P_i + \varepsilon_0 E_i \tag{1.4.1}$$

Here $\varepsilon_0 = 8.85 \times 10^{-12}$ C/v·m, is the permittivity of free space.

For most ferroelectric ceramics, the second term in Equation 1.4.1 is negligible, and therefore a D-E loop and P-E loop become interchangeable. In this thesis, no distinction is made between the dielectric displacement and polarisation.

In addition to the P-E loop, domain switching also leads to a strain-electric field hysteresis curve. A typical strain-field response curve is shown in Fig. 1.4.2 (right-top). The shape resembles that of a butterfly, and it is often referred to as "butterfly" hysteresis loop.

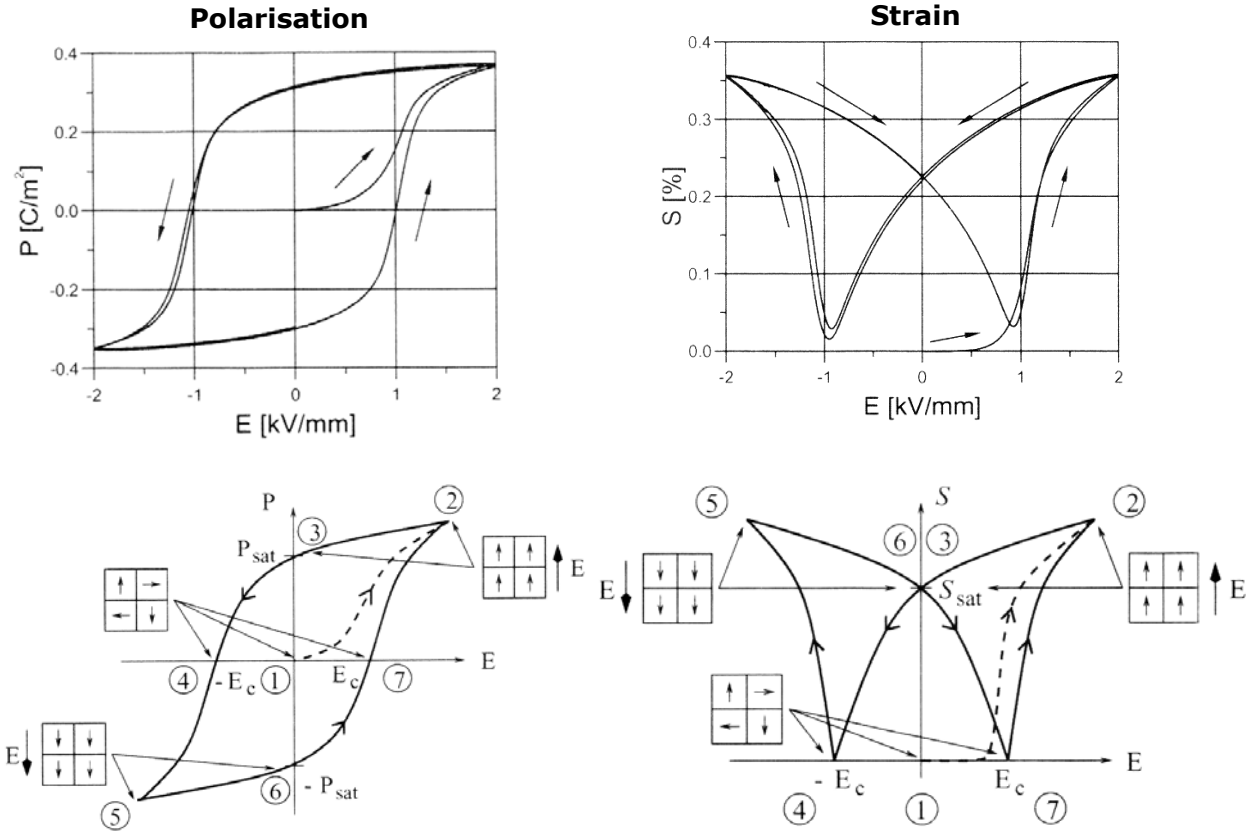

Figure 1.4.2. Polarisation (left-top) and strain (right-top) hysteresis loops induced by cycling electric field loading of PIC151 soft PZT ceramics. Schematic sketch of hysteresis loops (below) with number from ① to ⑦ used for indication of domain states [After Kamlah, 2001].

In Fig. 1.4.2 (below), the number sequence from ① to ⑦ in the schematic sketch represents the corresponding domain states in one electric field loading cycle. Detailed descriptions of the domain switching processes during a full cycle of electric field loading can be found in the paper of Lynch [Lynch, 1996] and the review article of Kamlah [Kamlah, 2001].

At the initial state ①, the domains in this thermally depoled state are randomly distributed in the ceramics, the spontaneous polarisation and strain of each domain cancelling each other out. As a result, no macroscopic polarisation and strain can be observed. With an application of a sufficiently small electric field, the material will exhibit a linearly reversible dielectric behavior.

With further increment of the E-field, after it reaches the so-called coercive field E_c, domain switching is initiated. The domains are gradually aligned to the loading direction, thus we can observe a fast development of polarisation and strain. This significant strain increment is due to two different kinds of contributions. One irreversible part is from the increasing number of domains reoriented with their longer *c*-axes (for the ferroelectric phase with tetragonal structure) parallel to the E-field. The other reversible part is from the inverse piezoelectric effect originating from the gradually increasing remnant polarisation.

Then at state indicated by ②, the reservoir of switchable domains is exhausted, and the switching processes are completed. Only the piezoelectric contribution leads to further changes of the strain, and the increase of polarisation becomes linear and reversible.

During unloading, the E-field is reduced from its maximum value to zero (state ③), the poled domain structure is preserved. Consequently, the material possesses a remnant polarisation (P_r) and a remnant strain (S_r). The poled state is important for technical applications, since it exhibits an approximately linear piezoelectric behavior for electric fields with small amplitude.

If an opposite direction electric field is applied, the previously fully orientated domain state is disturbed, the ordering degree of domains is reduced. This processing is called electric depolarisation; as a consequence, the remnant polarisation decreases. At the same time, the depolarisation leads to the loss of the inverse piezoelectric effect, and the distribution of the *c*-axes of unit cells becomes more and more random, the summary of these two effects causes the decrement of strain.

At state ④, the E-field reaches the negative direction coercive field ($-E_c$), now the lowest degree of domains ordering is reached, the polarisation becomes zero and the strain goes through a sharp minimum. With further increasing electric field, domain switching is initiated

again. At state ⑤, all the domains are aligned in a new direction parallel to the negative E-field, the resultant polarisation is in the opposite direction, whereas the strain is still elongate. Upon reversing the electric field again, the material responds in the same manner as before (⑥-⑦-②).

2. *Ferroelastic domain switching*

Domain switching can also be induced by a mechanical stress loading. This is the so-called ferroelastic domain switching. Schematic illustration of ferroelastic switching for a single domain is shown in Fig. 1.4.3, and we can see that no matter the stress is tensile or compressive, only non-180° domain switching (here use 90° domain switching as a representation) can be induced by the mechanical stress.

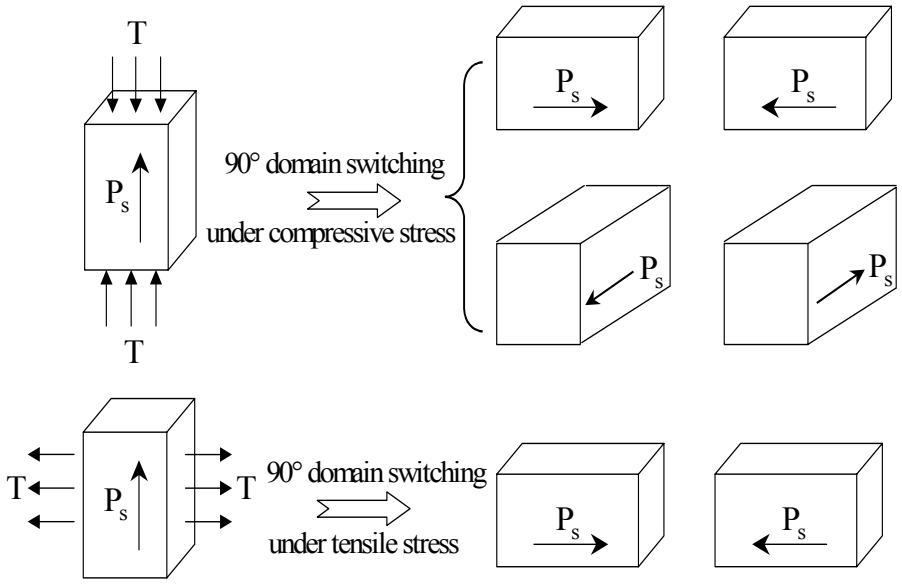

Figure 1.4.3. Schematic illustration of ferroelastic domain switching induced by mechanical stress loading with sufficiently high magnitude ($|T| \geq T_{coer.}$). Only non-180° (here use 90° switching as representation) switching can occur by stress loading [After Kamlah, 2001].

Fig. 1.4.4 shows the changes of polarisation (left) and longitudinal strain (right) as a function of compressive stress for a fully pre-poled PIC151 soft PZT ceramic material, respectively. The number sequence from ① to ③ represents the different domain states. At state ①, the material was fully pre-poled by an electric field, all the domains are assumed to be aligned to the pre-loaded E-field direction, hence the material possesses both remnant polarisation and remnant strain. Upon a sufficiently small stress load at this state, the change of polarisation approximately represents the direct piezoelectric effect, and the stress-strain relationship is

nearly linear elastic. After the compressive stress passing a limit value, which will be called *coercive stress* ($T_{coer.}$), domain switching processes are initiated. The microscopic spontaneous polarisation vector of the unit cells gradually become randomly distributed within or close to a plane perpendicular to the increasing compression load. Consequently, the earlier poling process induced remnant polarisation and strain become smaller and smaller. Significantly non-linear curves can be observed for both polarisation and strain responses. This process is called mechanical depolarisation. At state ②, as the compressive stress has become sufficiently high, the ferroelastic switching processes are completed, and all the domains are switched perpendicular to the stress. After unloading (state ③), the material possesses a compressive stress induced remnant strain, and the remnant polarisation is nearly zero. The polarisation change from ② to ③ is nearly vertical, this indicates that the electric state becomes independent of the change of stress. The domain states at ② and ③ are transversely isotropic, consequently, the material possesses no macroscopic piezoelectric effects [Kamlah, 2001].

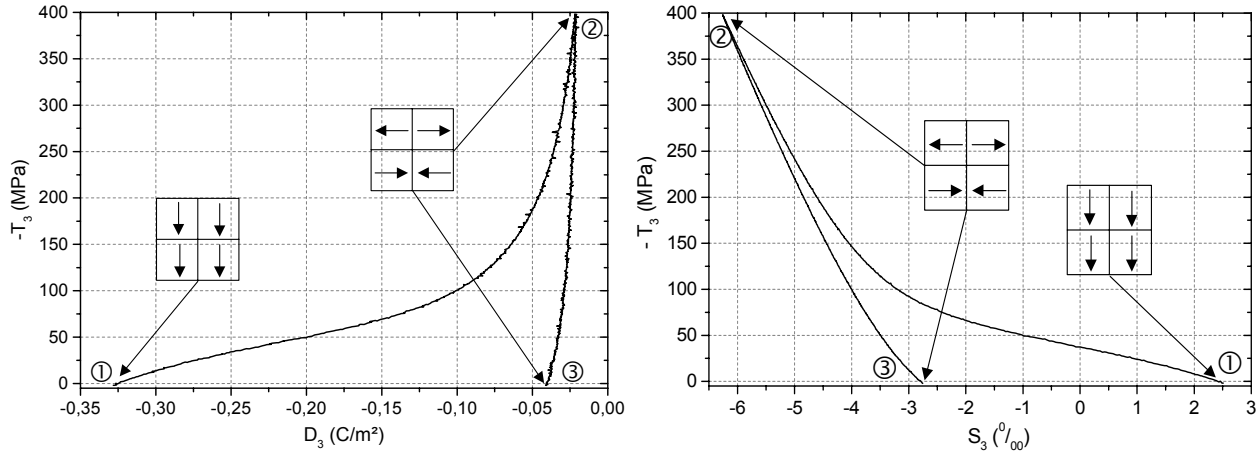

Figure 1.4.4. Compressive mechanical stress induced depolarisation (left) and strain (right) curves of fully pre-poled (with negative value remnant polarisation) PIC151 soft PZT ceramic. Corresponding domain state was also schematically illustrated.

3. *Research motivation of the non-linear behavior of piezoceramics*

For the pre-poled piezoelectric ceramics under small signal electric field or stress loads, a set of linear piezoelectric equations are used in the practical engineering applications to describe the electromechanical coupling phenomena. (see Equation 1.2.3). However, the domain switching related non-linear behavior must be taken into account for the practical devices design, electromechanical coupling calculation, and service life/reliability evaluation. This is due to the following reasons:

(1). In order to get a large strain/stress output, actuators are sometimes subjected to large signal loads (E field and/or stress);

(2). The design of modern active devices becomes increasingly more complex. For instance, in case of multi-layer actuators, an electric field concentration will occur at the tips of inner electrodes, and stress will also concentrate at the tips of micro-cracks inside the structure.

Therefore, the traditional linear assumption is insufficient to represent the practical behavior of materials accurately.

The main objective of this work is to experimentally characterise the response of piezoceramics under large signal pure electric field, pure mechanical stress, and combined electromechanical loading conditions, respectively. Based on these experimental results, a more suitable constitutive model extending over the full range of linear and non-linear behavior can be developed.

4. *Current state of research works on non-linear constitutive behavior*

Investigations of the non-linear behavior for the reliability assessment of piezoceramics can be traced back to as earlier as 1960s. Krueger reported the compressive stress induced non-linearity as well as permanent deformation of piezoelectric ceramics, with stress applied parallel or perpendicular to the poling axis [Krueger, 1967, 1968]. Schnell reported non-linear depolarisation of piezoelectric ceramics under uni-axial pressure tests and time dependence of this behavior [Schnell, 1980].

Since the rapid expansion of civil and military application market, research works on the non-linear constitutive behavior of piezoceramics become animated again in recent years. One direction of these efforts is the experimental investigation; the other one is the modelling of the observed behavior.

Investigation of frequency dependence of polarisation and strain versus E field curves has been performed on a kind of soft ferroelectric material ($0.7Pb(Mg_{1/3}Nb_{2/3})O_3 - 0.3PbTiO_3$) with various maximum field strength by Viehland and Chen. Strong frequency dependent phenomena were observed in case of an electric field amplitude $\leq E_c$, especially exhibited most pronounced at $E = E_c$. In addition, the coercive field E_c was also found to be frequency dependent, decreasing with measurement frequency decrement [Viehland and Chen, 2000].

Pure mechanical stress induced non-linear behavior of piezoelectric ceramics was usually experimentally investigated under uni-axial compressive stress loading. As an important

replenishment, measurements of soft PZT ceramics under tensile stress loading were performed by Fett et al. [Fett et al., 1998, 1999, 2000]. In addition, partial unloading tests were carried out the same PZT material to evaluate the change of Young's modulus during both compressive stress loading and unloading processes [Fett et al., 2002].

Cao and Evans attributed the mechanical non-linearity of piezoceramics to ferroelastic domain switching processes. They compared the strain and depolarisation behavior of soft and hard PZT subjected to loading-unloading cycles with different stress amplitudes, and found that soft PZT was more sensitive to a compressive stress, where even very small stresses would induce non-recoverable strains and depolarisation after unloading. In case of stresses applied normal to the pre-poling direction, the resultant stress/strain curves exhibited only limited non-linearity [Cao and Evans, 1993].

Calderon-Moreno et al. investigated the response of irreversible strain of PZT ceramics under cyclic stress loading with different amplitudes. Their results showed that the irreversible strain increased significantly with loading cycle numbers and eventually became saturated. This cumulative irreversible strain behavior was more pronounced for lower stress amplitudes, due to more loading cycles were needed for saturation [Calderon-Moreno et al., 1999, 2001].

Domain switching related non-linear responses of $(Pb,La)(Zr,Ti)O_3$ (PLZT) piezoceramic material were thoroughly analysed in the work of Lynch. He also reported the responses of polarisation and strain versus electric field hysteresis loops under various compressive stress preload conditions, where the coercive field, remnant polarisation and remnant strain gradually decreased as a consequence of increasing compression load [Lynch, 1996]. Similar investigations were carried out for another kind of soft PZT material by Chaplya and Carman, and their results were interpreted in terms of two successive non-180° domain switching processes [Chaplya and Carman, 2001].

Schäufele and Härdtl investigated the non-linear compressive strain and depolarisation behavior of soft and hard PZT with different Zr:Ti ratio. The stress induced remnant strain and depolarisation had their maximum values at the MPB, whereas the coercive stress ($T_{coer.}$, defined in their work as the stress value corresponding to the inflection point of the non-linear stress - strain curve) was smallest at MPB. Superimposed co-axial E field had a significant influence on the magnitude of coercive stress, which linearly increased with parallel bias E field increment. [Schäufele and Härdtl, 1996].

Recently, Chaplya and Carman published their experimental results of stress-strain curves under bias electric field preload conditions for PZT ceramics. With an increment of a positive bias E field (parallel to pre-poling direction in their experiments), two phenomena were detected: (1) stress-strain curves became effectively closed after mechanical unloading; (2) the stresses needed for the beginning and ending of domain wall motion increased and finally became saturated [Chaplya and Carman, 2002].

Time-dependence of soft PZT ceramics under constant E field loading was experimentally investigated by Weber et al. Both polarisation and strain exhibited creep like changes during the hold time of a constant E field, and this behavior became more pronounced next to the coercive field [Weber, et al., 2000]. Time effects of piezoceramics under compressive or tensile stress loads can be found in the thesis of Alatsathianos [Alatsathianos, 2000] and the book of Munz and Fett [Munz and Fett, 1999].

Recently, Huber et al. published their experimental results of proportional electromechanical coupling tests for soft PZT material, in which a uni-axial compressive stress and a parallel electric field were applied simultaneously with varying magnitude proportions. A switching ("yield") surface was obtained to determine the onset conditions of domain switching [Huber et al., 2002].

To characterise the biaxial and multi-axial constitutive behavior of ferroelectric materials, Huber et al. measured the changes of dielectric displacement for a sample exposed to an electric field acting or compressive stress loading under a given angle with respect to the initial poling direction [Huber et al., 2000].

In the work of Chen and Lynch, internal and external pressures accompanied by a simultaneous axial compressive stress were applied to a tubular PLZT specimen to map out the ferroelastic domain reorientation surface [Chen and Lynch, 2001].

In contrast to the conventional macroscopic strain measurements, microscopic strain evaluation by high resolution X-ray diffraction method was found to be an effective approach to distinguish the intrinsic effect (lattice deformation) from the extrinsic effect (domain wall motion) in the total strain response. In the works of Hoffmann et al. [Hoffmann et al., 2001] and Endriss et al. [Endriss et al., 1999], electric field induced strain response was investigated for lanthanum doped soft PZT ceramic material. The influence of Zr:Ti ratio and grain size on the material properties was characterised. The total strain of the rhombohedral sample was dominated by the intrinsic piezoelectric effect (lattice deformation), while domain switching was negligible. Domain wall motion related extrinsic effect was found to be the significant

contribution to the total strain response of the tetragonal material. These results were confirmed by the Acoustic Emission (AE) studies.

Besides the experimental investigations, constitutive models have been developed to describe the macroscopic non-linear behavior of piezoceramics. Basically, two kinds of constitutive theories have been invented: (1) phenomenological approaches making constitutive assumptions directly on the macroscopic level of consideration; (2) micromechanically based constitutive laws, which simulate the macroscopic ferroelectricity by modelling the underlying microscopic switching mechanisms. In the review article of Kamlah, these models have been thoroughly discussed and compared [Kamlah, 2001].

Chapter 2 Experimental Method and Set-up

To characterise the large signal non-linear behavior of piezoelectric ceramic materials under high electric field or combined electromechanical loading conditions, the extremely challenging tasks are to avoid high voltage damages to the experimental apparatus and to get the correct measurement signals. For this purpose, meticulous cares should be taken for the specimen preparation and for the designs of measurement circuits and test fixtures, etc..

2.1 Material characteristics and specimen preparation

PIC151 PZT ceramic material, which is commercially available from PI Ceramic Company (Lederhose, Germany), was selected for the measurements in this thesis. The exact compositional formulation for PIC151 is proprietary to PI Ceramic Company. It is known that this material is a kind of $Pb(Ni_{0.33}Sb_{0.67})O_3$-$PbTiO_3$-$PbZrO_3$ ternary system , where Sb^{5+} in the composition acts as donor to make the material soft, therefore it is a kind of soft PZT. In order to get the maximum electromechanical coupling efficiency, the composition is formulated in the vicinity of the morphotropic phase boundary of PZT in the tetragonal range, with an average grain size of 6 μm. The breakdown voltage of this material is about 5kV/mm. Some of the technically important characteristics are given in Table 2.1.1. More information about this material can be found at the company homepage of *www.piceramic.de*.

Table 2.1.1. Some technical properties of PIC151 soft PZT ceramic material.

PZT Characteristics	Notation	PIC151
Density ($\times 10^3$ kg·m^{-3})	ρ	7.80
Curie Temperature (° C)	Θ_c	250
Relative Permittivity	$\varepsilon^T_{33}/\varepsilon_0$ $\varepsilon^T_{11}/\varepsilon_0$	2400 1980
Dielectric Loss ($\times 10^{-3}$)	tan δ	15
Resistivity (Ω·m)	ρ	10^{11}
Coupling Factors	k_p k_{33} k_{31}	0.62 0.69 0.34
Charge Constants ($\times 10^{-12}$ mV^{-1})	d_{31} d_{33} d_{15}	-210 450 580
Voltage Constants ($\times 10^{-3}$ VmN^{-1})	g_{31} g_{33}	-11.5 22.8
Elastic Constants ($\times 10^{-12}$ m²N^{-1})	s^E_{11} s^E_{33}	15.0 19.0

The samples ordered from the company were cut to 5×5×15 mm³ rectangular blocks, polished, then burned silver electrodes into the two 5×5 mm² surfaces at 850 °C.

The choice of sample geometry is constrained by several factors like: the magnitude of the electric field required for poling the material; the size of strain gauges which must be bonded on the sample; and finally proper aspect ratio to get a uniform stress and strain state in the center of sample.

The maximum capability of the high voltage power supply (HCB 15 – 30 000, F. u. G. Elektronik GmbH, Rosenheim, Germany) is 30 kV, such that the corresponding maximum E-field applied on the specimen is 2 kV/mm, which is about two times than the coercive field of this material. By this electric field, the specimen can be fully polarized. The aspect ratio of 3:1 can ensure that a significant middle portion of the sample is experiencing a uni-axial stress and strain uniformly.

Flow chart of the specimen preparation procedure is shown in Fig. 2.1.1. For the experiments performed under a pure electric field or combined electromechanical loading, due to the high voltage, the following meticulous considerations have to be taken for the preparation of specimens.

(1). Sample cleaning

The sample surfaces should be strictly cleaned during the whole preparation procedure and before the measurement, since any contamination (e.g., greasy stains, trivial fibres, etc.) will enhance the probability of arcing at high voltage.

(2). Strain gauges selection

Two special kinds of strain gauges from Measurements Group Inc.* (Raleigh, North Carolina, USA) were used for the strains measurement in this thesis. One named CEA-06-125UN-350 was used to measure the longitudinal direction strain; another one named EA-06-062ED-120 (with Opinion E) was used for the transverse direction strain measurement. The selection of strain gauges is first for the consideration of specimen geometry, and second for the reason of safety under high voltage loading.

Both of these two types of strain gauges have a tough and flexible polyimide backing. Their measuring gauge grids are completely encapsulated in the protective polyimide, leaving only a part of copper-coated tabs exposed for lead wire soldering.

∗ Measurements Group Inc. was out of business at the end of 2001. The products now can be ordered from Vishay Measurements Group GmbH (Heilbronn, Germany).

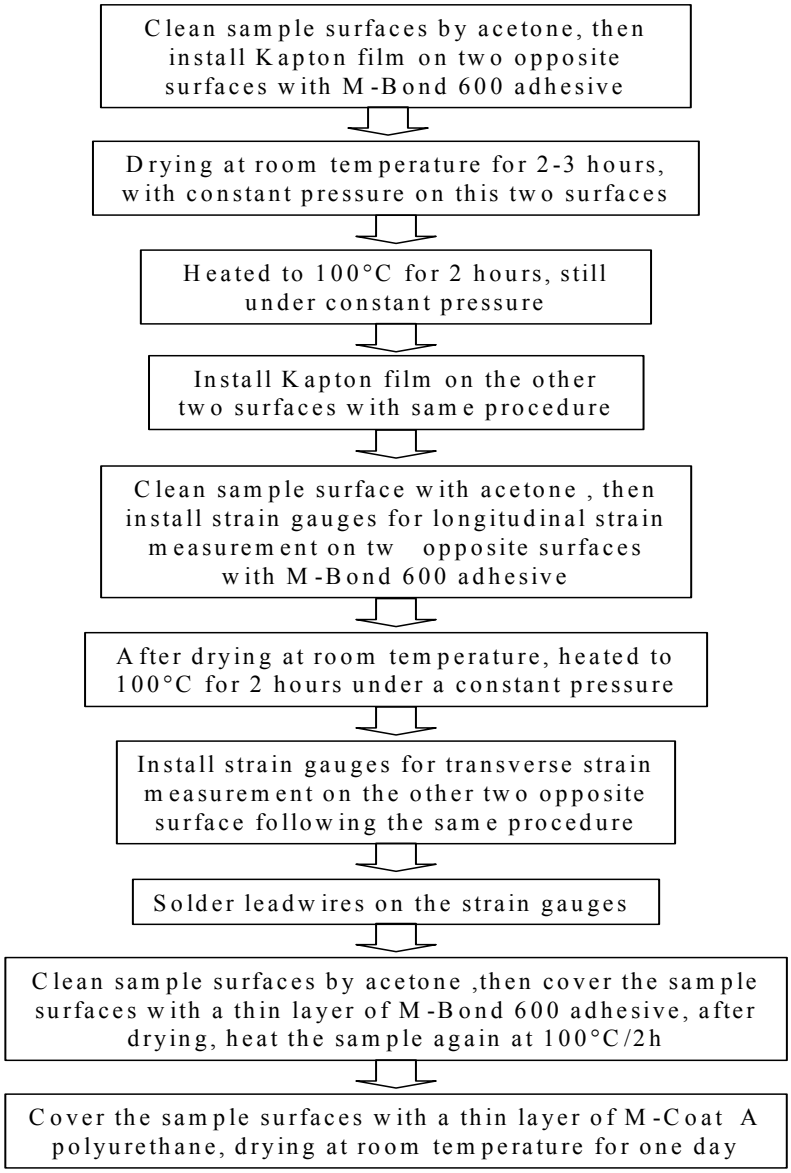

Figure 2.1.1. Specimen preparation procedure for experiments under a pure electric field or combined electromechanical loading.

(3). Strain gauges position on the specimen

Under a mechanical compression load, the two ends of the sample are effectively clamped due to friction between the specimen surfaces and loading device. This clamping effect could give rise to non-uniform stress distributions within a sample, which would produce inaccuracies for the strain measurements. For this reason, the measuring grids of strain gauges should be installed at the central portion of a specimen, since most homogenous deformation state is present there. At the same time, in order to minimize the probability of arcing, the strain

gauges should be attached as far as possible away from the electrode connected to the high voltage potential.

(4). Soldering joints

To minimize the local electric field intensification, the soldering joints between the lead wires and solder tabs of strain gauges should be smooth and as small as possible.

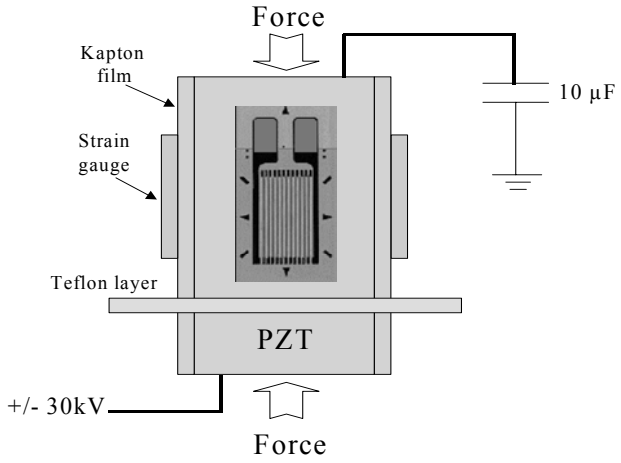

Figure 2.1.2. A completely prepared specimen ready for pure electric field or combined electromechanical loading experiments.

A completely prepared specimen configuration is schematically shown in Fig. 2.1.2. For the experiments performed with high electric field application, the specimen was placed in a bath filled with *fluorinert liquid* (FC-40, 3M Company, St. Paul, MN, USA). This is a kind of clear, colourless, thermally stable and fully-fluorinated liquid, with dielectric strength of 18 kV/mm, which is much higher than that of the air. When applying a high electric field, some contaminants (e.g., trivial fibres, moisture) inside the fluorinert liquid might align themselves from high electrical potential to low potential and form some discharge paths. Therefore, as shown in Fig. 2.1.2, a Teflon shield was installed on the specimen between the strain gauges and the high potential electrode to prevent arcing by cutting the discharge paths.

For strain measurement under a pure mechanical stress load, the strain gauges are normally directly installed on the specimen. At the initial stage of experiments, the specimens were also prepared by this simple way to evaluate the strain response under high electric field load. However, the experiences from many failed tests indicate that when the applied voltage closely achieves its maximum value, it is nearly impossible to avoid high voltage discharge (arcing) damage to the samples prepared by this simple method. Three examples of arcing damaged specimens are shown in Fig. 2.1.3.

It can be seen that, usually, the arcing will primarily originate at the corners of the high potential electrode, and then pass through the specimen edges to a strain gauge or a lead wire soldering point. Obviously, the harmful high voltage during discharge is extremely dangerous for the experimental apparatus, e.g., strain amplifiers, electrometer, computer for data acquisition, and so on.

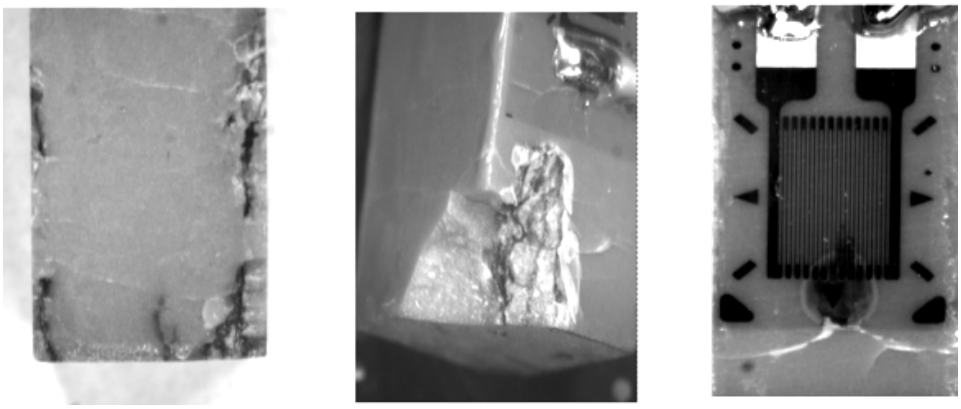

(a) (b) (c)

Figure 2.1.3. Examples of damaged specimens by high voltage discharge. (a) high voltage discharge path along the specimen edges; (b) a seriously damaged specimen corner; (c) a burned-out point by arcing at a strain gauge's grid end.

This challenge was finally effectively solved by attaching a thin layer of Kapton polyimide film between the strain gauges and the specimen (see Fig. 2.1.2). The Kapton polyimide film was ordered from Measurements Group Inc., with the thickness of 0.02 mm**.** Its dielectric strength is 236 kV/mm, with volume resistivity on the order of 10^{12} Ω·cm, and the relative dielectric constant is about 3.9.

In the following discussion, we will see that, at the region near a strain gauge, the electric field concentration inside the PZT ceramic sample will be significantly reduced by attaching a thin layer of Kapton film between the gauges and specimen. As a result, the probability of arcing is effectively minimized.

As shown in Fig. 2.1.4 (a), if there is no strain gauge on the specimen, the electric field distribution inside the material will be approximately parallel from the high potential electrode to ground potential electrode. However, when there is a strain gauge attached on the specimen surface, since the strain gauge is also nearly at ground potential, the parallel electric field distribution will be disturbed. Local E-field concentration will occur near the strain gauge region. The distance from the strain gauge grid end or lead wire soldering point to the specimen's high potential electrode is relatively short (only about 6mm). As a result, the

maximum electric field between them could be as high as 5 kV/mm (if consider the maximum output from the high voltage power supply is 30 kV). This E-field is nearly equal to the breakdown field of PIC151 soft PZT. Consequently, the arcing can be hardly avoided as the applied voltage approaching its maximum value.

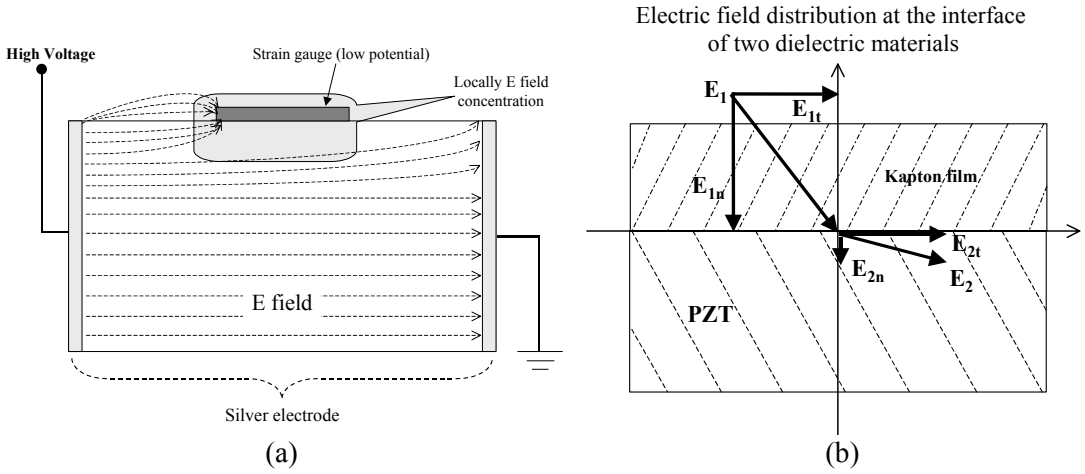

Figure 2.1.4. Electric field distribution in case of strain gauges attached on the specimen surface. (a) without Kapton film; (b) with a thin layer of Kapton film attached between the strain gauge and specimen.

When a thin layer of Kapton film is attached between the strain gauges and specimen, near the strain gauge region, the excessive E-field concentration inside the specimen will be minimized. A sketchy analysis is given below. As illustrated in Fig. 2.1.4 (b), in case of an incident of electric field from the Kapton film into the sample or vice versa, refraction will occur at the interface of these two different dielectrics. The tangential components of the E-field in these two different materials are equal.

$$E_{1t} = E_{2t} \tag{2.1.1}$$

Where E_{1t} and E_{2t} are the tangential components of electric field in the Kapton film and PZT specimen, respectively.

In the Kapton film, the electric displacement (D_k) induced by the normal electric field component (E_{1n}) is

$$D_k = \varepsilon_0 \varepsilon_{rk} E_{1n} \tag{2.1.2}$$

Where ε_0 is the vacuum dielectric constant, and ε_{rk} = 3.9, is the relative permittivity of Kapton film.

In the PZT ceramic specimen, if treated simply as a linear dielectric, the electric displacement (D_P) induced by the normal electric field component (E_{2n}) is

$$D_p = \varepsilon_0 \varepsilon_{rp} E_{2n} \tag{2.1.3}$$

Where $\varepsilon_{rp} = 2400$, is the relative permittivity of PIC151 soft PZT.

According to the Gauss's Law, $D_k = D_p$, therefore

$$\varepsilon_0 \varepsilon_{rk} E_{1n} = \varepsilon_0 \varepsilon_{rp} E_{2n} \tag{2.1.4}$$

$$\varepsilon_{rk} / \varepsilon_{rp} = E_{2n} / E_{1n} \tag{2.1.5}$$

Since $\varepsilon_{rk} << \varepsilon_{rp}$, yields $E_{2n} << E_{1n}$. It is clear that, with a thin layer of Kapton film attached between the strain gauges and specimen, the normal component of the electric field will be mainly concentrated inside the Kapton film. The breakdown strength of the Kapton film is about 236 kV/mm, which is much higher than PZT ceramics, therefore the arcing probability is effectively minimized.

The second purpose of using Kapton film in the experiments is to get the correct strain measurement results by strain gauges. The longitudinal strains, measured by LVDT (abbreviation for linear variable differential transformer) and strain gauges at the same time, are compared in Fig. 2.1.5 and Fig. 2.1.6. Here we use the strain measured by LVDT method as a standard result.

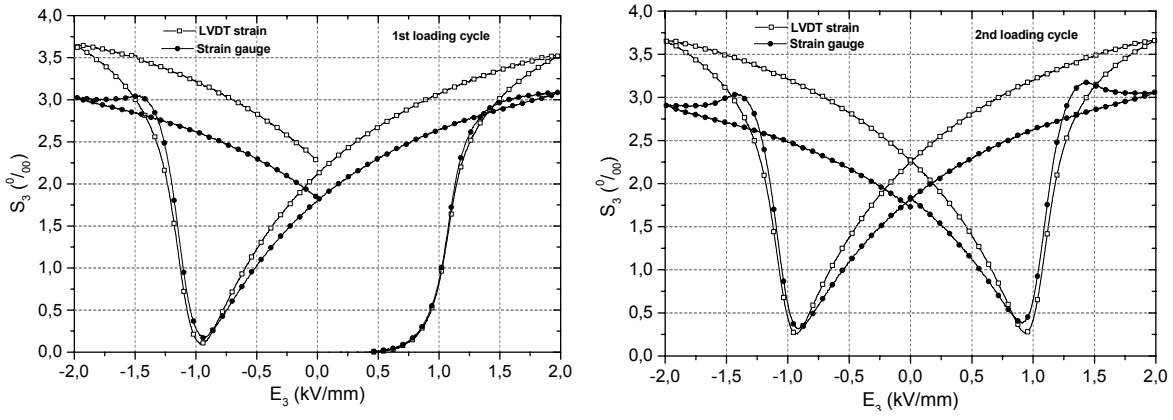

(a) (b)

Figure 2.1.5. Comparison of longitudinal strains measured by LVDT and strain gauge method. There was no Kapton polyimide thin film glued between the strain gauge and specimen. (a) first E field loading cycle; (b) second loading cycle.

In case of Fig. 2.1.5, there was no Kapton film glued between the strain gauge and specimen. At the beginning of the first E-field loading cycle, the strains measured by strain gauge and LVDT developed in the similar way. However in further cycles, when the E-filed reached about +/-1.5kV/mm, the signal from the strain gauge reached a maximum value, and as

responding to further E-field increment, it became apparently smaller in contrast to the strain measured by LVDT method.

A tentative explanation for this strange behavior is: as discussed earlier, the electric field will be concentrated at the region near strain gauge. Without Kapton film, the concentration occurs inside the PZT specimen, and it would induce abnormal domain switching at this region. We know that, the strain measured by strain gauge represents the local deformation, whereas the strain monitored by LVDT represents the macroscopic body deformation. Due to the abnormal domain switching at the region near strain gauge, the strains measured by these two methods are consequently quite different.

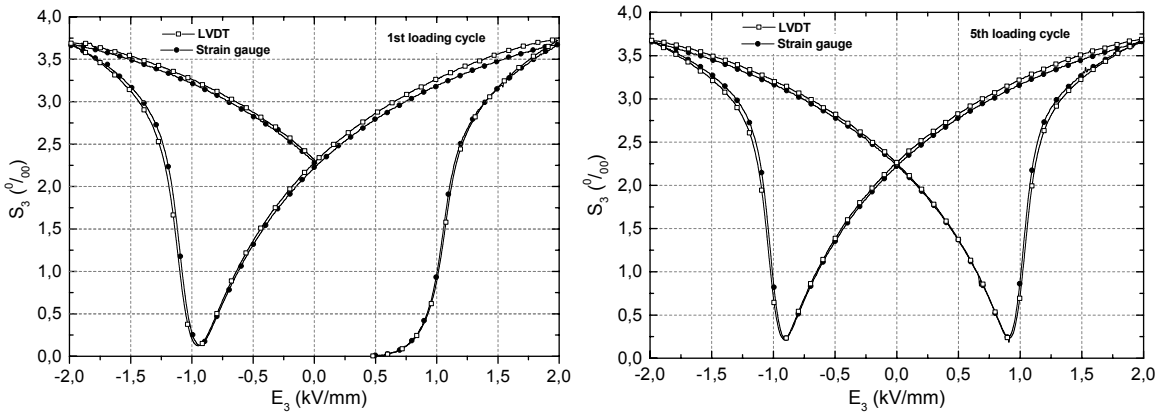

(a) (b)

Figure 2.1.6. Comparison of longitudinal strains measured by LVDT and strain gauge method. There was a thin layer of Kapton polyimide film attached between the strain gauge and specimen. (a) first E field loading cycle; (b) fifth E field loading cycle.

When there is a thin layer of Kapton film attached between the strain gauge and specimen, as discussed earlier, the concentration of E-field mainly occurs inside the Kapton film, and there is almost no abnormal domain orientation at the region near strain gauge. Consequently, as shown in Fig. 2.1.6, the strains measured by strain gauge and LVDT are nearly same during the whole E-field loading cycle.

2.2 Principles of polarisation and strain measurement

1. *Polarisation measurement*

Shunt method, virtual ground and Sawyer-Tower method are three popular techniques for dynamic polarisation hysteresis measurement of ferroelectric materials in response to electric field loading. In this thesis, since the experiments were performed under "quasi-static"

loading conditions, polarisation was measured by the Sawyer-Tower method. The measuring circuit is shown in Fig. 2.2.1.

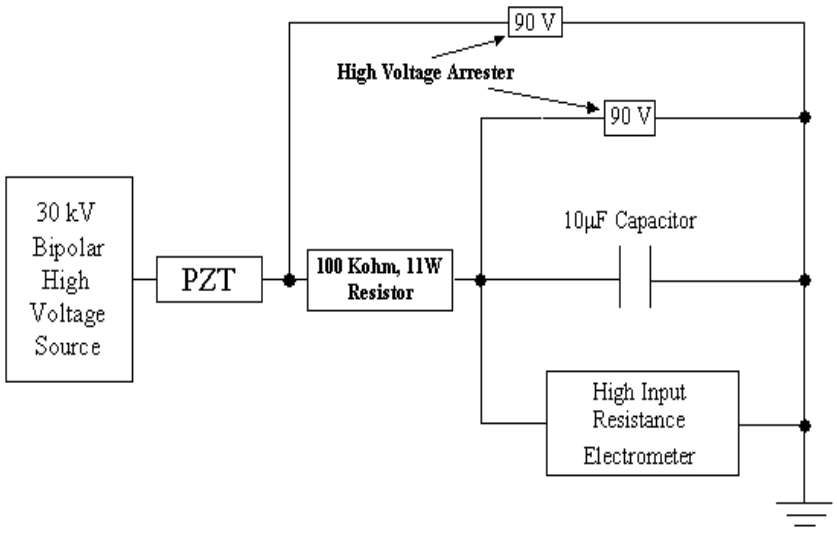

Figure 2.2.1. Schematic electric circuit in principle of Sawyer-Tower method for polarisation measurement.

The specimen can be considered as a capacitor (C_s) with approximate capacitance of 35 pF, which can be calculated as

$$C_s = \varepsilon_0 \varepsilon_r \frac{A}{d} \tag{2.2.1}$$

Here ε_0 is the permittivity of vacuum (8.85×10^{-12} F/m), $\varepsilon_r = 2400$, is the relative permittivity of PIC151 soft PZT, A is the specimen electrode area (= 25 mm²), and d is the distance between the two electrode surfaces (= 15 mm).

As shown in Fig. 2.2.1, a 10 μF reference capacitor (C_r) is connected in series to the specimen. Since the capacitance of the specimen is much smaller than that of the reference capacitor, almost all of the electric potential of the high voltage source acts on the specimen.

By definition, polarisation is the value of dipole moment per unit volume or amount of charges accumulated on per unit area. Polarisation of the specimen induced by electric field loading, P_{sample}, is given by

$$P_{sample} = \frac{Q_s}{A} \tag{2.2.2}$$

Here, Q_s is the amount of charges accumulated on the electrode of the specimen, and A is the electrode area.

Since the reference capacitor is connected in series to the specimen, their amounts of charges are equivalent.

$$Q_s = Q_r \tag{2.2.3}$$

Where Q_r is the amount of charges accumulated on the reference capacitor.

On the other hand, the amount of charges on the reference capacitor is equal to

$$Q_r = UC_r \tag{2.2.4}$$

Where U is the voltage over the reference capacitor, and C_r =10 μF, is the capacitance of the reference capacitor.

Then the polarisation induced by electric field loading can be calculated as

$$P_{sample} = \frac{UC_r}{A} \tag{2.2.5}$$

Consequently, by monitoring the voltage over the reference capacitor, polarisation of the specimen can be measured. In the experiments, this voltage was measured by a *Keithley 6517A* high input resistance electrometer (Keithley Instruments, Inc., Cleveland, Ohio, USA). In order to eliminate the influence of moisture on the accuracy of measurement, the electrometer was encapsulated in a chamber with drier.

Even though the specimens have been carefully prepared by the method introduced before, arcing might still occasionally occur during the experiments. To avoid the damages to the electrometer and the DA/AD data acquisition card inside the computer, as seen in Fig. 2.2.1, two 90 V range *high voltage arresters* were connected parallel to the reference capacitor. When arcing occurs, the harmful high voltage can go through the arresters to the ground.

Furthermore, a high power (11 W) 100 kΩ resistor was designed in series with the reference capacitor. During the normal tests, due to the "quasi-static" loading rate and very small current in the circuit, this resistor has nearly no influence on the measurement results. When the arcing happens, the instantaneous current will be very high. The resistor can share part of the harmful high voltage, and consequently provide a protection to the reference capacitor and connected equipments.

2. *Strain measurement*

The measurements under a pure electric field loading were performed by using the experimental set-up developed by Weber et al. (for details of this set-up, see next section). In this case, the electric field induced strains were measured by strain gauges and LVDT method at the same time. LVDT is an electrometric device that produces an electrical voltage

proportional to the displacement of a movable magnetic core. A *W1T3* type LVDT ordered from Hottinger Baldwin Messtechnik GmbH (Darmstadt, Germany) was used in the experiments.

For pure mechanical stress loading and the coupled electromechanical tests, to apply the compression load and isolate the test frame from high voltage, the specimen was placed between two large alumina ceramic blocks. Technically, it is difficult to install the LVDT on the experimental set-up to measure the direct strain response from the specimen. Due to this reason, only strain gauge technique was used for strain measurement in these experiments. The measuring principle for strain gauges is based on the *Wheatstone Bridge Circuit.* An example of a Wheatstone Bridge Circuit is shown in Fig. 2.2.2.

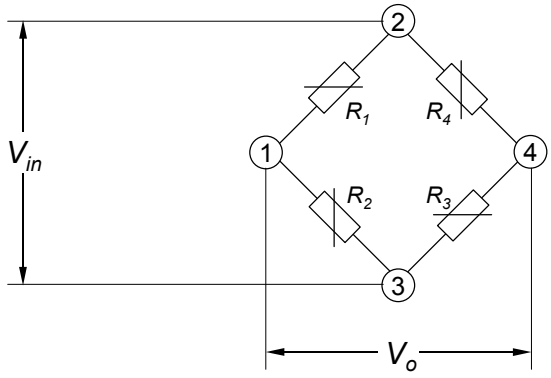

Figure 2.2.2. Schematic of Wheatstone Bridge Circuit for strain measurement.

An approximate equation is used in practice to provide sufficiently accurate results for the measurement.

$$\frac{V_o}{V_{in}} = \frac{1}{4}\left(\frac{\Delta R_1}{R_1} - \frac{\Delta R_2}{R_2} + \frac{\Delta R_3}{R_3} - \frac{\Delta R_4}{R_4}\right) \tag{2.2.6}$$

Where V_o is the output voltage of the bridge, V_{in} is the input voltage of the bridge, R is the resistance of one bridge arm, and ΔR is the resistance change of one arm.

For a strain gauge, the change of resistance corresponds to a certain induced strain.

$$\frac{\Delta R}{R} = kS \tag{2.2.7}$$

Where k is the gauge factor, S is the strain.

If all of the four arms of a Wheatstone Bridge are strain gauges, Equation 2.2.6 becomes

$$\frac{V_o}{V_{in}} = \frac{k}{4}\left(s_1 - s_2 + s_3 - s_4\right) \tag{2.2.8}$$

In the experiments performed for this thesis, the half bridge technique was used for the strain measurement, and one arm of the half bridge was a standard reference resistor ($\Delta R = 0$), thus Equation 2.2.8 is in the form of

$$\frac{V_o}{V_{in}} = \frac{k}{4} s \tag{2.2.9}$$

Therefore, the strain measured by one strain gauge is

$$s = \frac{4}{k}\frac{V_o}{V_{in}} \tag{2.2.10}$$

A *KWS 3073* 5kHz carrier frequency amplifier (Hottinger Baldwin Messtechnik GmbH, Darmstadt, Germany) was used to monitor the strain. Before the measurements, all the amplifiers were carefully calibrated by the shunt method [Hoffmann, 1989].

In order to avoid arcing damages to the strain gauges and to the amplifiers, as shown in Fig. 2.2.3, *diodes* and *high voltage arrestors* were connected parallel to both of the two soldering tabs of a strain gauge. When arcing happens, the harmful high voltage can be quickly conducted to the ground line.

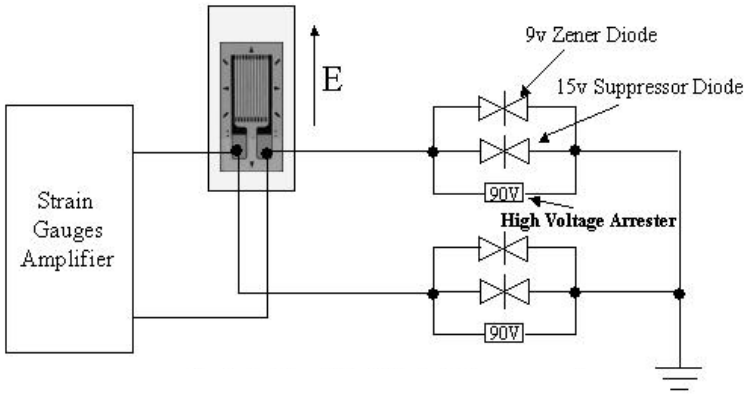

Figure 2.2.3. Schematic of electric circuit for strain measurement by strain gauge method.

2.3 Experimental set-up for electromechanical loading

The test fixture and total signal transmission system for the pure electric field loading experiments are shown in Fig. 2.3.1. Details of this experimental set-up had been described in the work of Weber et al. [Weber, et al., 2000]. Here it will not be redundantly explained again.

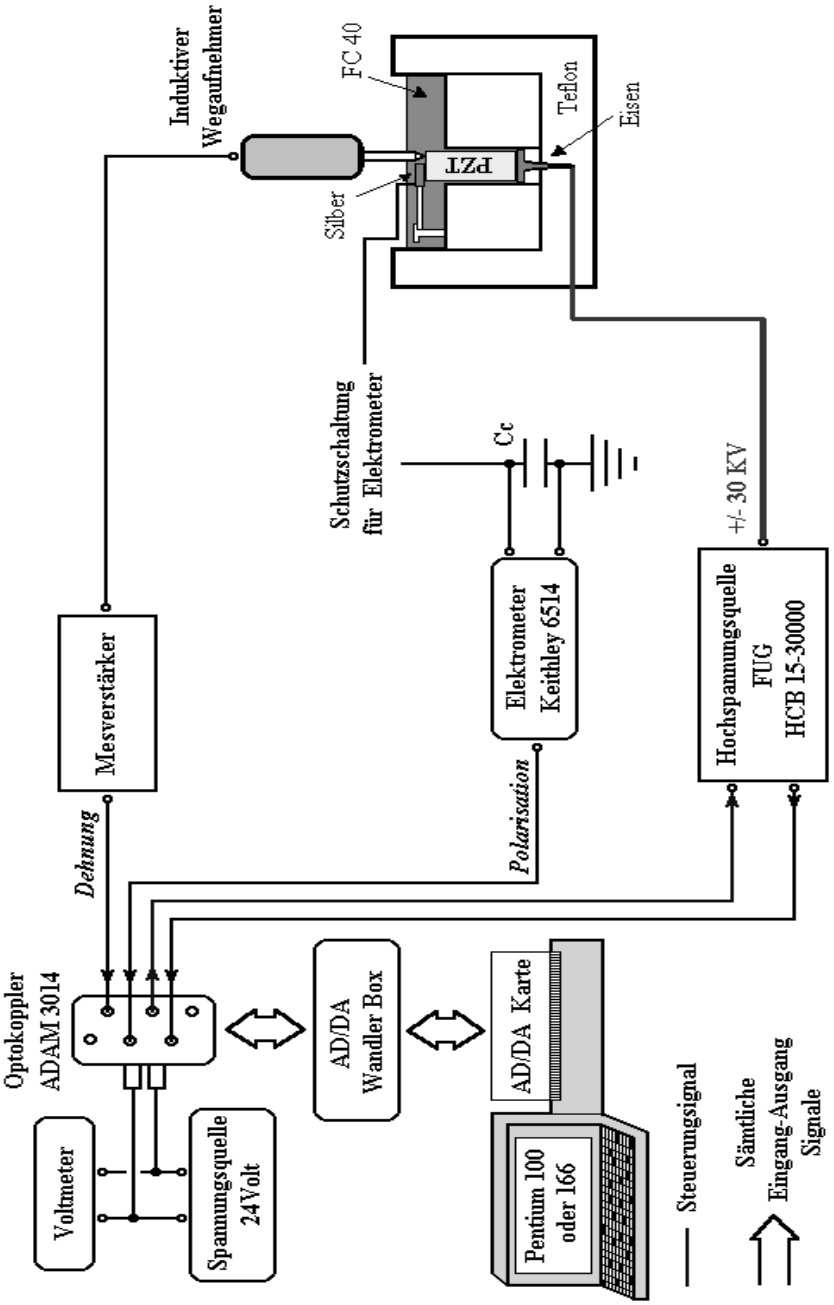

Figure 2.3.1. Schematic of experimental set-up for polarisation and strain measurements under pure electric field loading condition.

For the combined electromechanical loading experiments, it is most important to isolate all the apparatus from the high voltage and eliminate occasional discharge damages. As shown in Fig. 2.3.2, a special set-up was built for this purpose.

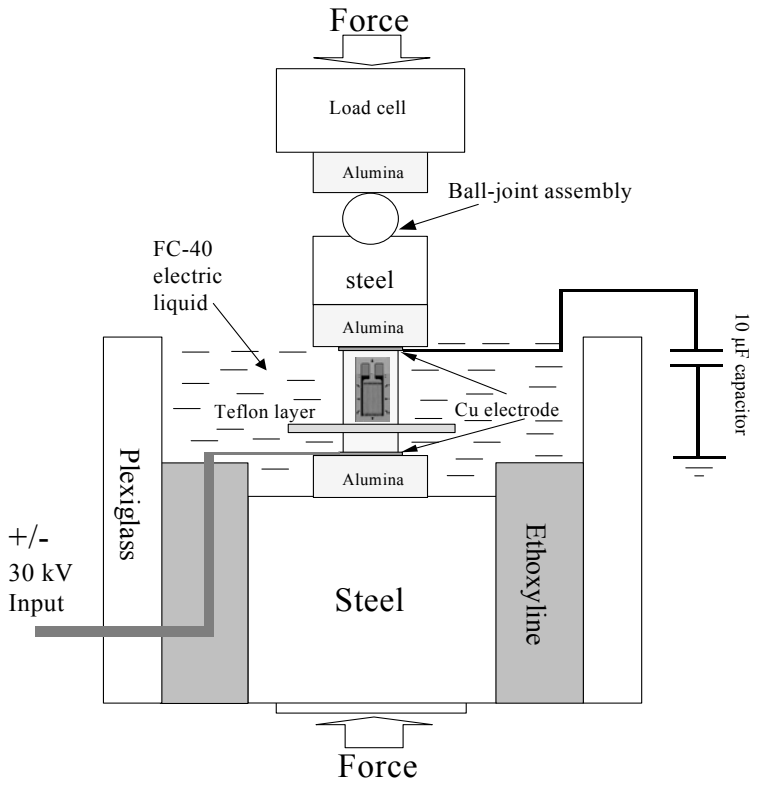

Figure 2.3.2. Schematic of test fixture for combined electromechanical loading experiments.

A polymer material container was installed on the *servo-hydraulic test frame* (Instron, Model 1361). During the experiment, the container was filled with FC-40 fluorinert liquid. Two alumina ceramic spacers were used to isolate the Instron machine from the high voltage. Bipolar high voltage was applied to the specimen through copper electrodes, which were glued on the alumina ceramic blocks. A uni-axial compressive stress was supplied by the Instron servo-hydraulic test frame. A *ball-joint assembly* was used to minimize the bending effects. For polarisation measurement, a 10 μF capacitor was in series connected to the specimen.

Four strain gauges were attached to the specimen for the strains measurement. Readings from two strain gauges mounted on the opposite sides were used to monitor the longitudinal direction strain; another two were used for transverse strain monitoring. Prior to every experiment, the specimen was first carefully positioned in the centre between the alumina

blocks. Then within a very small stress range, the specimen was subjected to compression loading /unloading cycles, and the strain outputs from opposite direction strain gauges were compared. If the difference was too large, the specimen position would be carefully re-adjusted again to minimize the bending effects caused by any misalignment. Until it was sure that the uni-axial compressive stress was applied on the specimen geometry centre, the experiment could begin. To further minimize the bending effects, when finishing the experiment, the recorded data from oppositely attached strain gauges were averaged to plot the curves.

The total measurement system is schematically illustrated in Fig. 2.3.3. A computer equipped with a *DAP 1216a/16* DA/AD data acquisition card and the *DASYLab 4.0* software package (National Instruments Services GmbH & CoKG, Mönchengladbach, Germany) was used to control the Instron machine and the high voltage power supply simultaneously. All the equipment output signals first went through the *isolated DC input/output signal- conditioning modules* (optocoupler) and then were recorded by the computer. The isolated DC input/output signal-conditioning module was used for further isolation of the computer from high voltage discharge.

To get a visual impression, Fig. 2.3.4 shows two photographs of the test fixture with a specimen emplaced between two alumina disks in the polymer container and a part of the total experimental system.

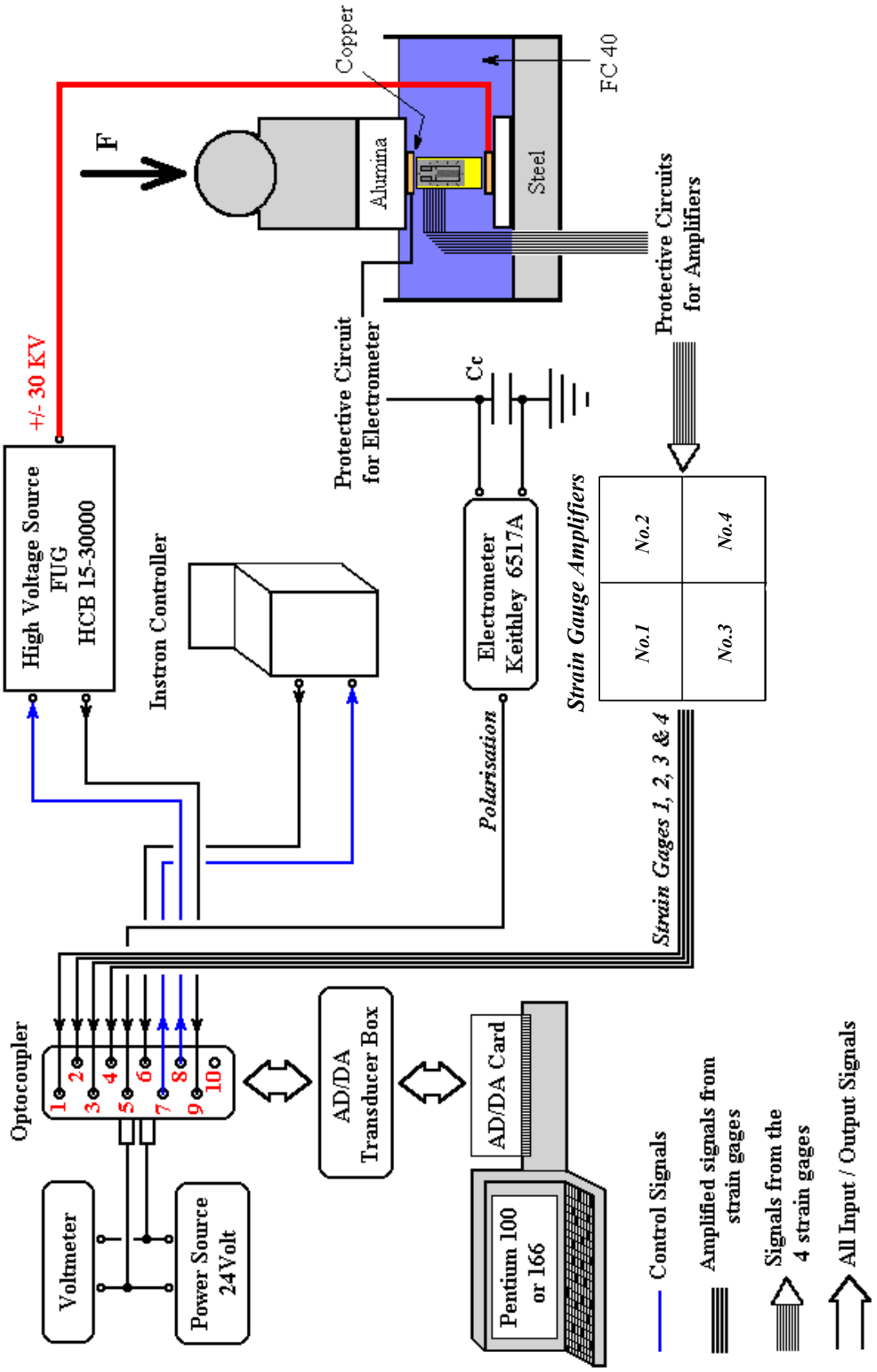

Figure 2.3.3. Schematic of experimental system for combined electromechanical loadling.

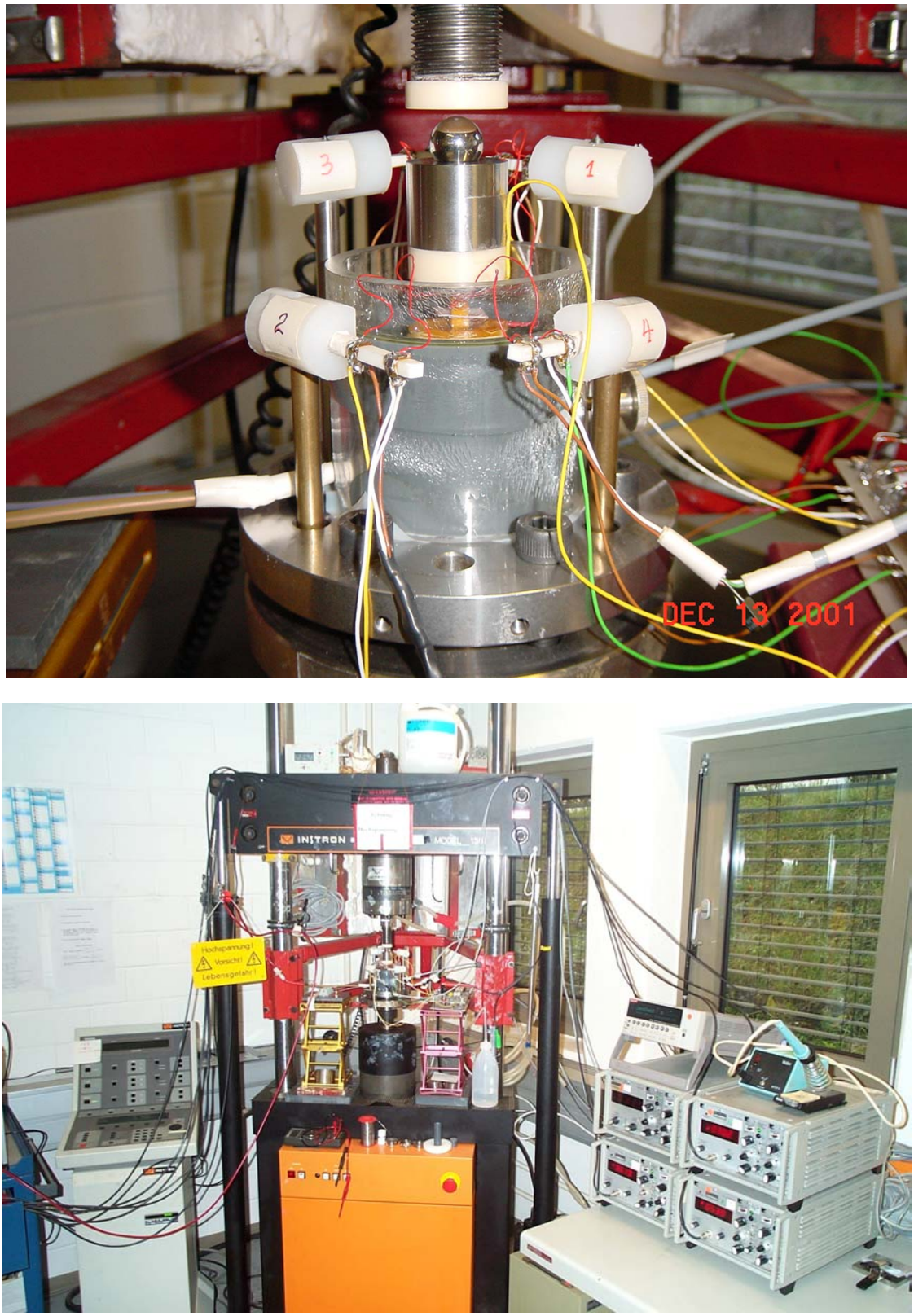

Figure 2.3.4. Photographs of the experimental set-up for combined electromechanical tests. (up) test fixture consisted of a polymer container, a spherical joint and alumina disks; (down) a part of the total experimental system with Instron machine, electrometer and four strain amplifiers.

Chapter 3 Experiments under Pure Electric Field Loading Conditions

This chapter summarizes the experimental results of PIC151 soft PZT ceramic material under pure "quasi-static" electric field loading conditions. The polarisation and strain responses of this material are found to depend on the amplitude, frequency and other features of the applied E field. Additionally, this material also exhibits significant time-dependent effects under constant electric field loading, where both polarisation and strain will develop in a creep-like manner.

3.1 Fundamental polarisation and strain behavior

1. *Polarisation and strain vs. electric field hysteresis loops*

The polarisation, longitudinal and transverse strain hysteresis loops are shown from Fig. 3.1.1 (a) to Fig. 3.1.1 (c), respectively, where a triangle waveform cyclic electric field was applied to an initially unpoled specimen, with the amplitude of +/- 2 kV/mm and a loading rate of 0,08 kV/mm per second (corresponding to 0.01 Hz). A total of ten cycles of the E field was applied to the specimen. For the reason of better illustration, only curves of the first, second and tenth loading cycles are plotted.

As shown in Fig. 3.1.1, during the quasi-static electric field cycling, typical polarisation and butterfly-like strain hystersis curves are observed. Generally speaking, two types of effects will provide contributions to the P-E and S-E hysteresis loops of a ferroelectric ceramic material: one is the normal linear dielectric response corresponding to polarisation and linear inverse piezoelectric effect related to strains, respectively; the other effect is due to the ferroelectric domain switching process, which will give rise to the hysteresis and non-linearity of the curves. Simple but instructive descriptions of the polarisation/strain hysteresis loops in terms of ferroelectric domain switching process have been given in Chapter 1 (section 1.4).

By definition, the values of polarisation and strain at zero field are called remnant polarisation (P_r) and remnant strain (S_r), respectively. The E field necessary to bring the polarisation to zero is called coercive field (E_c), which corresponds to the intersection of the P-E hysteresis loop with the field axis. It should be mentioned that the remnant polarisation/strains and coercive field are not absolute values for a certain material, they are a function of the external conditions, e.g. environment temperature, superimposed stress states, and the features of the E field loading history, like the amplitude, frequency, and so on [Damjanovic, 1998].

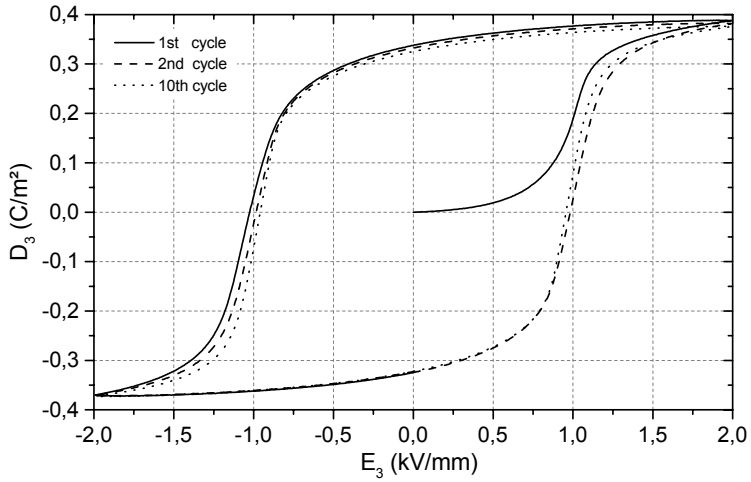

(a)

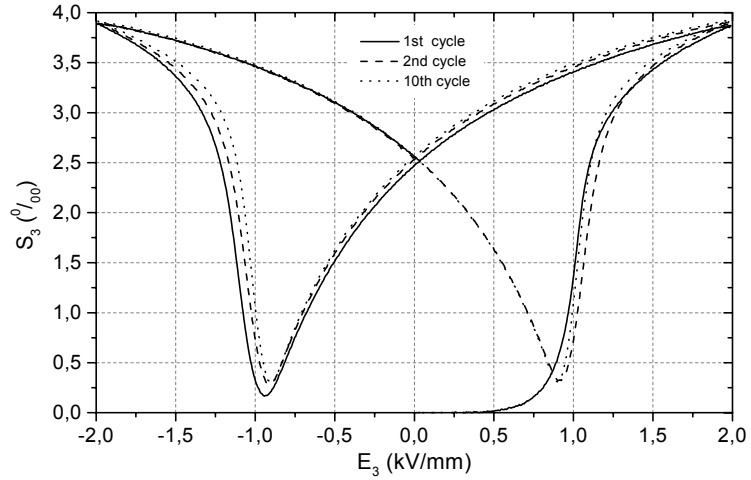

(b)

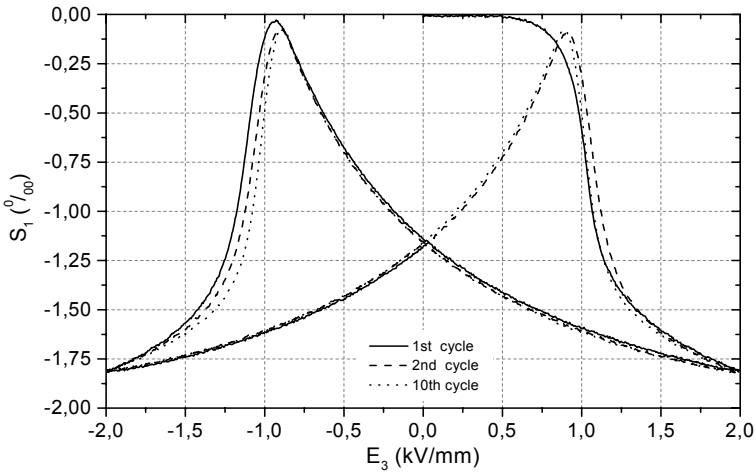

(c)

Figure 3.1.1. Responses of PIC151 soft PZT ceramic material as a function of AC electric field, with the amplitude of +/- 2 kV/mm and a loading rate of 0.08 kV/mm per second; (a) D_3-E_3, (b) S_3-E_3, and (c) S_1-E_3. Curves of the 1st, 2nd and 10th loading cycles are illustrated.

In case of the experiment shown in Fig. 3.1.1, the polarisation and strain hysteresis loops are found to become stable after several loading cycles. The variations of positive/negative direction remnant polarisations and coercive fields as a function of the loading cycle numbers are plotted in Fig. 3.1.2 and Fig. 3.1.3, respectively (for the negative remnant polarisation and coercive field, the absolute values are used).

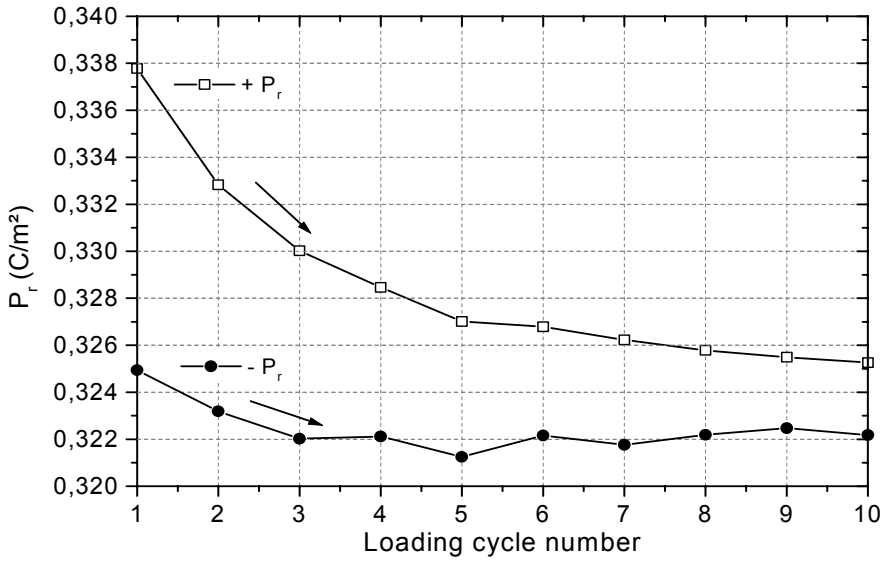

Figure 3.1.2. Positive direction remnant polarisation ($+P_r$) and negative direction remnant polarisation ($-P_r$) in response to electric field loading cycle numbers.

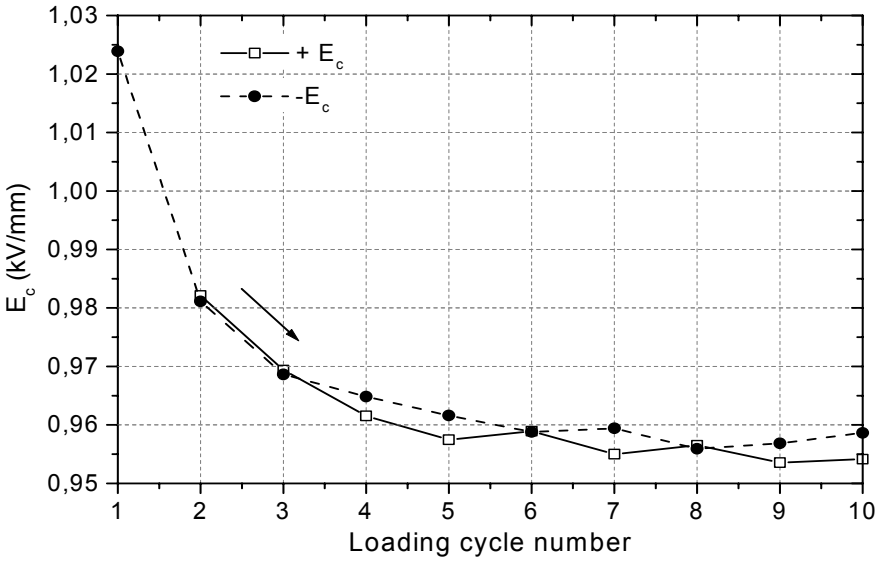

Figure 3.1.3. Positive direction coercive field ($+E_c$) and negative direction coercive field ($-E_c$) in response to electric field loading cycle numbers.

It can be seen that the absolute values of remnant polarisation and coercive field initially decrease with increasing cycle number, and eventually become relatively stable after about six loading cycles. One of the notable features which can be detected from the above two figures is that the negative direction coercive field - E_c and the positive direction remnant polarisation + P_r decrease more significantly than +E_c and – P_r, respectively. For example, the + P_r induced in the first E field loading cycle is about 0.338 C/m², and it decreases to 0.325 C/m² at the tenth loading cycle, whereas, the – P_r at the first cycle is about – 0.325 C/m², and its new value at the tenth cycle is – 0.322 C/m². The negative direction coercive field – E_c in the first cycle is about – 1.024 kV/mm, and it decreases to – 0.959 kV/mm at the tenth cycle.

2. *Strains vs. polarisation (S-P) curves*

In addition to the usually used P-E and S-E relationships, investigation of the strain *vs.* polarisation (S-P) curves was also supposed to be an effective approach to a better understanding of the polarisation reversal mechanisms in ferroelectric materials. In case of relaxor ferroelectric materials, e.g. $Pb(Mg_{1/3}Nb_{2/3})O_3$, a plot of strain against polarisation would form a completely anhysteretic parabolic curve, which indicates that these materials mainly exhibit electrostrictive behavior. Therefore, the induced strain and electric displacement are related by a quadratic relation [Kuwata, 1980]. Investigations of $(Pb,La)(Zr,Ti)O_3$ ferroelectric ceramics (PLZT) indicated that, no matter the material being designed in the tetragonal phase or in the rhombohedral phase, the plots of the S-P curves always exhibited a significant hysteresis [Krueger, 1976; Gerthsen and Krueger, 1976; Schmidt, 1981]. Through systematically experimental investigations and theoretical calculations, these authors confirmed that polarisation reversal in these materials was primarily determined by non-180° domain switching processes (71° and 109° for rhombohedral phase and 90° for tetragonal phase), and the large hysteresis of S-P curves could also be attributed to the predominant non-180° domain switching. Pan et al. observed that the S-P curves became increasingly quadratic as the lanthanum content increased in the PLZT ceramics. They believed that, as the lanthanum content increased, the induced strain of the materials near the morphotropic phase boundary became more electrostrictive in nature [Pan et al., 1988].

Based on the polarisation and strain measurements, the longitudinal and transverse strains *vs.* polarisation curves are plotted in Fig. 3.1.4. We can see that both the S_3-D_3 and S_1-D_3 curves display significant hysteresis. To thoroughly understand this behavior, the polarisation and

strains versus E field curves are plotted in one diagram in Fig. 3.1.5 (left) for the purpose of easier comparison, and the related domain reorientation processes are schematically sketched in Fig. 3.1.5 (right). Letters marked on the curves from *A* to *G* in Fig. 3.1.4 and Fig. 3.1.5 represent different domain states during one electric field loading cycle.

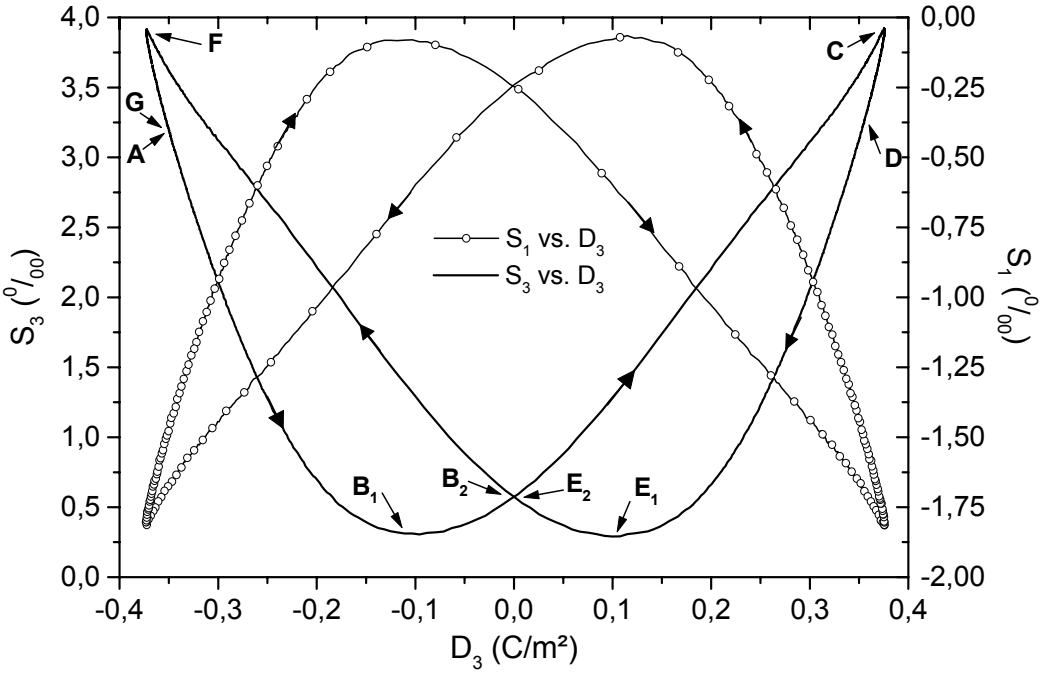

Figure 3.1.4. Longitudinal strain (S_3) and transverse strain (S_1) in response to polarisation (D_3) in the tenth electric field loading cycle.

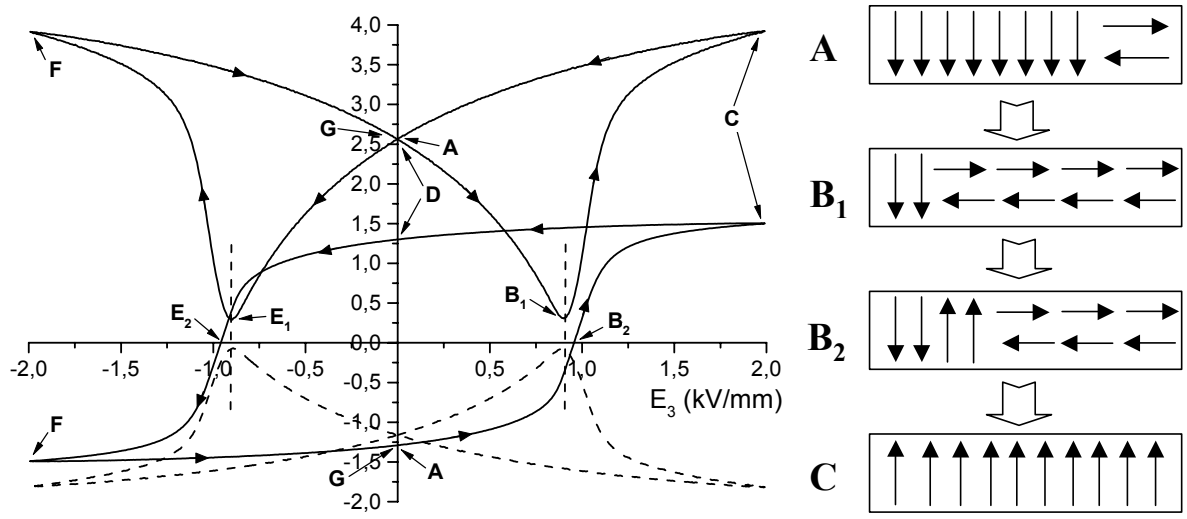

Figure 3.1.5. A tentative explanation of the domain switching processes in one electric field loading cycle. (left) D_3-E_3, S_3-E_3 and S_1-E_3 curves plotted in one diagram, where the polarisation value was timed four for better illustration; (right) domain switching processes. Letters from *A* to *G* represent different domain states in one loading cycle.

The experimental phenomena will be interpreted in terms of two successive 90° domain switching processes. In the works of Chaplya and Carman, a similar approach was used to explain their experimental results of PZT ceramics under combined electromechanical loading conditions [Chaplya and Carman, 2001, 2002]. Investigations by *in situ* X-ray diffraction (XRD) method also confirmed that the polarisation reversal in tetragonal phase PZT piezoelectric ceramics was predominated almost exclusively by 90° domain reorientation processes [Tsurumi et al., 1997].

Starting from point *A* in the P-E and S-E hysteresis loops, most of the domains have been aligned by previous E field loading with the negative direction. The material possesses remnant polarisation and strains, with the values of P_r = - 0.322 C/m², $S_{3(r)}$ = 2.565 $^0/_{00}$ and $S_{1(r)}$ = - 1.159 $^0/_{00}$, respectively. While, as pointed out by Arlt et al., after removal of the E field, a small portion of the domains would relax by 90° switching process and gradually change their spontaneous polarisation directions to the initial states before poling [Arlt et al., 1987]. The corresponding domain configuration is sketched as state *A* in the right panel of Fig. 3.1.5.

The remnant polarisation and strains are quickly removed with the application of a positive electric field, and most of the domains inside the material experience the first time 90° reorientation during this E field depolarisation process. At point B_1, the first 90° switching process is nearly completed. Consequently, we can see the strains achieve their minimum absolute values. Whereas, as shown in Fig. 3.1.5 (right), there are still some domains remaining their orientations parallel to the previous poling direction at state B_1; therefore, some negative residual polarisation can still be observed and the minimum strain values are not zero. With further electric field increment, prior to the reorientation process of those unswitched domains, some domains with orientation perpendicular to the E field loading will begin their second time 90° switching process. At point B_2, the amounts of domains with opposite spontaneous polarisation direction are equal. As a result, now the net polarisation is zero, however, the strains have already been increased to higher values. The electric field at point B_2 is corresponding to the usually called coercive field. Since the polarisation and strains do not achieve their minimum values simultaneously, the resultant S-P curves will exhibit significant hysteresis. The second time 90° domain switching process will be completed with further increasing positive electric field, at point *C*, nearly all the domains are aligned parallel to the poling direction, the variations of polarisation and strains become saturated. For these unswitched domains shown at states B_1 and B_2 (domains which remain

their orientations parallel to the previous negative poling direction), they will experience 180° or two successive 90° switching process to align their spontaneous polarisation direction parallel to the positive E field, but have no significant influence on the tendency of the S-P hysteresis curves. Domain switching process from *C* to *G* is nearly as same as it from *A* to *C*, only the direction is opposite.

3. *Volumetric strain vs. electric field curves*

The change of specimen's volume during a full electric field loading cycle was also investigated in this experiment. Since the measurement is carried out under uni-axial loading conditions, the transverse strains S_1 and S_2 are equivalent. Therefore, from the trace of strain tensor, the relative change of the material's volume (defined as *volumetric strain* – S_{volume}) can be calculated as

$$S_{volume} = S_3 + 2 \times S_1 \tag{3.1.1}$$

For an initially unpoled specimen prior to external load, since $S_3 = 0$ and $S_1 = 0$, Equation 3.1.1 yields $S_{volume} = 0$.

Based on the longitudinal and transverse strains measurement results, the corresponding volumetric strain as a function of electric field is plotted in Fig. 3.1.6, in which interesting butterfly-like curves are observed.

As discussed earlier, according to the conventional thought for strain response, there are mainly two kinds of effects induced by the electric field loading inside a ferroelectric ceramic material. One is the ferroelectric domain switching processes, which could be both 180° and non-180° reorientation. Experimental investigation by Lynch indicated that, there was no volume change associated with the pure domain switching processes [Lynch, 1996]. The other effect induced by E field is the inverse piezoelectric effect, by which the lattice could be elongated or contracted along the spontaneous polarisation axis (e.g., *c* axis for tetragonal phase). In case of the experiments performed in this chapter, the electric field loading was uni-axial. As a result, the inverse piezoelectric effect can be expressed as

$$\begin{aligned} S_3 &= d_{33} \times E_3 \\ S_1 &= d_{31} \times E_3 \end{aligned} \tag{3.1.2}$$

Then Equation 3.1.1 appears in the form

$$S_{volume} = (d_{33} + 2d_{31})E_3 \tag{3.1.3}$$

Due to the inverse piezoeffect, linear response of the volumetric strain can be induced by the electric field loading at both microscopic and macroscopic scales. From Equation 3.1.3, we

can see that the magnitude of volumetric strain should be proportional to the applied E field with the slope of $(d_{33} + 2d_{31})$. After removal of the E field, the induced linear volumetric strain will be reduced to zero.

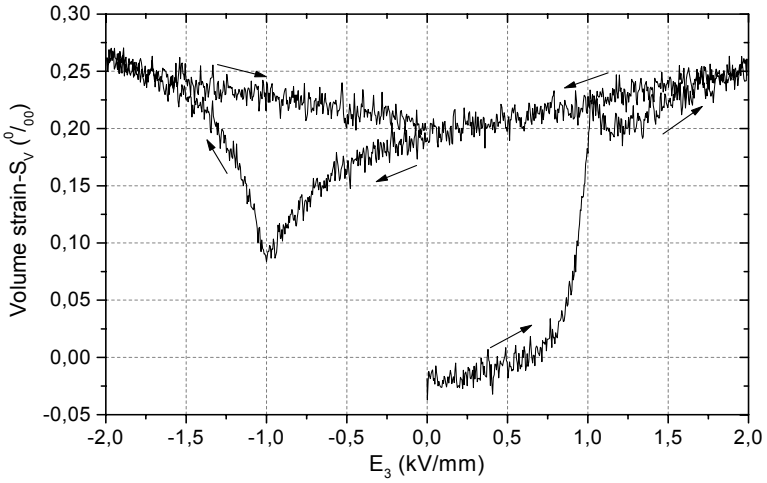

(a)

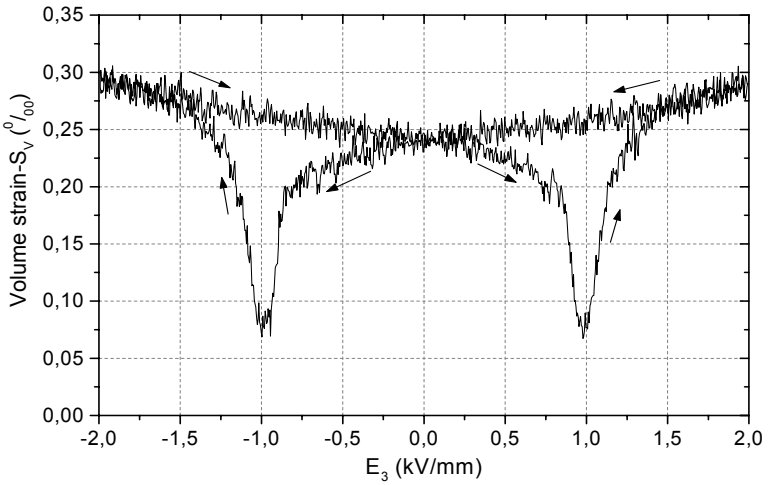

(b)

Figure 3.1.6. Volumetric strain as a function of electric field; (a) First loading cycle, and (b) Tenth loading cycle.

The apparent remnant volumetric strain and the hysteretic butterfly shape curves illustrated in Fig. 3.1.6 can not be solely explained by the combination of pure switching process and inverse piezoeffect. Electric field induced phase transition, which is seldom mentioned for the discussion of non-linear phenomena of ferroelectric materials, might be a reasonable mechanism responsible for the observed volumetric strain behavior.

As introduced in Chapter 1(see section 1.3), most PZT materials of technological importance have compositions near the morphotropic phase boundary (MPB). PZT ceramics usually

exhibit their maximum dielectric permittivity and electromechanical coupling coefficient close to this phase boundary. Although the MPB is represented by a nearly vertical line in the phase diagram (see Fig. 1.3.4), it is commonly observed that the tetragonal and rhombohedral phases are actually coexisting in a finite range of compositions around this phase boundary in each ceramic grain [see Soares et al., 2000, and papers cited there]. If the chemical formulation of PZT ceramics is given by $Pb(Zr_{1-x}Ti_x)O_3$, the MPB at room temperature is located at $x = 0.47$; and the two phases coexistence region is limited in the range of $0.451 \leq x \leq 0.488$. Out of this coexistence interval, the material will only possess a pure tetragonal or a pure rhombohedral phase. X-ray diffraction analysis indicates that, within the phase coexistence region, the unit cell volume of the tetragonal phase is larger than that of the rhombohedral phase [Soares et al., 2000].

Theoretical calculations according to the Devonshire phenomenological theory indicated that a phase transition (also called "shift of MPB" by the author) could be induced by uni-axial external electric field or mechanical stress load. The electric field can cause transition from the rhombohedral phase to the tetragonal phase. This phase transition direction is reversed by compressive stress load, whereas a tensile stress has the same effect as E field [Stotz, 1987].

Recently, Fan and Kim experimentally investigated the electromechanical properties of polycrystalline $Pb(Zn_{1/3}Nb_{2/3})O_3$-$Pb(Zr_{0.47}Ti_{0.53})O_3$ materials. By adjusting the chemical composition, the materials could possess a pure rhombohedral phase, a pure tetragonal phase, or be located near the MPB with two ferroelecctric phases coexisting. An X-ray diffraction method was used to evaluate the changes of microstructure before and after the electric field poling process. Their work confirmed that, for the material with composition near the MPB, a relative small electric field (maximum 2 kV/mm in their experiment) would induce phase transition from the rhombohedral symmetry to the tetragonal symmetry, with a polarisation rotation from the diagonal [111] direction of the rhombohedral phase changed to the *c*-axis [001] of the tetragonal phase. In case of materials with pure rhombohedral or tetragonal phases, the phase transition phenomena were not observed [Fan and Kim, 2002].

The chemical composition of PIC151 soft PZT is formulated in the vicinity of the morphotropic phase boundary in tetragonal range [Nuffer et al., 2000]. Therefore, two ferroelectric rhombohedral and tetragonal phases should be coexisting in the material. As pointed out by Soares et al., if the material composition is formulated in the tetragonal side near the MPB, the rhombohedral phase is metastable in relation to the tetragonal phase [Soares et al., 2000].

According to the above discussion, a phase transition can be induced in PIC151 soft PZT by an external load. As seen in Fig. 3.1.6 (a), prior to the electric field load, the volumetric strain value of an initially unpoled specimen is about zero. With an E field application, positive volumetric strain is induced and achieves a significant increment near the coercive field. When the E field is higher than E_c, most of the domains have been oriented parallel to the poling direction, further change of the specimen's volume is deemed to be determined by the inverse piezoeffect. For example, the unit cells of the tetragonal phase will be elongated parallel to the *c* axis and contracted along the *a* axis. Consequently, we can see the volumetric strain traces a linear curve to increase. During the unloading process (from + 2 kV/mm to 0), the volumetric strain due to inverse piezoefffect gradually decreases along a nearly straight line. However, after removal of the E field, positive remnant volumetric strain is apparently observed. The significantly permanent change of the specimen's volume should be due to phase transition contribution, which a part of the rhombohedral phase is transformed into the tetragonal phase by electric field loading.

At the beginning of a negative direction electric field application, inverse piezoeffect is still the main contribution, which will cause contraction along the *c* axis and expansion along the *a* axis of unit cells with tetragonal phase. Therefore, the volumetric strain is observed to decrease linearly. As the E field approaching $-E_c$, from the P-E curve (see Fig. 3.1.1), we can see that the E field now works analogously like a compressive stress to cause depolarisation process. As a result, part of the previously transformed rhombohedral phase will be transited back to their original states (Theoretical calculation from Stotz indicated that a uni-axial compressive stress would induce phase transition from the tetragonal phase to the rhombohedral phase [Stotz, 1987]). Therefore, in Fig. 3.1.6 (a), we can see that, near $-E_c$, the volumetric strain curve deviates from the straight line and decreases quickly with an approach to zero. When the E field is higher than the coercive field, the rhombohedral to tetragonal phase transition occurs again, and in the following, the volumetric strain curve will repeat the same behavior presented above. After several loading cycles, as seen in Fig. 3.1.6 (b), a stable butterfly shape volumetric strain *vs*. E field curve is obtained.

So far, contributions of phase transition together with the inverse piezoeffect are used to explain the experimentally observed volumetric strain behavior under uni-axial cyclic electric field loading condition. In Fig. 3.1.6, we can see that most of the irreversible remnant volumetric strain is induced as the E field load approaching the coercive field, at where the

material also possesses most pronounced domain switching process. The interrelationship between domain switching and phase transition processes is still not clear.

The charge constants d_{33} and d_{31} are given by the company as 450×10^{-12} mV^{-1} and - 210×10^{-12} mV^{-1}, respectively. Therefore, Equation 3.1.3 appears in the form

$$S_{volume}/E_3 = 30\times10^{-12} mV^{-1} \tag{3.1.4}$$

The volumetric strain induced by pure inverse piezoeffect is proportional to the electric field with the constant of proportionality of 30×10^{-12} mV^{-1}.

From Fig. 3.1.6 (b), slope of the linear part of the experimental curve during unloading period is measured as 25×10^{-12} mV^{-1}, which agrees well with the calculated value. This result gives us further evidence that the linear part of the volumetric strain *vs*. E field curves can be attributed to the inverse piezoeffect.

According to the microstructure analysis results given by Soares et al. [Soares et al., 2000], for PZT ceramic material with the chemical composition near the morphotropic phase boundary (MPB), the average unit cell volume is about 67.8833 $Å^3$ for the tetragonal phase and 67.5667 $Å^3$ for the rhombohedral phase, respectively. The phase fraction in PIC151 soft PZT is not very clear. Since its chemical composition is located in the tetragonal side near the MPB, we might assume there are 70% tetragonal phase and 30% rhombohedral phase coexisting inside the material. Based on these parameters, the amount of phase transition is calculated. Right after the tenth loading cycle, the remnant volumetric strain is about $0.24^0/_{00}$. This is corresponding to about 5% transition from the rhombohedral phase to the tetragonal phase. This acceptable value confirms the explanation of permanent remnant volumetric strain by phase transition mechanism is reasonable [private discussion with Prof. M. Hoffmann, IKM, Uni. Karlsruhe].

3.2 Loading rate dependence of polarisation and strain

To provide more insight into the electric field induced non-linear behavior, systematic polarisation and strain measurements have been performed on PIC151 soft PZT material with various loading rates (frequencies). Triangle waveform electric fields with different amplitudes were used in two sets of experiments, respectively. In the first set of tests, the E field was limited in the range of +/- 1 kV/mm, which is approaching the material's coercive field. The second set of tests was carried out with an amplitude of +/- 2 kV/mm, which is about two times than E_c. For each set of tests, the electric field loading rate was limited in "quasi-static" regime, with different values of 0.02, 0.08 and 0.8 kV/mm per second, respectively. Fig. 3.2.1 and Fig. 3.2.2 show the polarisation and strains hysteresis curves of these two sets of experiments, respectively.

As seen in Fig. 3.2.1, in case of an electric field applied with amplitude near the coercive field, a strong loading rate dependence of the polarisation and strains responses is observed. Upon increasing the loading rate, the induced residual* polarisation (P^{res}) and strains (S^{res}_3 and S^{res}_1 for longitudinal and transverse strains, respectively) at E = 0 significantly decrease. Experimental data corresponding to the tenth loading cycle are summarized in Table 3.2.1 for comparison. We can see that, in case of the loading rate of 0.02 kV/mm per second, the residual polarisation and strains are about two times than the values induced at the loading rate of 0.8 kV/mm per second.

Table 3.2.1. Residual polarisation, longitudinal and transverse strains in response to different loading rates; E field amplitude is +/- 1kV/mm, data are corresponding to the 10th cycle.

E field loading rate (kV/mm per second)	+ P^{res} (C/m³)	- P^{res} (C/m³)	S^{res}_3 ($^0/_{00}$)	S^{res}_1 ($^0/_{00}$)
0.8	0.098	- 0.091	0.727	- 0.290
0.08	0.171	- 0.154	1.369	- 0.552
0.02	0.211	- 0.168	1.569	- 0.643

* As seen in Fig. 3.2.1, in case of the experiments performed with the maximum electric field amplitude of 1 kV/mm, the P-E and S-E hysteresis loops are not saturated. Therefore, the induced polarisation and strain values after removal of the E field loading is called *"residual"* to distinguish them from the real *remnant* values induced at saturated conditions.

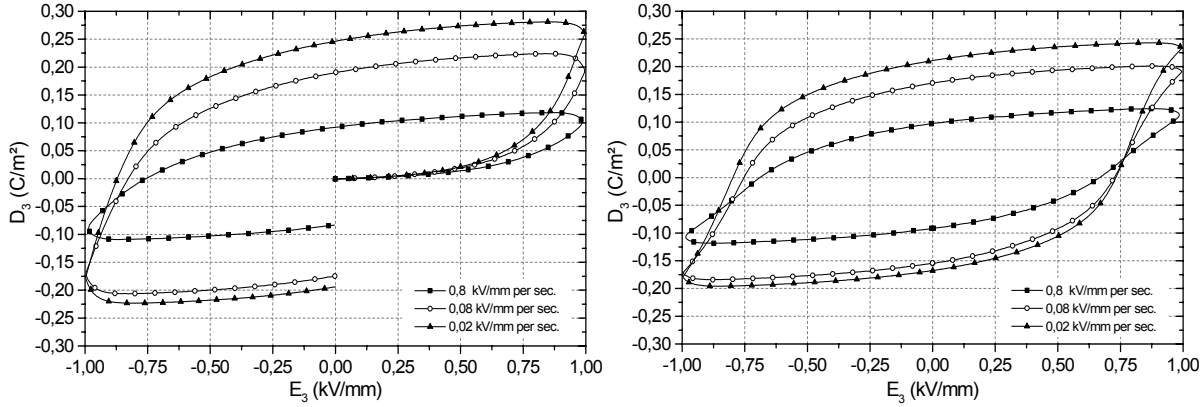

(a) Polarisation (D_3) *vs*. electric Field

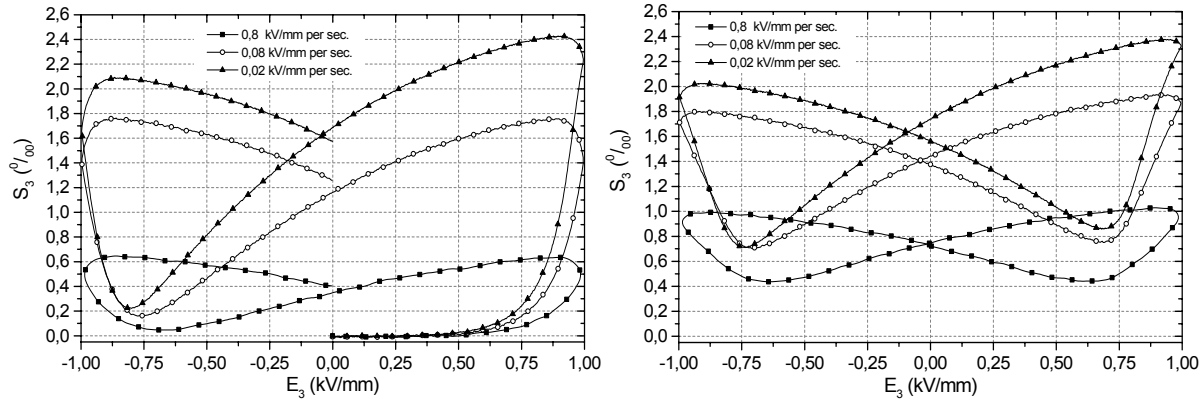

(b) Longitudinal strain (S_3) *vs.* electric field

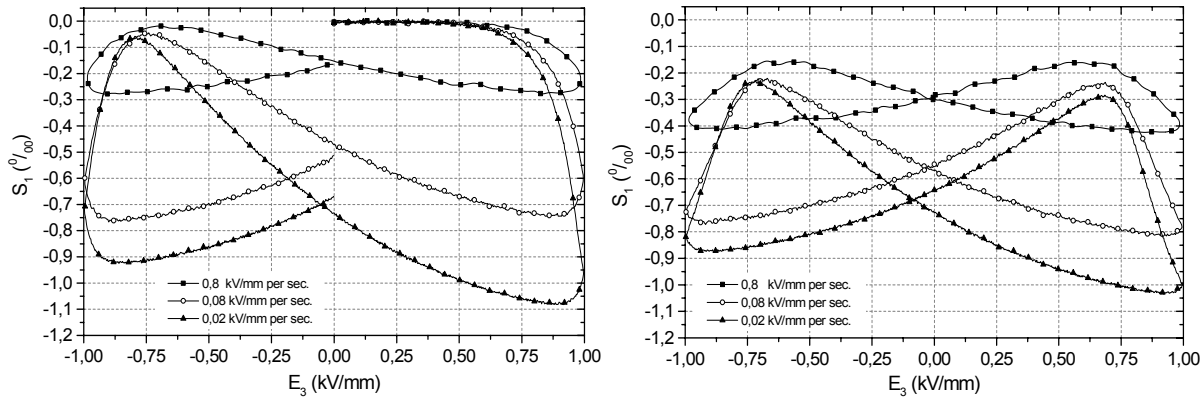

(c) Transverse strain (S_1) *vs*. electric field

Figure 3.2.1. Polarisation, longitudinal and transverse strains in response to electric field loading. The E field range was limited between +/- 1 kV/mm, with different loading rates of 0.8, 0.08 and 0.02 kV/mm per second, respectively. Left panel is corresponding to the responses of the first loading cycle; and right panel is corresponding to the results of the tenth loading cycle.

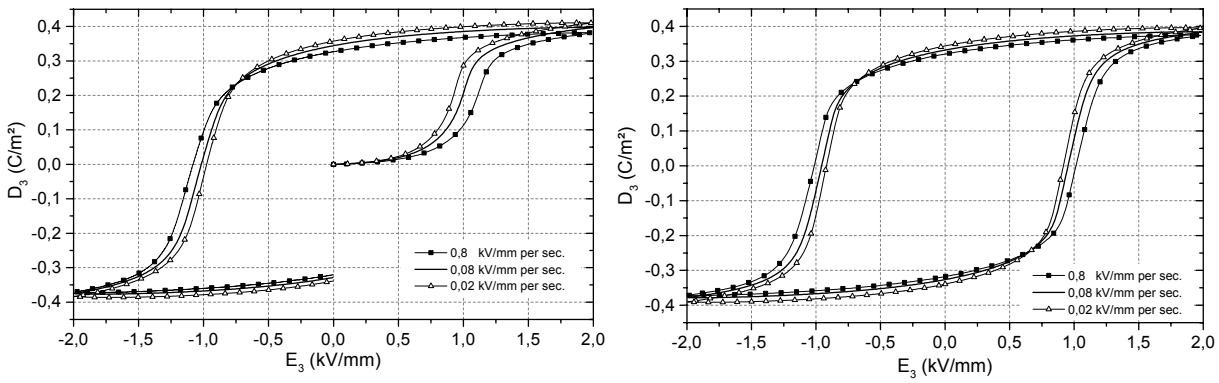

(a) Polarisation (D_3) *vs*. electric field

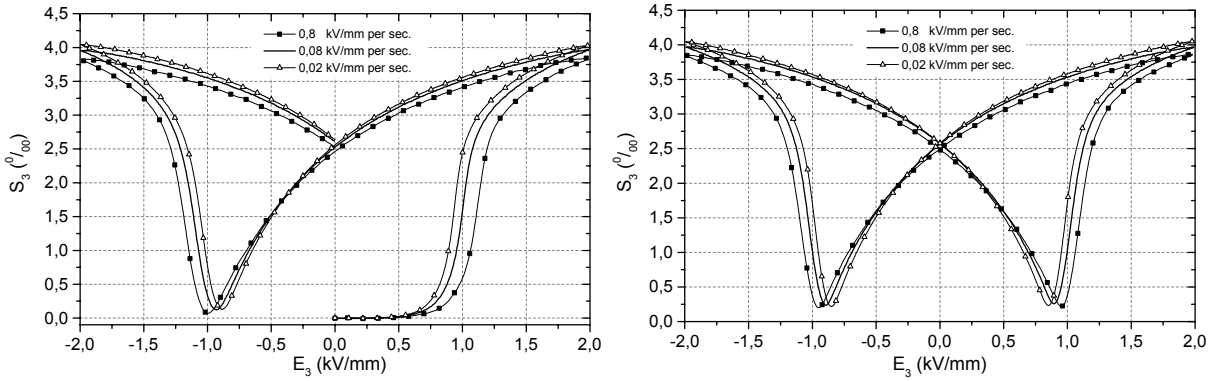

(b) Longitudinal strain (S_3) *vs*. electric field

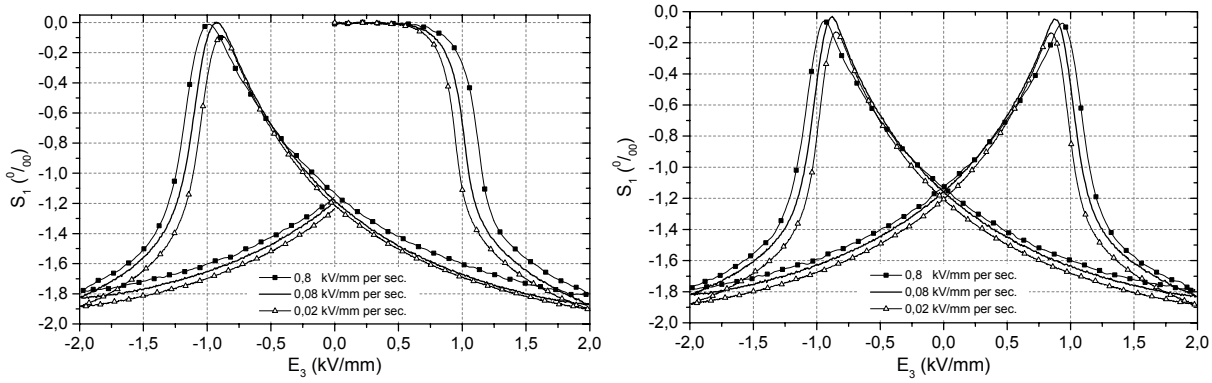

(c) Transverse strain (S_1) *vs*. electric field

Figure 3.2.2. Polarisation, longitudinal and transverse strains *vs*. E field hysteresis loops. The E field amplitude is +/- 2 kV/mm, with different loading rates of 0.8, 0.08 and 0.02 kV/mm per second, respectively. Left panel is corresponding to the first E field loading cycle, and right panel is related to the sixth cycle.

For the second set of tests with an electric field amplitude of +/- 2 kV/mm, typical polarisation and strains *vs*. E field hysteresis curves are observed at various loading rates (see Fig. 3.2.2). The remnant polarisation and strains also exhibit a decrease with increasing loading rate, however, the values do not show such a pronounced difference as seen in the first set of tests. In addition, from the D_3-E_3 curves in Fig. 3.2.2, we can find that the coercive field E_c is loading rate dependent too, decreasing with decreasing loading rate. Experimental data corresponding to the sixth loading cycle of the second set of tests are summarized in Table 3.2.2 for comparison. Meanwhile, remnant polarisation and strain values measured after 10 minutes removal of the E field loading are also given in this Table.

Table 3.2.2. Experimental data of electric field loading tests with different loading rates. E field amplitude is +/- 2 kV/mm. Data are corresponding to the 6th loading cycle and after 10 minutes removal of the E field.

Loading rate (kV/(mm s))	$+P_r$ (C/m²)	$-P_r$ (C/m²)	$+E_c$ (kV/mm)	$-E_c$ (kV/mm)	$S_{3(r)}$ ($^0/_{00}$)	$S_{1(r)}$ ($^0/_{00}$)	D_3 after 10 minutes stop (C/m²)	S_3 after 10 minutes stop ($^0/_{00}$)	S_1 after 10 minutes stop ($^0/_{00}$)
0.8	0.321	-0.318	1.010	-1.011	2.502	-1.137	-0.305	2.344	-1.049
0.08	0.332	-0.326	0.949	-0.954	2.569	-1.158	-0.315	2.431	-1.083
0.02	0.344	-0.340	0.916	-0.917	2.574	-1.207	-0.329	2.454	-1.141

The experimental results are consistent with the works of Viehland and Chen. In their experiments, the loading rate (frequency) dependence of P-E and S-E behavior was investigated for $0.7Pb(Mg_{1/3}Nb_{2/3})O_3$-$0.3PbTiO_3$ ferroelectric ceramics. They found that the responses of polarisation and strain displayed a significant frequency dependence for the circumstance of $E \leq E_c$, whereas, in case of $E >> E_c$, the frequency dependent phenomenon was not very pronounced. The coercive field E_c was also found to increase with increasing loading frequency [Chen and Viehland, 2000; Viehland and Chen, 2000].

To study the stability characteristics of piezoelectric ceramics, for the second set of tests, right after removal of the cyclic electric field, the changes of polarisation and strains with time were measured. As seen in Fig. 3.2.3, the general observation is that, after poling, the remnant polarisation and strains decrease with time. The decrease is most pronounced at the very beginning of removing the E field. Thereafter, the changes tend to be saturated with further time increase.

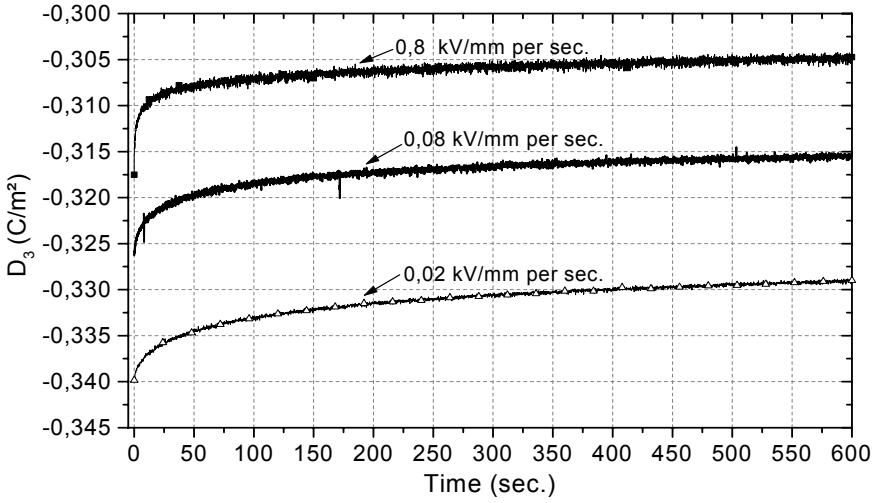

(a) Polarisation

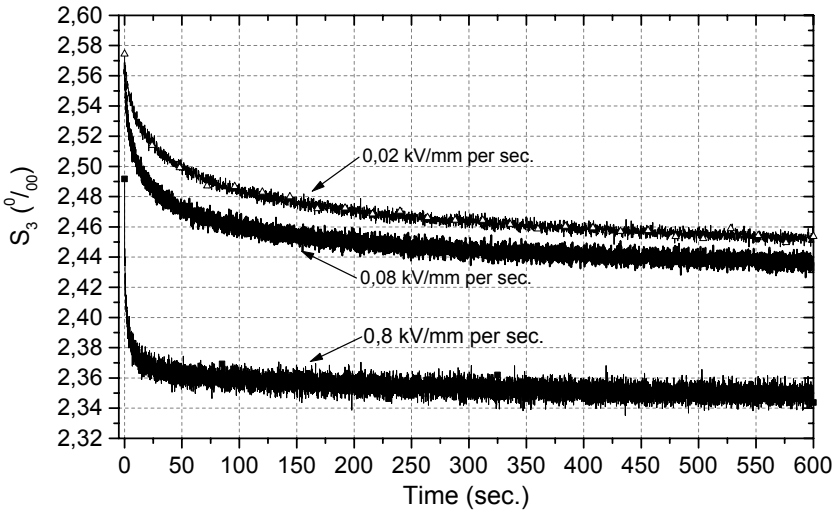

(b) Longitudinal strain

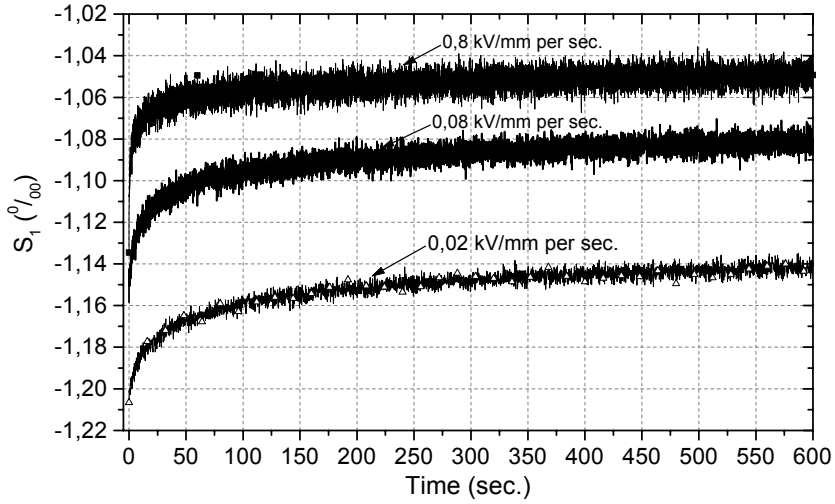

(c) Transverse strain

Figure 3.2.3. After six cycles of electric field loading with different loading rates, changes of remnant polarisation, longitudinal and transverse strains with time.

After major stimulations, e.g. electric field poling processes in this experiment, changes of the material properties with the passing of time are defined as ageing effects [Xu, 1991]. Therefore, the observed gradual decrease of the remnant polarisation and strains phenomenon in Fig. 3.2.3 belongs to the ageing effects of piezoceramics.

To explain the origin of ageing of ferroelectric materials, several different models have been proposed by relating this effect to gradual changing of domain configuration with time. In general, the physical process of ageing observed in this experiment may be described qualitatively as follows: During the cyclic electric field loading, ferroelectric domain switching will be induced. Meanwhile, inside the material, internal stress will build up due to the non-180° domain reorientation processes. After removal of the E field excitation, the internal stress will be gradually released by back switching of some domains to their initial states prior to the external load [Damjanovic, 1998]. This process will reduce the amount of domains parallel to the pre-poling direction, as a result, the remnant polarisation and strains are observed gradually decreasing with time.

Ageing effects are also found to be loading rate dependent. As seen in Fig. 3.2.3, in case of higher pre-loading rate (e.g., 0.8 kV/mm per second), a very steep initial slope and a faster tendency to saturation are observed in the polarisation and strains *vs*. time curves. While, for the circumstance of lower pre-loading rate (e.g., 0.02 kV/mm per second), the variations of polarisation and strains exhibit a more gradually decreasing tendency with the passage of time. According to these observations, it should be true that slower E field loading can orient more domains parallel to the poling direction, and the established domain configurations are relatively more stabilized. Consequently, the remnant polarisation and strains induced by lower rate E field loading are slightly larger than the values induced in case of higher loading rate, and also display slower decreases after removal of the E field.

3.3 Time-dependence of piezoceramic response under constant electric field load

1. *Experimental results*

To investigate the time-dependence of the material response under constant electric field loading conditions, initially unpoled PIC151 soft PZT ceramic specimens were subjected to four full cycles of a ramp-like E field, with the loading rate of 0.08 kV/mm per second (corresponding to a frequency of 0.01 Hz). During both loading and unloading periods, the electric field was interrupted repeatedly by keeping it at a constant level for 300 seconds. The constant E field holding levels were selected as +/-0.50, +/-1.00, +/-1.50 and +/-2.00 kV/mm, respectively. A total of four cycles of polarisation and longitudinal strain *vs*. E field hysteresis curves are shown in Fig. 3.3.1.

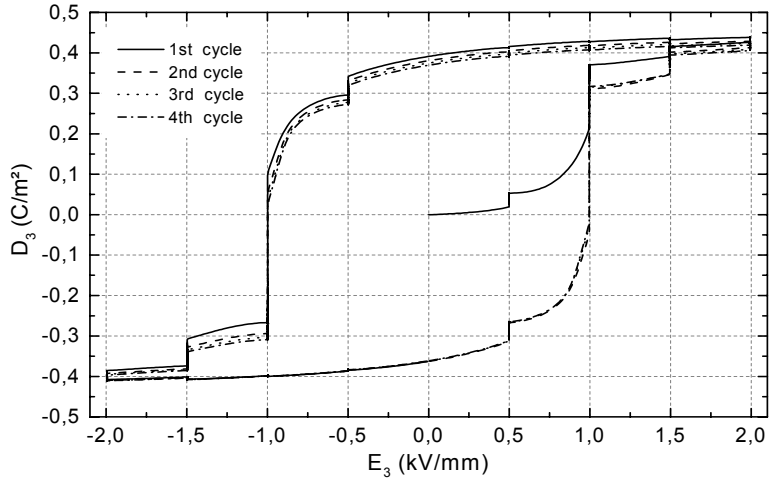

(a)

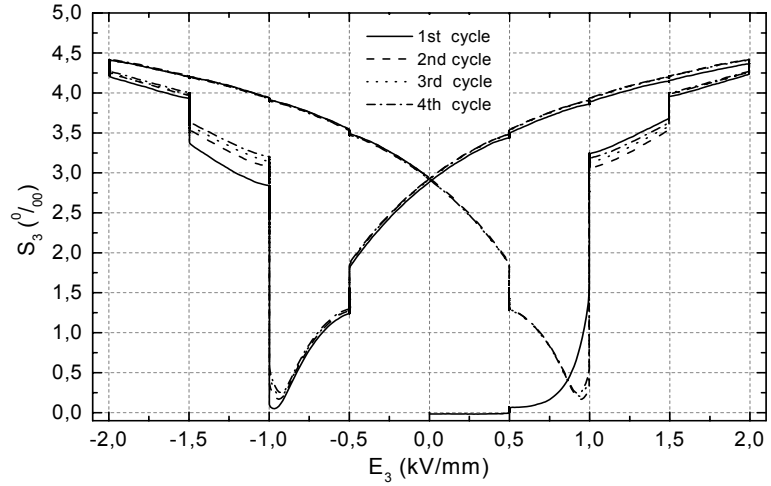

(b)

Figure 3.3.1. A total of four cycles of D_3-E_3 (a) and S_3-E_3 (b) hysteresis loops. During both loading and unloading processes, the E field was hold at constant levels of +/ 0.50, +/- 1.00, +/- 1.50 and +/- 2.00 KV/mm for 300 seconds, respectively.

Clearly, changes of the polarisation and strain during the duration of a constant E field can be observed in Fig. 3.3.1. For the initial ¼ period of the first loading cycle, (electric field increasing from zero to + 2 kV/mm), changes of polarisation and strain at constant E fields of 0.50, 1.00, 1.50 and 2.00 kV/mm are plotted *vs*. hold time in Fig. 3.3.2.

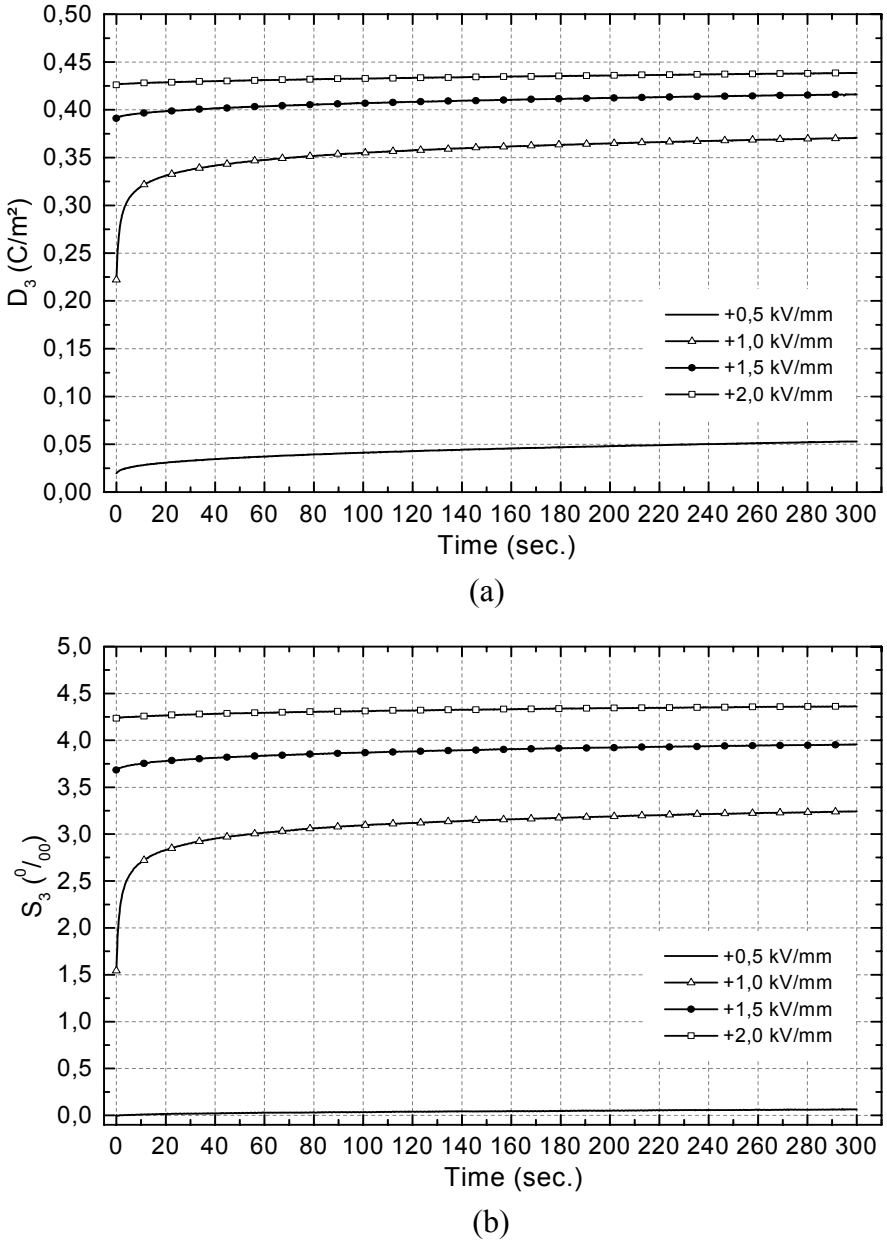

Figure 3.3.2. Changes of polarisation (a) and strain (b) versus electric field hold time. Experimental condition: during the initial E field increasing period (from 0 to + 2kV/mm) of the first loading cycle, the E field was kept constantly at 0.50, 1.00, 1.50 and 2.00 kV/mm for 300 seconds, respectively.

We can see that both polarisation and strain exhibit a creep-like increase under a constant E field loading. With the hold time increment, the changes gradually slow down and tend to be

saturated eventually. The creep-like increasing behavior is most pronounced at 1.00 kV/mm, which is close to the coercive field of PIC151 soft PZT. For example, the initial polarisation and strain at the beginning of hold time are 0.222 C/m² and $1.544^{0}/_{00}$, respectively, and they increase up to 0.371 C/m² and $3.243^{0}/_{00}$, respectively, after five minutes of E field holding.

For the period of electric field unloading from + 2 kV/mm to zero of the first loading cycle, changes of polarisation and strain at constant field levels of 1.50, 1.00 and 0.50 kV/mm are plotted as a function of hold time in Fig. 3.3.3.

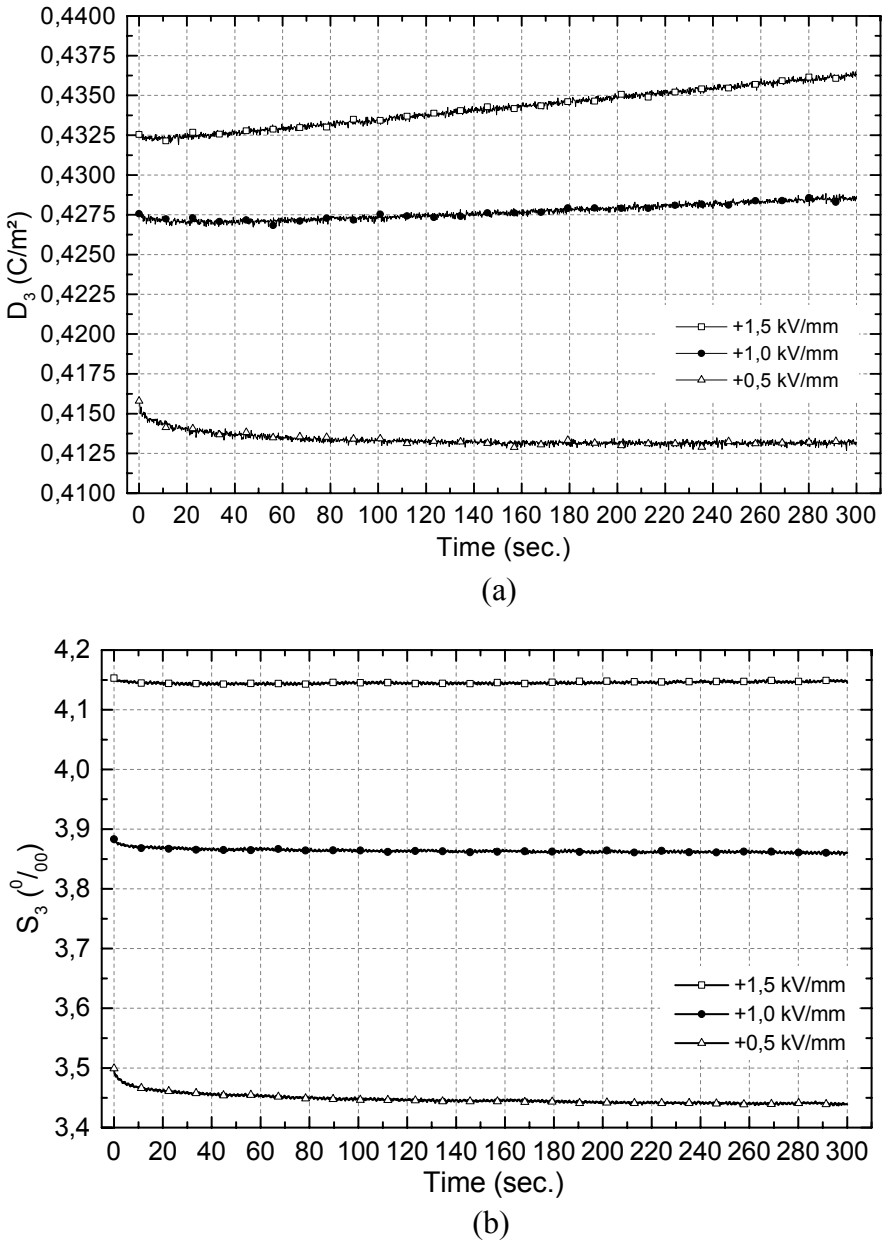

Figure 3.3.3. Changes of polarisation (a) and longitudinal strain (b) *vs.* E field hold time. Experimental condition: during the period of unloading process from 2 kV/mm to zero of the first loading cycle, the E field was kept constantly at 1.50, 1.00 and 0.50 kV/mm for 300 seconds, respectively.

From Fig. 3.3.3, it's found that the responses of polarisation and strain during the unloading process are different. The polarisation exhibits an apparent increase with the hold time increment at 1.50 and 1.00 kV/mm, and the increase is especially significant at 1.50 kV/mm. Whereas, the strain displays only a slight decrease at these two constant E field levels. At 0.50 kV/mm, both polarisation and strain exhibit a decrease during the hold time.

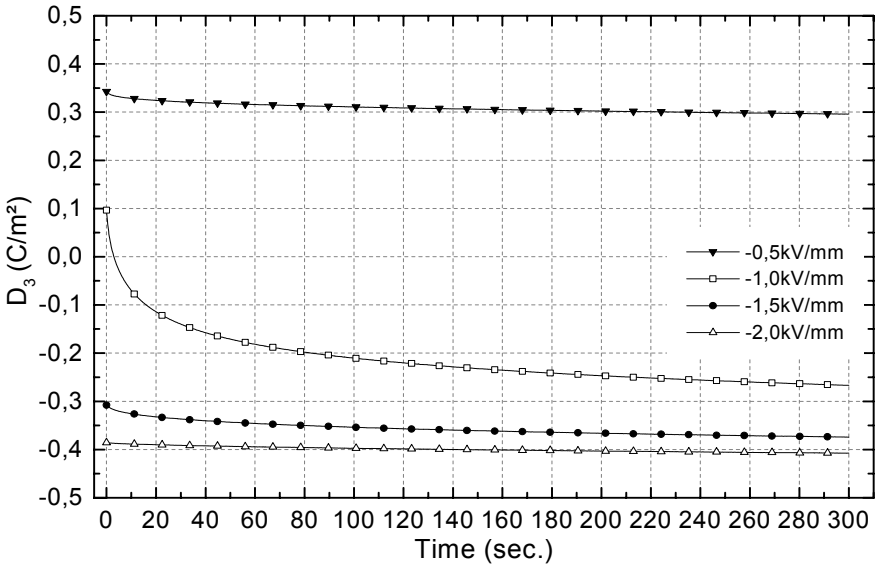

(a)

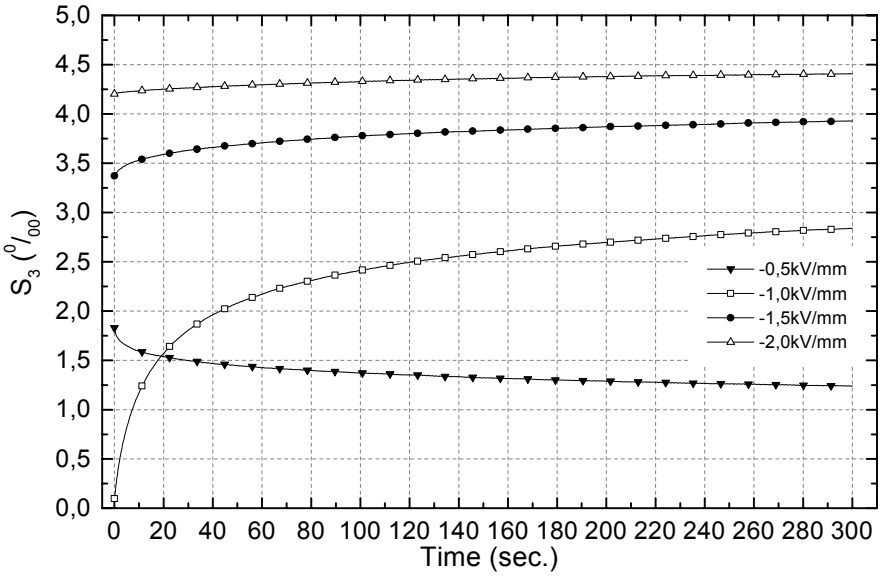

(b)

Figure 3.3.4. Changes of polarisation (a) and longitudinal strain (b) with hold time. Experimental condition: during the negative direction E field loading period (from 0 to – 2kV/mm) of the first cycle, the E field was hold constantly at – 0.50, - 1.00, - 1.50 and – 2.00 kV/mm for 300 seconds, respectively.

Fig. 3.3.4 shows the changes of polarisation and strain versus hold time during the negative E field loading history of the first cycle. Most prominent creep-like responses are observed as holding at – 1.00 kV/mm (close to the negative direction coercive field of this material), where the polarisation traces a line with an initially steep slope to develop from positive towards negative value, and finally tends to be saturated at the end of hold time. The initial longitudinal strain value at – 1.00 kV/mm is approaching zero, with the hold time increment, at first the strain experiences a significant increasing, and afterwards, the changing slows down and becomes saturated eventually. The material now possesses negative polarisation, but still exhibits elongation in the negative poling direction.

2. *Discussion of time-dependent effects*

The experimental results clearly indicate that the response of piezoelectric ceramics exhibits significant time-dependent effects in particular during a constant E field loading. This phenomenon is inconsistent with the conventional thought of ferroelectric materials under "quasi-static" loading conditions.

According to the traditional idea [Lines and Glass, 1977], in an initially unpoled material, no net polarisation exists. Once upon application of a small E field, a nearly linear polarisation change (due to the normal dielectric response) will be induced. The material response is *reversible* and will return to zero after removal of the E field. No residual polarisation and hysteresis are expected until a critical level of the E field is exceeded. This threshold value corresponds to the so-called coercive field (E_c). In case of $E \geq E_c$, polarisation reversal occurs by realignment of domains to the direction of applied field. As a result of this domain reorientation (or switching) process, remanence and hysteresis in the P-E and S-E curves are observed. The nature of domain or unit cell switching is normally regarded as an *instantaneous* process, which occurs in a very moment as soon as the threshold E field (E_c) is reached. Remnant polarisation and strain induced by domain switching correspond to the *irreversible* part of the total response. They will be preserved after unloading and will stay until an opposite E field of some critical strength is reached. In contrast to this, the *reversible* part of the total response corresponds to the linear dielectric behavior and the inverse piezoeffect of a poled piezoceramic material, and their values are proportional to the magnitude of the applied E field and change sign with it. According to this idealising thought, the hysteresis behavior of piezoelectric ceramics would be caused by pure *instantaneous* domain switching processes, and no time-effects play a role.

To thoroughly understand the time-dependent effects, as shown in Fig. 3.3.5, the first cycle P-E and S-E curves of this hold time experiment are compared with the results of another experiment performed with continuous E field loading. To simplify the discussion, we only consider the material response in the duration of E field loading from zero to + 2 kV/mm.

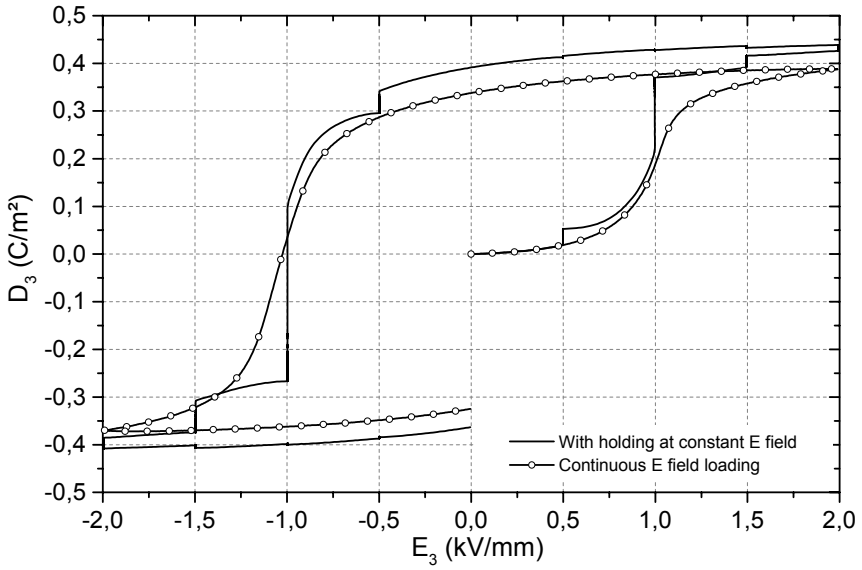

(a)

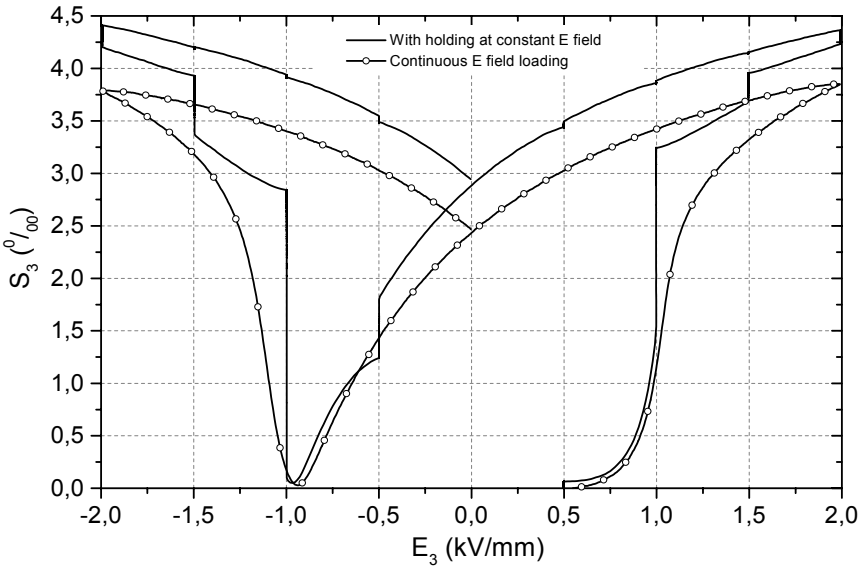

(b)

Figure 3.3.5. Comparison of polarisation (a) and longitudinal strain (b) responses of PIC 151 soft PZT as a function of continuous electric field loading and one full cycle of E field loading with 300 seconds holding at different constant levels. Only curves of the first loading cycle are illustrated.

For both of these two experiments, during the period of E field loading from zero to + 0.50 kV/mm, the polarisation and strain curves trace the same line, respectively, to increase. With E field holding at + 0.50 kV/mm for 300 seconds, even though this field level is much lower than the coercive field ($E_c \approx$ +/- 1 kV/mm for PIC151 soft PZT), we still can observe that more polarisation and strain are induced. This time-dependence under a low E field loading can not be explained by the traditional ferroelectric theory. As discussed earlier, according to the conventional thought, no *irreversible* contribution can be induced by electric field lower than E_c.

The macroscopic time-dependent responses of polarisation and strain can be interpreted by gradually induced more microscopic domain switching during the long hold time of a constant external E field.

As mentioned before, the commercial piezoceramics (e.g., PIC151 soft PZT used in the experiments of this thesis) are very sophisticatedly doped systems. In the sequence of decreasing length scale, a polycrystalline piezoceramic material consists of grains, domains, unit cells and defects. Grains with different crystallographic orientations are separated by grain boundaries, and domains walls separate domains with different spontaneous polarisation directions. Defects comprise vacancies, substituent or interstitial ions, and so on. With an external electric field application, the complicated microstructure will give rise to fluctuation of the microscopic electric field distribution inside the material. Theoretical simulations by the finite element method indicate that the local E field at some regions can be several times higher than the external E field, whereas, at some other regions, the local E field can be much smaller than the external E field or even possesses opposite direction [Fröhlich, 2001].

With application of an external electric field, due to the complicated microstructure, the internal E field distribution inside the material is inhomogeneous. At some regions, the local E field may be higher than the switching threshold, domain reorientation occurs *instantaneously*. While, for the other regions with lower local E field, domain switching process can not be initiated until the coercive field is reached. The local electric field strength can be increased by application of a higher external E field. As shown in Fig. 3.3.5, the polarisation and strain increase rapidly with increasing external E field. This is due to more and more domains being oriented parallel to the loading direction. As the reservior of the irreversible domain switching contribution is exhausted, the changes of polarisation and strain will become saturated. Later polarisation and strain increments induced by further E field

loading are due to the linear dielectric response and inverse piezoeffect contribution, respectively.

In case of holding the external E field at a constant level, the creep-like polarisation and strain behavior indicate that there are gradually induced further domain switching processes during the hold time. Since the external electric field was kept constantly, there must be some other kinds of time-dependent mechanism to change the local E field to induce more domain switching. One possibility of the mechanisms is the transient defect diffusion process activated by external E field load.

As discussed earlier, a real polycrystalline ferroelectric material contains many defects. Besides distributed within the domains, the defects can also be trapped in the domain-wall areas or in the grain boundary regions. For an initially unpoled or a prepoled piezoceramic sample, these defects (also called free electric charge carriers) act as pinning or clamping centers to inhibit the domain switching or domain-wall motion processes [Carl and Härdtl, 1978; Damjanovic, 1998]. The common mechanism of pinning effects of these defects on domain switching is the presence of internal bias fields in aged samples, i.e. in the samples with stabilised domain structure. The internal bias fields act as a kind of additional potential to restrict the domains. To initiate the domain switching process by an external load (E field or mechanical stress), such an internal bias field has to be overcome at first. Microscopic defects induced stabilisation (pinning) of the domain structure has been proposed to explain the macroscopic polarisation fatigue and ageing phenomena of ferroelectric ceramics or thin films under cyclic electric field load [Carl and Härdtl, 1978; Al-Shareef, et al., 1997; Robels and Arlt, 1993].

In case of this hold time experiment, microscopic defects in the specimen can be aligned by the constant external E field load through the migration process of dopant ions or vacancies. By reducing the internal bias fields of these pinning centers, such a process will lead to a redistribution of the internal electric field and an effective minimising of the clamping effects for those unswitched domains. When the coercive field for some unswitched domains is reached, ferroelectric switching will occur and contribute to the macroscopic polarisation and strian increment. The E field activated migration of microscopic defects is a time-dependent diffusion process, related to typical time constants by diffusion coefficients [Lohkämper, et.al., 1990]. With the passage of hold time, more defects will be aligned by the constant external E field load and reduce the pinning effects for more unswitched domains. As a result, the local E field may achieve the coercive field at various locations and give rise to more and

more domain reorientation. On the macroscopic level, creep like polarisation and strain behavior are consequently observed. On the other hand, the alignment of defect dipoles (e.g. oxygen vacancies and acceptor ions) will also contribute to the macroscopic polarisation and strain increment to some extent [Kamlah, 2001].

On account of the nature of electromechanical coupling effects of a piezocermic material, electric field loading will cause an inverse piezoeffect for either switched or unswitched domains and a consequent mechanical stress field existing in microscopic scale. Due to the inhomogeneous internal electric field distribution and the complicated microstructure, the microscopic stress distribution inside the material is also inhomogeneous. Local stress intensification may occur at some regions. When the coercive stress is reached, ferroelastic domain switching will be induced. This process will further change the internal electric field distribution (due to the resultant change of domain configuration and direct piezoeffect) and influence the material macroscopic responses.

So far, the time-dependent effect under constant electric field loading has been interpreted by the mechanism of changing of the local E field strength through the transient diffusion process of defects. At the same time, the nature of electromechanical coupling effects of a piezoceramic material has to be taken into consideration for the explanation of this time-dependent effect.

The time-dependent effect of this material is found to depend on the magnitude of the external electric field load. As seen in Fig. 3.3.5, only slightly more polarisation and strain are further induced during the hold time at + 0.50 kV/mm. This is because, under such a low external electric field load, most of the regions in the material possess a local E field lower than the coercive field. With the passage of time, only a slight amount of domain switching is further induced at some regions with the local E field approaching the coercive field. With further external electric field increase from 0.50 to 1.00 kV/mm, the coercive field will be reached at a lot of regions inside the material. A large amount of domain switching results in a significant polarisation and strain increment. For the continuous loading test, the induced polarisation and strain at + 1.00 kV/mm are about 0.189 C/m² and $1.174^{0}/_{00}$, respectively. While, for the hold time experiment, the polarisation and strain values at the beginning of holding at + 1.00 kV/mm are 0.222 C/m² and $1.544^{0}/_{00}$, respectively. The larger polarisation and strain values are apparently due to the contribution of time-dependent effect at + 0.50 kV/mm.

The most pronounced time-dependent effect is observed at + 1.00 kV/mm, which corresponds to the macroscopic coercive field of this material. During the hold time of 300 seconds, both polarisation and strain increase significantly. At the end of the hold time, the new values are 0.371 C/m² and $3.243^{0}/_{00}$ for polarisation and strain, respectively. To achieve the same values in the continuous loading test, the applied electric field has to be increased up to about + 1.70 kV/mm for polarisation and + 1.45 kV/mm for strain, respectively. The most pronounced time-dependent effect at + 1.00 kV/mm can be interpreted by the following way: under such a high external electric field loading, the local E field of most of the unswitched regions is already quite near the coercive field. During the hold time, transient defect diffusion processes will help these regions to achieve the coercive field. As a consequence of gradually induced further domain switching processes, significant creep-like polarisation and strain increases are observed.

Since most of the domains have been switched during the long hold time at + 1.00 kV/mm, from the end of holding at + 1.00 kV/mm to the beginning of holding at + 1.50 kV/mm, linear dielectric behavior and inverse piezoeffect should be the essential contributions to polarisation and strain responses in this loading period. For the subsequent E field holding at + 1.50 and + 2.00 kV/mm, the time-dependent effect can still be observed but becomes relatively weaker.

Another notable feature can be observed from Fig. 3.3.5 is that, for the experiment with E field holding at different constant levels, the induced maximum and remnant values of polarisation and strain are obviously higher than the values induced in the continuous loading test. Therefore, it should be true that, as high E field acting for a much longer time, the total amount of domains taking part in reorientation in the hold time test is more than the amount in the continuous loading test.

Chapter 4 Experiments under Pure Mechanical Stress Loading Conditions

For the objective of determining the optimum operating conditions of actuators and providing basic property measurements to the theoretical simulations, the focus of this chapter is to present the evaluation of characteristics of piezoelectric ceramics under pure uni-axial compressive stress loading conditions. When a sufficiently large mechanical load is applied, the small signal parameters become insufficient to represent the material behavior. At high stress levels, the stress-strain behavior exhibits significant non-linearity with a distinct irreversible strain present upon unloading. Furthermore, mechanical depolarisation will also be induced for the pre-poled materials. The non-linear responses can be interpreted in terms of ferroelastic domain switching processes, and they are found to be time dependent.

4.1 Compressive stress induced non-linear behavior

4.1.1 Experimental results

The first group of experiments were performed on initially unpoled PIC151 soft PZT ceramic specimens, which were subjected to three subsequent ramp-shape loading-unloading cycles by a compressive stress, with the amplitude of – 400 MPa and a loading rate of 5 MPa per second. The resultant longitudinal and transverse strains in response to the stress curves are given in Fig. 4.1.1 (a) and (b), respectively.

As seen in Fig. 4.1.1, during the first stress application cycle, both longitudinal and transverse strain curves exhibit a significant non-linearity at the initial loading period of the compression load. As the stress magnitude achieves higher values (approximately starting from – 200 MPa in this experiment), the stress-strain behavior becomes linear elastic. Upon unloading from – 400 MPa, a linear elastic response can be observed at first. When the compression load is lower than – 150 MPa, the plots show a slight non-linearity. After removal of the stress, final irreversible remnant strains are induced.

As pointed out by Kamlah and Lynch, the macroscopic non-linearity and the irreversible residual deformation are caused by microscopic ferroelastic domain switching processes [Kamlah, 2001 and Lynch, 1996]. The “virgin” state of material prior to stress loading is isotropic. Domains with different orientations are randomly distributed in the material.

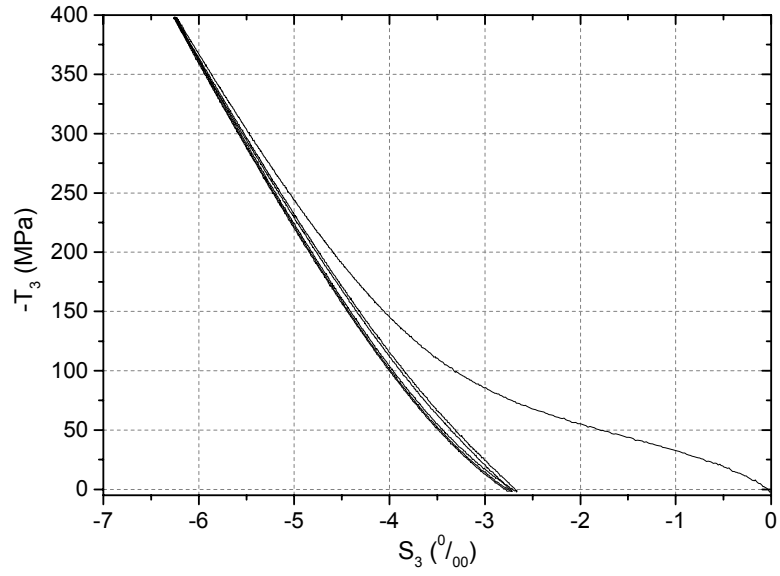

(a)

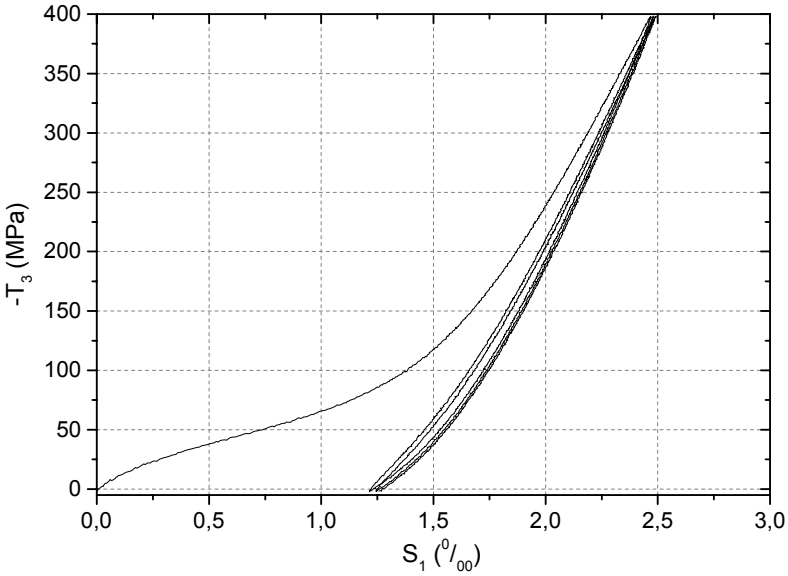

(b)

Figure 4.1.1. Three cycles of longitudinal (a) and transverse (b) strains versus compressive stress curves of initially unpoled PIC 151 soft PZT ceramic material. Stress loading and unloading rate was 5 MPa/sec.

With the application of a sufficiently high compressive stress, domains with orientations relatively parallel to the compression load will be switched as closely as possible to a plane, which is orthogonal to the stress loading. As discussed in Chapter 1 (section 1.4), this is a ferroelastic non-180° domain switching process and will give rise to a rapid increase of the strains. At higher stress levels, the switching process is nearly completed. Therefore, the material reacts more and more stiffly and approximately elastically. After unloading, the switched domain structure is preserved and leads to significantly remnant strains. For further

loading and unloading cycles, the stress-strain loops become quite narrow and only a slight hysteresis can be observed. This is because of the nearly complete exhaustion of the switchable domains after the first loading cycle.

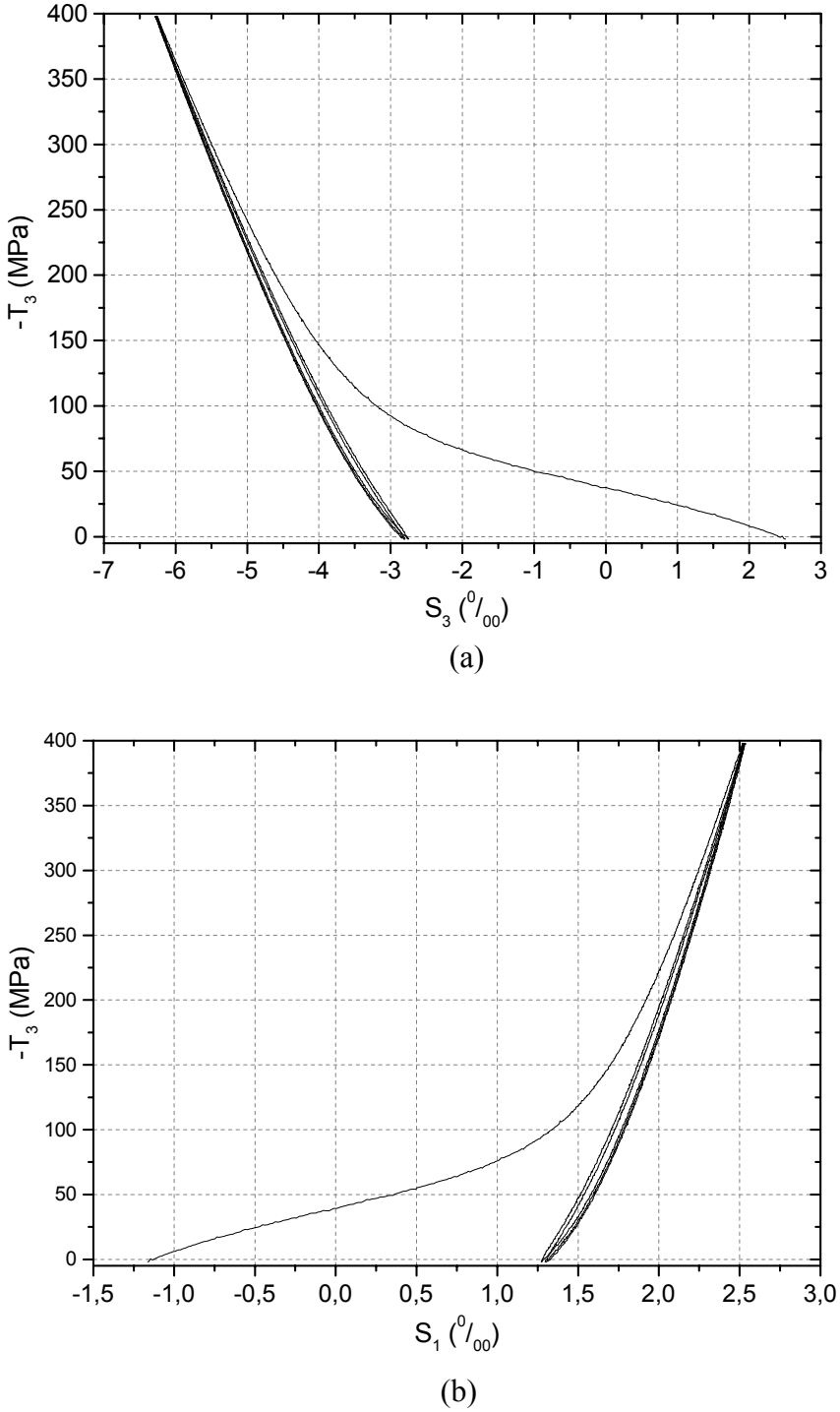

Figure 4.1.2. Three cycles of longitudinal (a) and transverse (b) strains versus compressive stress curves of a pre-poled PIC151 soft PZT ceramic specimen. Stress loading and unloading rate was 5 MPa/sec.

To evaluate the responses of polarised material, an initially unpoled PIC151 soft PZT specimen was first subjected to a total of five cycles of ramp-shaped electric field loading under mechanical load free state, with the amplitude of +/- 2 kV/mm and a loading rate of 0.08 kV/mm per second (0.01 Hz). Changes of strain and polarisation were monitored simultaneously. Right after removal of the E field, a uni-axial compressive stress parallel to the pre-poling direction was applied to the specimen. The stress loading-unloading history is as same as it was used in the experiments for unpoled material. By this procedure, the history of the material (remnant polarisation and strains) is clearly known. Fig. 4.1.2 (a) and (b) show the longitudinal and transverse strains in response to the total of three cycles of compression load, respectively.

Similar to the results of the unpoled material, a non-linear stress-strain response during the stress-increasing period of the first loading cycle is observed for the pre-poled specimen. This agrees well with the experimental results for PZT ceramics given by some other researchers [Cao and Evans, 1993; Schäufele and Härdtl, 1996].

The non-linear behavior of pre-poled material can also be attributed to stress induced ferroelastic domain switching mechanisms. As a consequence of the poling process, all the domains would be aligned as closely as possible parallel to the electric field loading direction; hence the material possesses remnant polarisation and strains. The E field induced remnant longitudinal and transverse strain values are $2.508^{0}/_{00}$ and $-\ 1.165^{0}/_{00}$, respectively. With application of an increasing compressive stress, the microscopic spontaneous polarisation vectors of unit cells will be gradually redistributed randomly within or close to a plane perpendicular to the compression load. In the course of this non-180° domain switching process, the original order of the domains in the previous poling direction is lost, therefore, the electric field induced remnant strains vanish little by little and the compressive stress induced irreversible strains are observed. The ferroelastic domain switching process will be nearly completed at a higher stress level. The stress-strain responses during further increased stress loading and the initial unloading period become approximately linear elastic. When unloading the compression load below about – 150 MPa, similar to the unpoled material, the plots display a slight non-linearity. The remnant longitudinal and transverse strains induced after the first compression load cycle are $-\ 2.755^{0}/_{00}$ and $1.273^{0}/_{00}$, respectively. Only very slightly more remnant stains can be further induced during subsequent cyclic stress loading.

Besides the non-linear stress-strain behavior, as shown in Fig. 4.1.3, ferroelastic domain switching induced by a compression load will simultaneously give rise to a gradual removal of the remnant polarisation of a pre-poled material. This phenomenon is called *mechanical depolarisation*. The shape of the depolarisation curve resembles the corresponding stress-strain behavior, suggesting that the origin of non-linear deformation is also responsible for the polarisation changes [Cao and Evans, 1993].

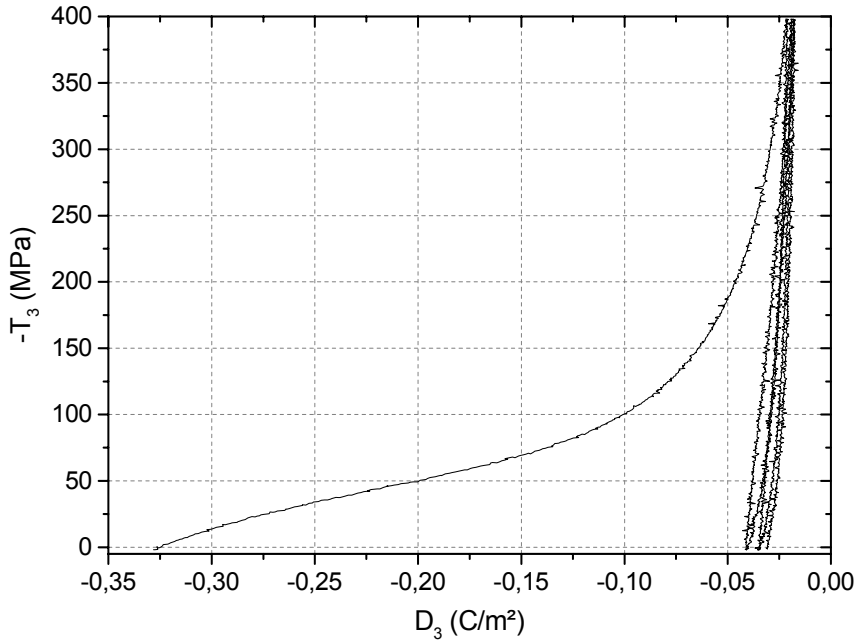

Figure 4.1.3. Three cycles of mechanical depolarisation curve of a pre-poled PIC151 soft PZT ceramic material. Stress loading and unloading rate was 5 MPa/sec.

The initial remnant polarisation induced by the poling E field is about – 0.328 C/m². With increasing of the compressive stress, the remnant polarisation non-linearly decreases. After achieving a much higher stress level (e.g., – 300 MPa), the change of the polarisation becomes quite slow for further increasing load. The remnant polarisation remained at – 400 MPa is about – 0.022 C/m². Therefore, the material can not be completely depolarised by a compressive stress loading with the maximum magnitude of – 400 MPa in this experiment. Upon unloading from – 400 MPa, the stress-depolarisation curve initially traces a nearly vertical line to develop. As pointed out by Kamlah, this phenomenon indicates that the specimen behaves electromechanically decoupled due to mechanical depolarisation (the electric state has become independent of the changes of mechanical stress) [Kamlah, 2001]. After about – 200 MPa, the unloading curve exhibits a slight non-linearity, which indicates that a small part of the polarisation can be gradually recovered. The remnant polarisation after

the first loading cycle is about – 0.041 C/m², which is apparently larger than the minimum value induced at – 400 MPa. A little bit more remnant polarisation can be removed by further stress loading cycles. Right after a total of three loading/unloading cycles, the remnant polarisation is about – 0.031 C/m².

When the stress magnitude is lower than a certain value during the unloading period, both strains and depolarisation curves are observed to deviate from the initially linear behavior and to exhibit slight non-linearities. A similar strain and polarisation *recovery phenomenon* was also reported in the experimental work of Calderon-Moreno et al. for PZT ceramic material, and they attributed this effect to some domains switching back to their initial states prior to depolarisation. High internal stresses, which would be generated inside the material during the external load induced domain reorientation process, were deemed to be the driving force for partial domains switching back [Calderon-Moreno et al., 1999].

For the first stress loading/unloading cycle of a pre-poled specimen, changes of longitudinal and transverse strains are plotted as a function of the depolarisation. The results are given in Fig. 4.1.4. Concerning the S_3-D_3 curve in Fig. 4.1.4 (a), during the initial stress loading period, the corresponding part of this strain-depolarisation curve can be approximately fitted by two long segments of straight line. They correspond to the major non-linear part of the related stress-strain/depolarisation curves (see Fig. 4.1.2 and Fig. 4.1.3, respectively). These two straight lines intersect at the stress value of about - 40 MPa. In the following discussion (section 4.1.2), we will see that this stress value just corresponds to the inflection point of the non-linear stress-strain curve. The initial linear relationship between strain and depolarisation indicates that their changes induced by the compressive stress loading are simultaneous and proportional. Consequently, this result gives us further evidence that the non-linear strain and depolarisation *vs.* compressive stress curves originate from the same non-180° domain switching mechanism.

As the stress achieves higher levels (approximately from - 200 MPa), domain switching processes are nearly completed. Further increasing of the stress mainly induces linear elastic deformation; therefore, the strain-depolarisation responses are observed to deviate from the linear curve.

During the initial unloading period from – 400 MPa, a nearly vertical line can be observed at first in the strain-depolarisation curves. This unloading period is dominated by a linear elastic deformation reduction process, and there is nearly no change of the polarisation. When the stress is lower than a certain magnitude (e.g., - 200 MPa), the strain-depolarisation curves exhibit a slight non-linearity, which is due to partial back switching of domains to their initial

states. However, in contrast to the stress loading process, the very short segment of the strain-depolarisation curves during the unloading period indicates that most of the switched domain configurations are preserved after removal of the stress; hence, significant remnant strains and depolarisation are permanently induced.

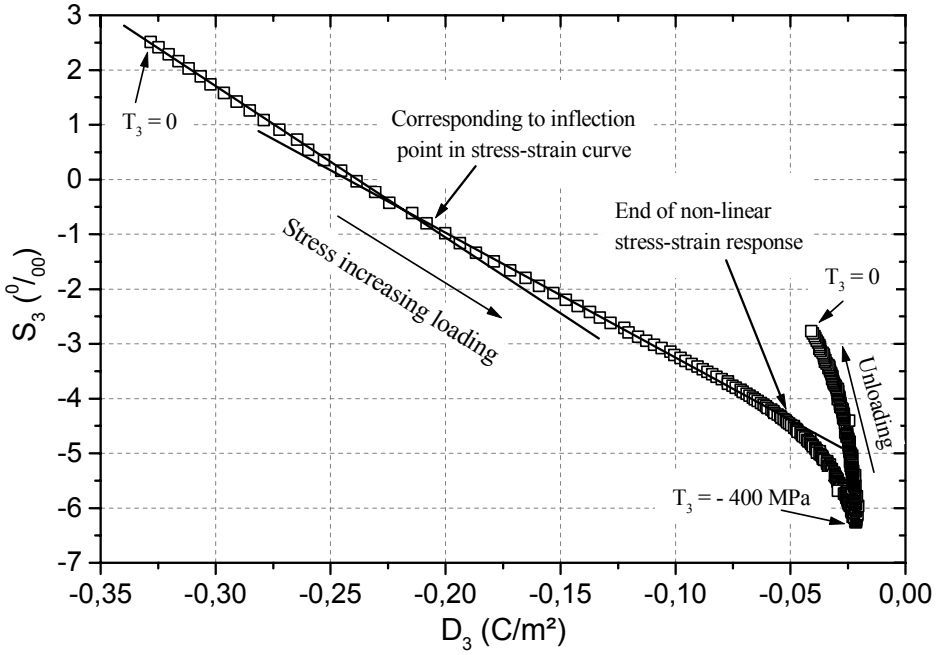

(a)

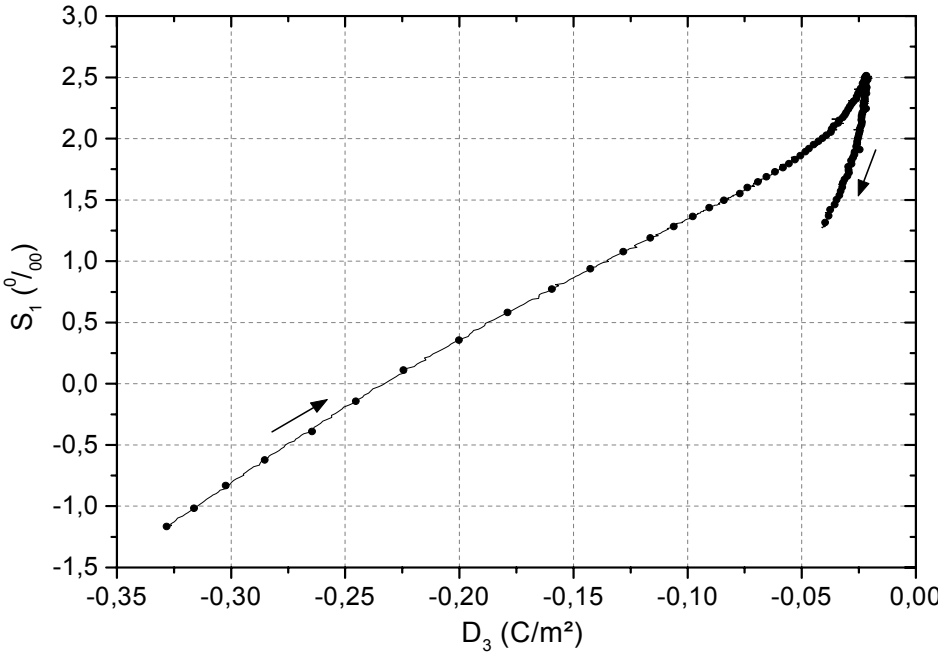

(b)

Figure 4.1.4. Longitudinal (a) and transverse (b) strains versus depolarisation curves during the first cycle of compressive stress loading of a pre-poled PIC151 soft PZT ceramic specimen.

For the initially unpoled and prepoled materials, the stress – strain curves induced during the first loading/unloading cycle are compared in Fig. 4.1.5.

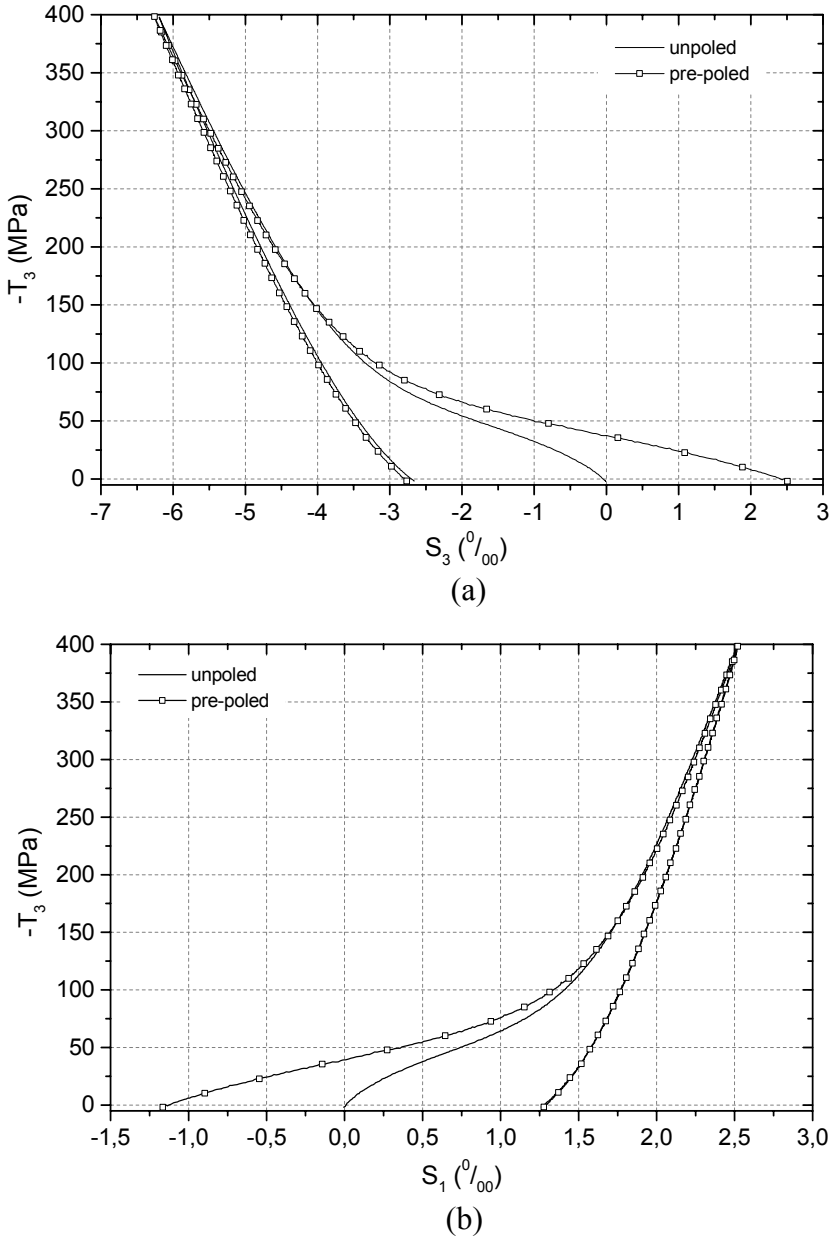

Figure 4.1.5. Comparison of the first cycle of longitudinal (a) and transverse (b) strains *vs.* stress curves of initially unpoled and pre-poled PIC151 soft PZT. Stress loading and unloading rate was 5 MPa/sec..

We know that in these two cases the materials possess completely different domain structures before the stress loading. Domains with different orientations are randomly distributed inside the initially unpoled specimen, while, for the pre-poled material, most of the domains have been aligned as closely as possible parallel to the poling field direction. From Fig. 4.1.5, we

can see that the initial domain configurations mainly influence the non-linear part of the stress-strain curves, which are observed to trace different paths to develop. As the compressive stress exceeds a certain value of approximate - 150 MPa, the non-180° ferroelastic domain switching processes are nearly completed; now, these two materials possess similar domain structures, which are isotropically distributed in the transverse direction (within or close to a plane perpendicular to the compression load). Therefore, we can see that the stress-strain curves nearly become coincident during further stress loading and unloading period and mainly exhibit linear elastic behavior. Finally, nearly the same remnant longitudinal and transverse strains (relative to the zero value) are induced after unloading.

4.1.2 Discussion

1. *Memory effects of piezocearmics*

Piezoelectric ceramics have memory abilities with respect to their polar state and shape. Permanent changes of polarisation and strains induced by mechanical loading can be brought back to their initial values by a subsequent application of an electric field to re-polarise the material.

To show this memory effect, for the pre-poled material, right after mechanical depolarisation by three cycles of compressive stress application, the sample was subjected to five cycles of a triangle waveform electric field loading at stress free state, with the amplitude of +/- 2 kV/mm and a loading rate of 0.08 kV/mm per second (0.01 Hz). The resultant polarisation, longitudinal and transverse strains *vs*. E field hysteresis loops are shown in Fig. 4.1.6, respectively.

Mechanical stresses induce only non-180° domain switching. Prior to the electric field loading, all the domains have been switched with orientations relatively perpendicular to the compression load. Therefore, the domain structure is completely different from the "virgin" state of an initially unpoled material. By an increasing electric field loading from 0 to + 2 kV/mm, the initial repolarisation process will reorient most of the domains back as closely as possible parallel to the pre-poling direction. As a result, strain and polarisation are observed to increase rapidly. It is worth mentioning here that, in this initial course of repolarisation, only non-180° domain switching can occur. Further cyclic electric field loading will give rise to the normal polarisation and strains hysteresis loops. Finally, remnant polarisation and strain are induced with the same values prior to depolarisation by the compression load. The material state can be considered recovered.

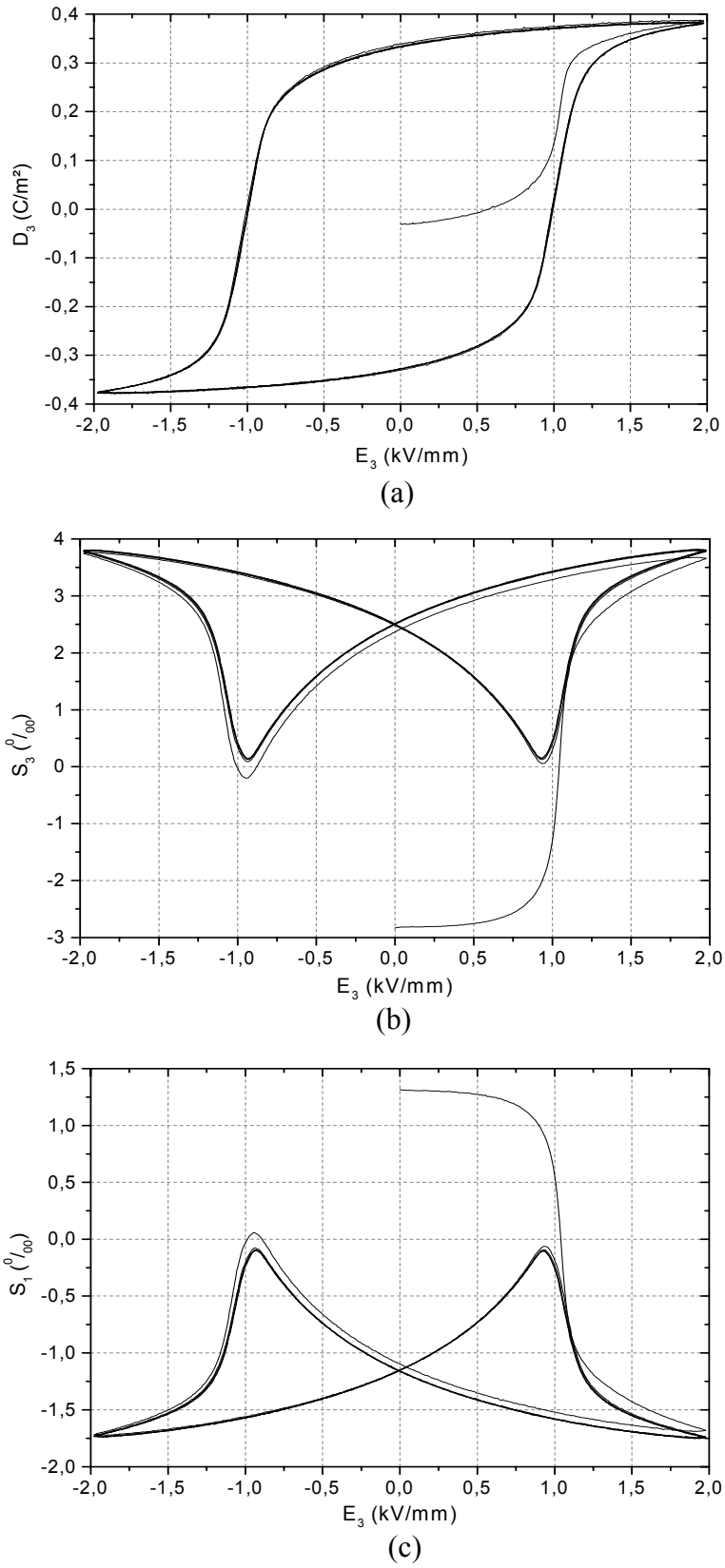

Figure 4.1.6. Repolarisation of a pre-poled PIC151 soft PZT material after three cycles of compressive stress load. (a) Polarisation *vs.* E; (b) Longitudinal strain *vs.* E; (c) Transverse strain *vs.* E. A total of five cycles of ramp-shaped electric field was applied to the specimen, with the amplitude of +/- 2 kV/mm and a loading rate of 0.08 kV/mm per second (0.01 Hz).

2. *Coercive stress for ferroelastic non-180° domain switching*

Theoretically speaking, within a sufficiently small stress loading range, the positive and negative ions inside the unit cells will be displaced only slightly from their equilibrium positions and the material just shows a linear elastic response and direct piezoelectric effect (Note that only the pre-poled material can exhibit macroscopic direct piezoeffect. For an initially unpoled material, the direct piezoeffect exists only in the microscopic scale.). After passing a critical stress load, ferroelastic domain switching processes will be initiated. This threshold stress value is defined as *coercive stress* ($T_{coer.}$) analogously to the definition of *coercive field* (E_c) in the dielectric case [Kamlah, 2001].

To give more insights into the mechanical stress induced non-linear behavior, as shown in Fig. 4.1.7, during the stress increasing part of the first loading cycle (from 0 to – 400 MPa), the derivative of the longitudinal strain with respect to stress ($\partial S_3/\partial T_3$) is plotted *vs*. the compression load (T_3) for an initially unpoled specimen and a pre-poled sample, respectively.

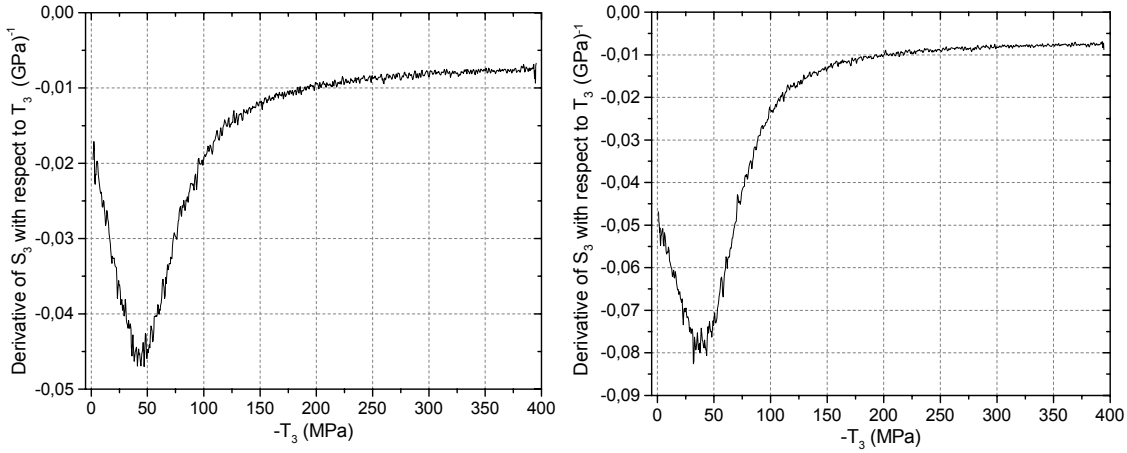

Figure 4.1.7. During stress increasing period of the first loading cycle, derivative of longitudinal strain S_3 with respect to compressive stress T_3 ($\partial S_3/\partial T_3$) as a function of compression load. (a) Initially unpoled PIC151 soft PZT; (b) Pre-poled PIC151 soft PZT.

PIC151 soft PZT is found to be very sensitive to the compressive stress. Even with a very small compressive stress load, ferroelastic domain switching processes can be initiated. This can be confirmed from the decrease of the derivative ($\partial S_3/\partial T_3$) at the very beginning of stress loading. The *coercive stress*, in the sense of completing of the linear elastic response and beginning of the ferroelastic domain switching, can be hardly determined (a linear elastic

response should correspond to a horizontal straight line in the derivative curve). For this reason, meticulous care should be taken during the operation of piezoceramic actuators. Slightly excessive compressive stresses in the poling direction will cause mechanical depolarisation.

The derivative of S_3 with respect to T_3 ($\partial S_3/\partial T_3$) at first decreases with increasing compression load. Large amount of ferroelastic domain switching gives rise to a rapid increase of the irreversible strain. The corresponding part of the stress-strain curve exhibits continuous decrease of the tangent modulus with increasing stress. After reaching a minimum value, the derivative increases with further stress increment. Now the stress-strain curve displays enhancive hardening behavior (tangent modulus increases with stress increment). As pointed out by Calderon-Moreno et al., the enhancive hardening behavior is because the amount of switchable domains is decreasing and those remaining are more difficult to be switched because of their microstructural configurations and the presence of opposing internal stresses [Calderon-Moreno et al., 1999]. At much higher stress levels, the changing of the derivative becomes saturated. A nearly horizontal straight line can be observed. Now, the ferroelastic domain switching processes are nearly completed, and the deformation becomes linear elastic.

The minimum value of the derivative corresponds to the inflection point of the non-linear stress-strain curve. In the work of Schäufele and Härdtl, the mechanical stress corresponding to the inflection point was defined as the *coercive stress* [Schäufele and Härdtl, 1996]. In the later presentation of time-dependent phenomena under constant compression load (see section 4.3), it will be interesting to find that, as the stress magnitude approaching this inflection point, the material exhibits most pronounced time-dependent effects. This indicates that the domains possess maximum mobility at the stress level close to this point.

From Fig. 4.1.7, we can see that, at the beginning of stress load, the derivative ($\partial S_3/\partial T_3$) value for the pre-poled specimen is significantly smaller than that for the unpoled sample. This indicates that, for a pre-poled material, the ferroelastic domain switching is relatively easier to be initiated; therefore, at the beginning of stress application, the stress-strain curve exhibits smaller tangent modulus. For the materials with different poling states, the stress values corresponding to the inflection points are also different. For the initially unpoled specimen, the stress value is about - 43.5 MPa; whereas, for the pre-poled sample, the value is about - 39 MPa, which is about 10% smaller than that of the unpoled material.

3. *Changes of volumetric strain during compressive stress loading*

Since the compression tests were carried out under uni-axial loading conditions, the transverse deformation is isotropic, yielding $S_1 = S_2$. Therefore, the relative change of specimen's volume (*volumetric strain* - S_{volume}) can be expressed as

$$S_{volume} = S_3 + 2S_1 \tag{4.1.1}$$

Based on the longitudinal and transverse strains measurements for the total three stress loading/unloading cycles, changes of the volumetric strain as a function of compressive stress are plotted in Fig. 4.1.8 for the initially unpoled and pre-poled specimens, respectively.

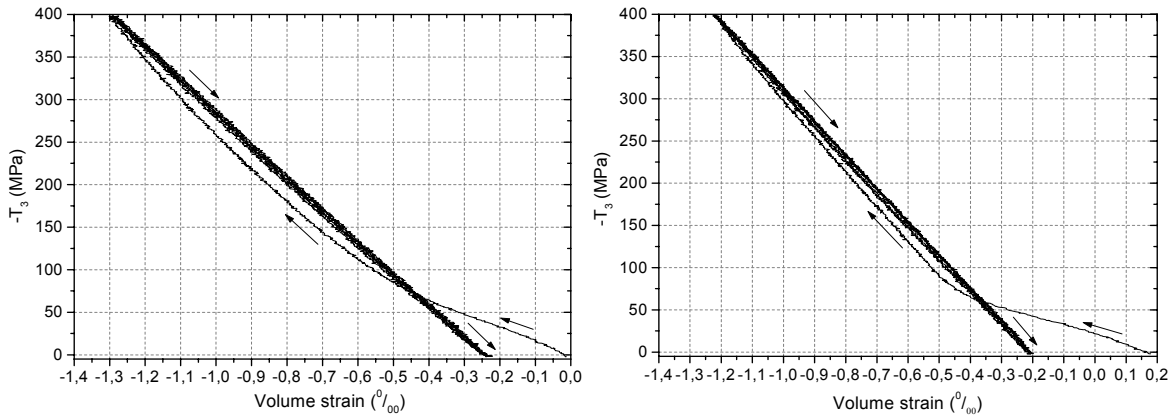

Figure 4.1.8. Changes of volumetric strain as a function of a total of three cycles of compressive stress loading. (a) Initially unpoled PIC151 soft PZT specimen; (b) Pre-poled PIC151soft PZT sample.

The volumetric strain of an initially unpoled material before mechanical load is taken as zero. With increasing magnitude of the compressive stress, the induced volumetric strain traces a non-linear curve to negative values. At higher stress levels, the curve becomes approximately linear. A nearly straight line can be observed during the unloading process. Finally, a significant negative remnant volumetric strain is induced.

The volumetric strain-stress curve of a pre-poled specimen resembles that of the unpoled specimen. The initial volumetric strain prior to stress loading is positive. As discussed in Chapter 3 (section 3.1), this can be attributed to the electric field induced phase transition (from the rhombohedral phase to the tetragonal phase) during the pre-poling process. The positive volumetric strain non-linearly decreases with compression load increment and eventually becomes negative. After achieving a certain higher stress level, the volumetric strain –stress curve becomes linear during further stress loading and unloading processes. Finally, an irreversible negative remnant volumetric strain is observed.

As seen in Fig. 4.1.8, for both unpoled and pre-poled specimens, the permanent volume change is mainly induced during the non-linear part of the first loading cycle. For further stress loading cycles, the volumetric strain-stress curves become a nearly straight line, and hardly any hysteresis can be detected. This observation demonstrates that the material now only exhibits elastic volumetric deformation. The change of the volumetric strain is reversible, and nearly no further remnant volumetric strain can be induced.

The compressive stress is usually considered providing two contributions to the total strain responses, i.e. elastic deformation and ferroelastic domain switching. Experimental results from Lynch confirmed that there was no volume change associated with a pure ferroelastic non-180° domain switching process [Lynch, 1996]. Elastic deformation will induce negative volumetric strain, whereas, this relative change of specimen's volume should be linear and reversible. In particular, after removal of the mechanical load, no remnant volumetric strain should be observed. Consequently, there must be some other mechanism responsible for the negative remnant volumetric strain observed in the experiments.

As discussed in Chapter 3 (section 3.1), theoretical calculations based on Devonshire phenomenological theory indicated that, for PZT ceramic materials with a chemical composition near the morphotropic phase boundary (MPB), a uni-axial compressive stress would induce a transition from the tetragonal phase (F_T) to the rhombohedral phase (F_R) [Stotz, 1987]. A microstructure analysis of PZT ceramics given by Soares et al. shows that, within the phase coexistence region near the MPB, the unit cell volume of the rhombohedral phase is smaller than that of the tetragonal phase [Soares et al., 2000]. Therefore, the experimentally observed negative remnant volumetric strain induced by compressive stress loading can be attributed to the phase transition from the tetragonal symmetry to rhombohedral symmetry.

Based on the parameters (i.e., fraction and average unit cell volume of F_T and F_R phases) given in Chapter 3 (section 3.1) and the experimentally obtained remnant volumetric strain values, the amount of phase transition induced by a compression load is calculated. For the initially unpoled specimen, after one cycle stress loading, about 5% of the tetragonal phase is transformed into the rhombohedral phase. For a pre-poled specimen, the pre-poling E field has induced some transition from the rhombohedral phase to the tetragonal phase. Therefore, more opposite phase transition will be induced by the stress loading. The calculation shows that about 8% transition from F_T to F_R is induced after the first stress loading cycle.

4.2 Loading rate dependnce of stress-strain behavior

In order to investigate the loading rate dependence, initially unpoled PIC151 soft PZT ceramic specimens were subjected to a ramp-shaped uni-axial compressive stress loading, with the amplitude of – 400 MPa. Three different loading rates of 0.4, 4 and 40 MPa/sec. were used in the experiments, respectively. The resultant longitudinal and transverse strains versus stress curves are shown in Fig. 4.2.1.

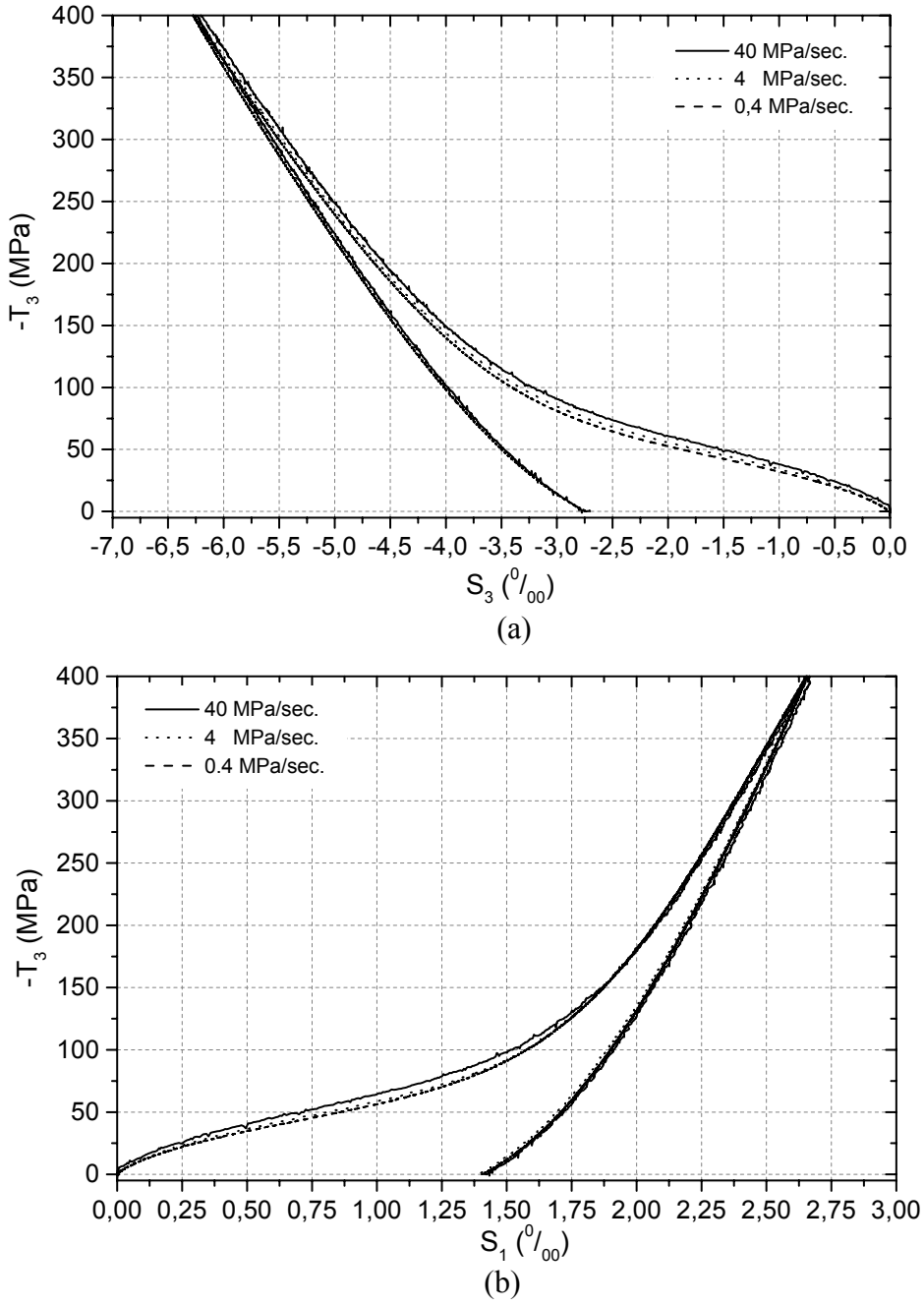

Figure 4.2.1. Longitudinal (a) and transverse (b) strains in response to compressive stress with different loading rates. The material is initially unpoled PIC151 soft PZT.

The material exhibits a similar non-linear stress-strain behavior at different loading rates. One of the notable features observed in Fig. 4.2.1 is that, to achieve the same strain value, a slightly higher stress is need in the case of a higher loading rate. Compressive stress values corresponding to the inflection points of these three stress-strain curves are about - 44.5, - 50 and - 53.5 MPa, respectively, increasing with the loading rate increment.

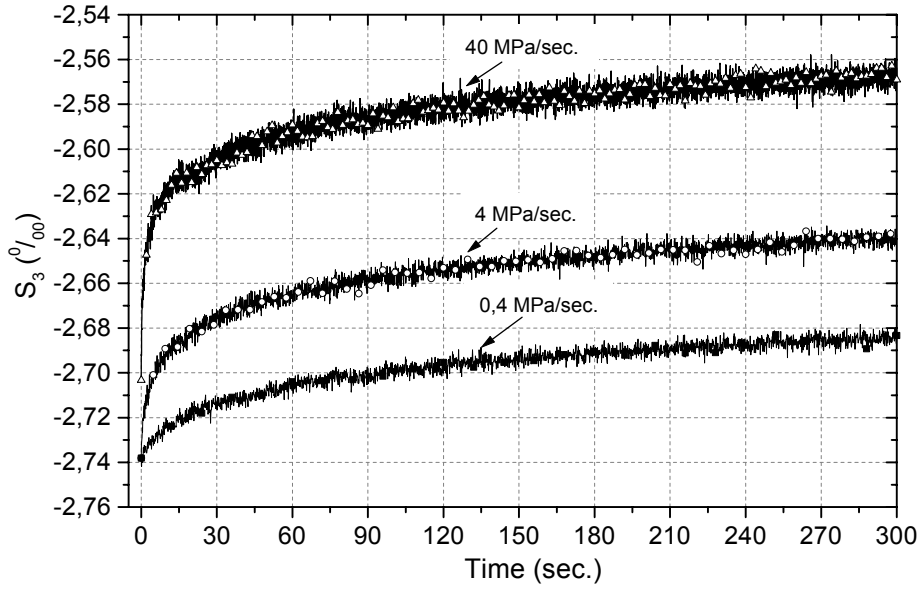

(a)

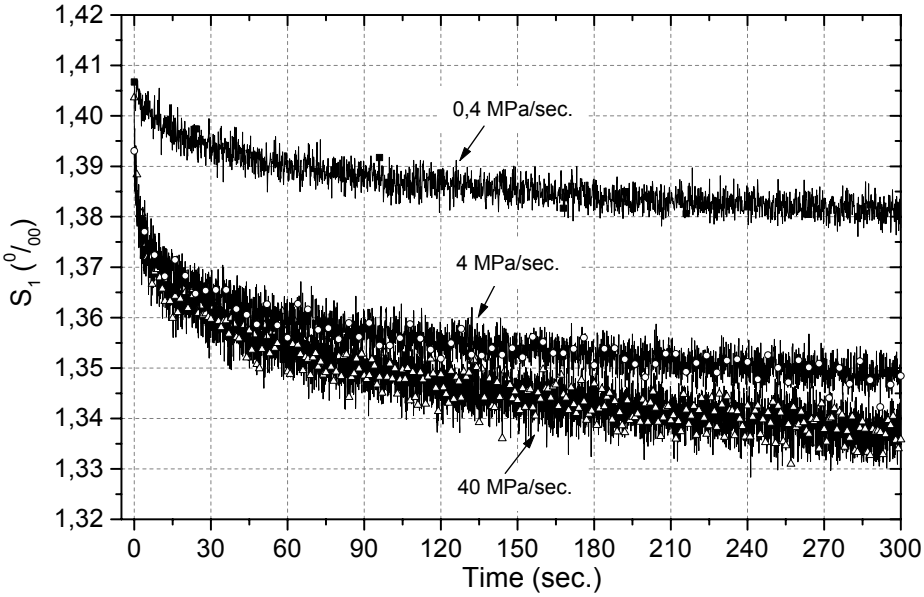

(b)

Figure 4.2.2. Changes of longitudinal (a) and transverse (b) strains with time, after removal of one cycle stress loading with the amplitude of – 400 MPa and different loading rates of 0.4, 4 and 40 MPa/sec., respectively.

After one cycle of loading, the stress was reduced to zero and the changes of the remnant longitudinal and transverse strains versus time were measured. Comparing the strain values at the beginning of stress removal, in Fig. 4.2.2, we can see a slightly larger remnant strain can be induced in case of a lower loading rate. Schäufele and Härdtl found the similar results for hard PZT ceramic materials subjected to compression loads with different loading rates, and they attributed this phenomenon to a more stabilized domain configuration built up inside the material during a longer compression loading duration [Schäufele and Härdtl, 1996].

Compression load induced remnant strains are found to decrease with time after unloading. The decrease is most pronounced at the very beginning of stress removal, thereafter, the changes tend to be saturated with further time increase. According to the definition given in Chapter 3 (section 3.2), the phenomenon of strain recovery after stress loading can also be attributed to the ageing effects. As explained by Calderon-Moreno et al., high internal stresses will be generated inside the material during the compression load induced ferroelastic domain switching process. After unloading, due to the internal stresses, the strain recovery is produced by switching some domains back to their original states [Calderon-Moreno et al., 1999].

Analogous to the electric field loading condition, ageing effects after compressive stress loading are also found to be loading rate dependent. As seen in Fig. 4.2.2, in case of a higher pre-loading rate (e.g., 40 MPa/sec.), a much steeper initial slope and a faster tendency to saturation are observed in both longitudinal and transverse strains *vs*. time curves. While, in the circumstance of a lower pre-loading rate (e.g., 0.4 MPa/sec.), the variation of the remnant strains exhibits a more gradual decrease with the passage of time.

4.3 Time-dependence of stress-strain behavior under constant compression load

To investigate the time-dependent effects of piezoceramics under pure mechanical stress loading conditions, an initially unpoled PIC151 soft PZT ceramic specimen was subjected to uni-axial ramp-shaped compressive stress load, with the amplitude of – 400 MPa and a loading rate of 4 MPa/sec.. During both loading and unloading periods of the first cycle, the stress load was interrupted repeatedly by holding it at different constant levels for 240 seconds. Longitudinal and transverse strains were measured simultaneously. The first cycle of stress-strain curves are shown in Fig. 4.3.1.

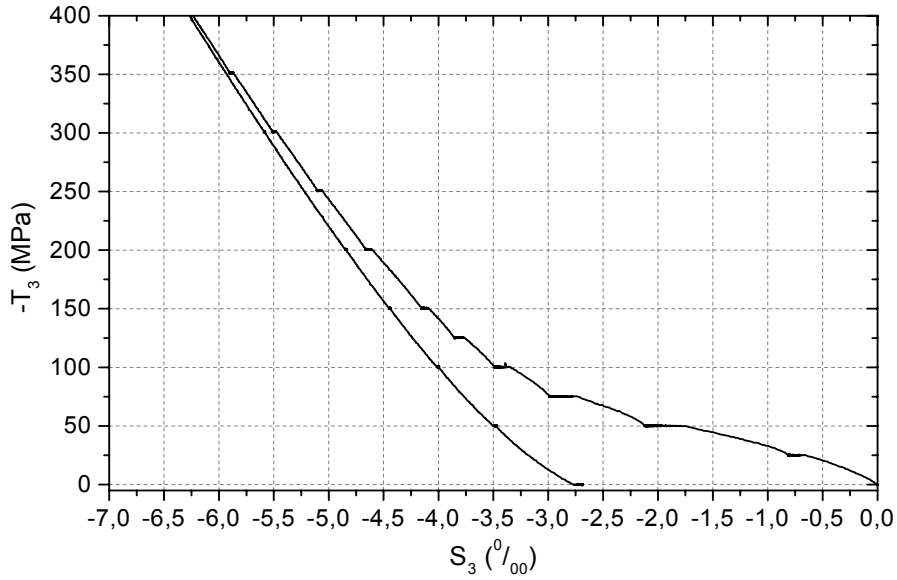

(a)

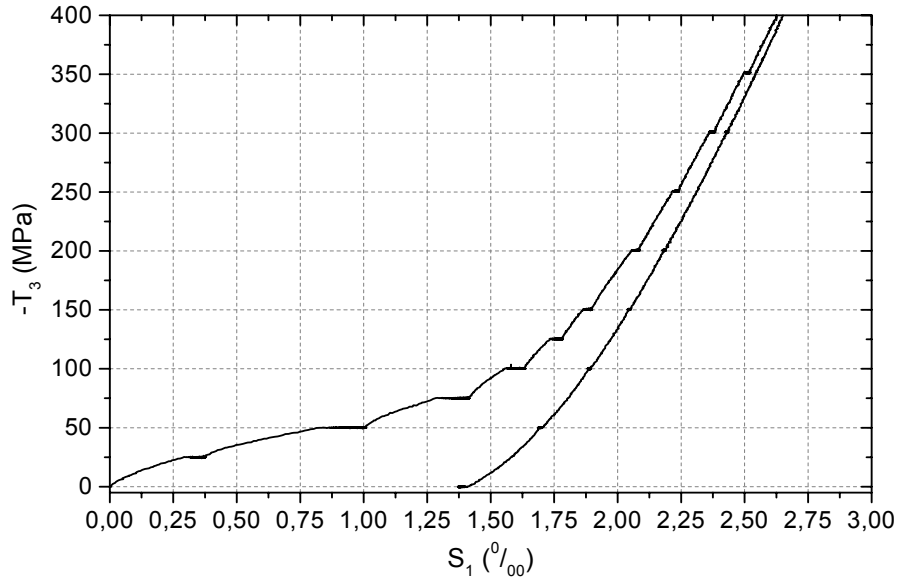

(b)

Figure 4.3.1. Longitudinal (a) and transverse (b) strains *vs.* compressive stress curves of initially unpoled PIC151 soft PZT ceramic material. Stress was kept at different constant values for 240 seconds during both loading and unloading process.

Similar to the time-dependent effects under pure electric field loading conditions, strains induced at each constant stress level during the stress increase loading period exhibit creep-like *increasing* behavior. Changes of longitudinal and transverse strains with time under constant stress levels of - 50, - 100, and - 400 MPa are given in Fig. 4.3.2, respectively.

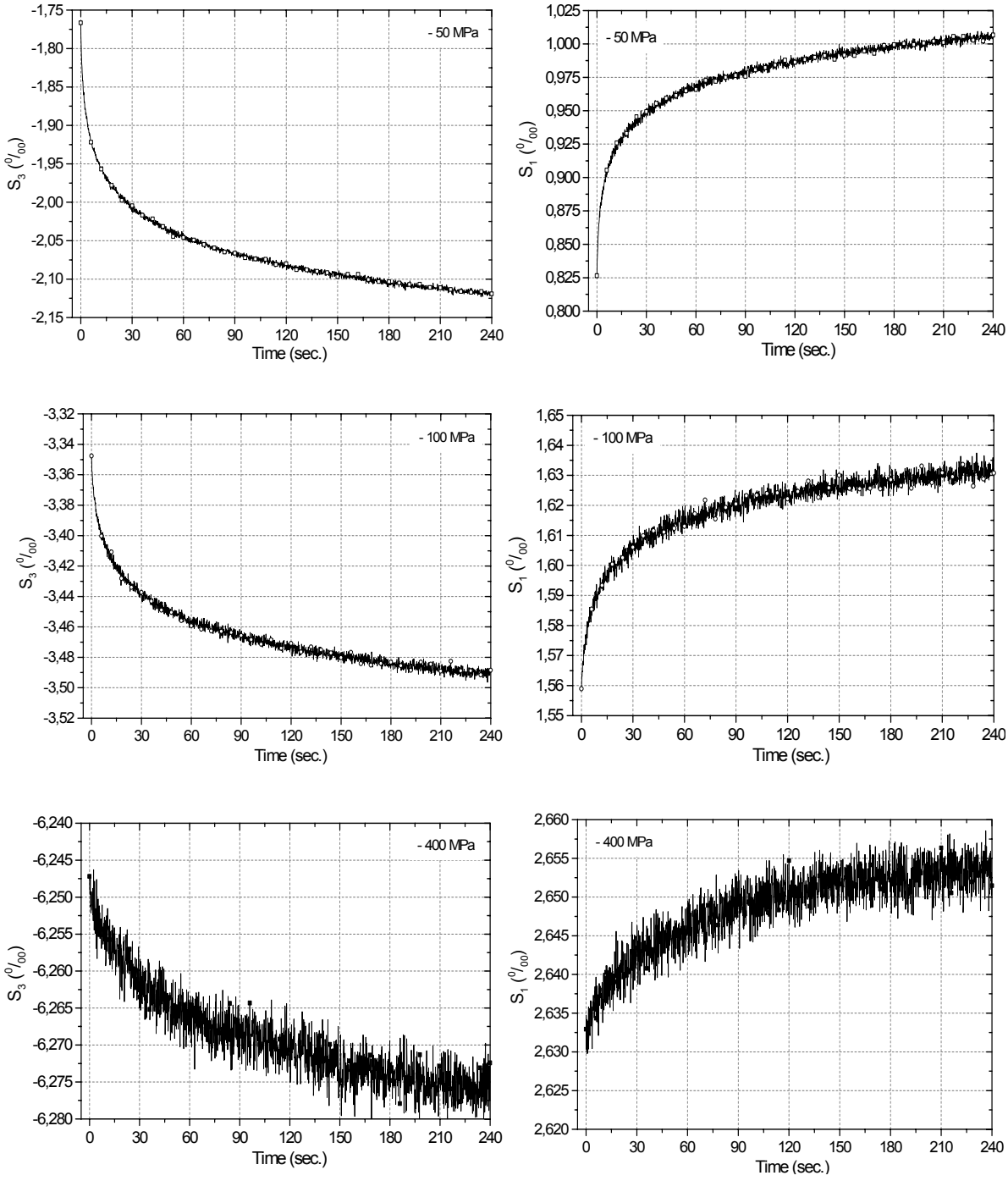

Figure 4.3.2. Changes of strains versus hold time at –50, -100 and – 400 MPa, respectively. The compression load was held constant during the stress increase loading period. Left panel is corresponding to the longitudinal strain, and right panel is the response of transverse strain.

At the beginning of a stress hold time, the strains initially experience a fast increase with a very steep slope. With further holding time increment, the changes gradually slow down and tend to be saturated eventually. Similar time-dependent effects were also found in the tensile stress loading tests of PIC151 soft PZT ceramic material [Munz and Fett, 1999].

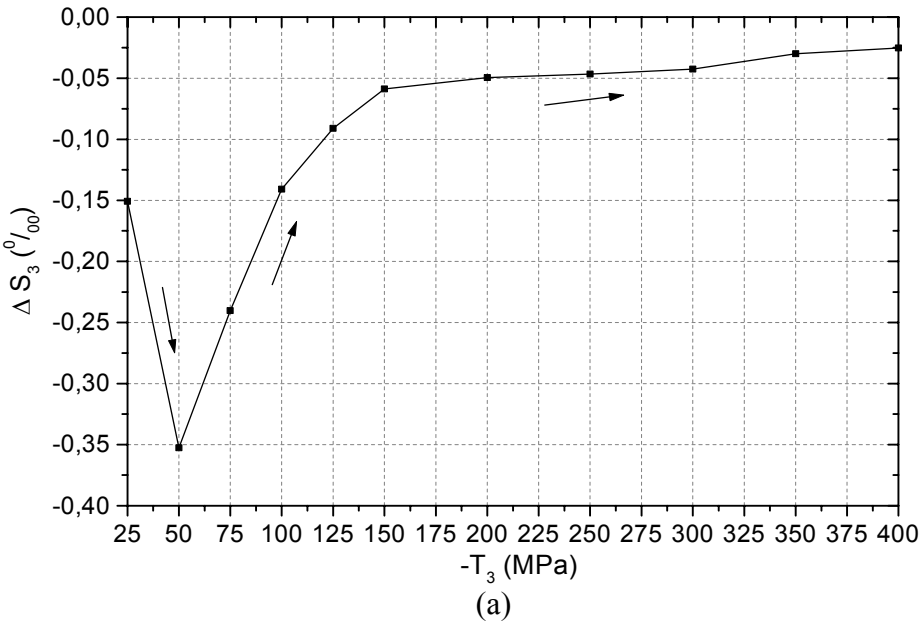

(a)

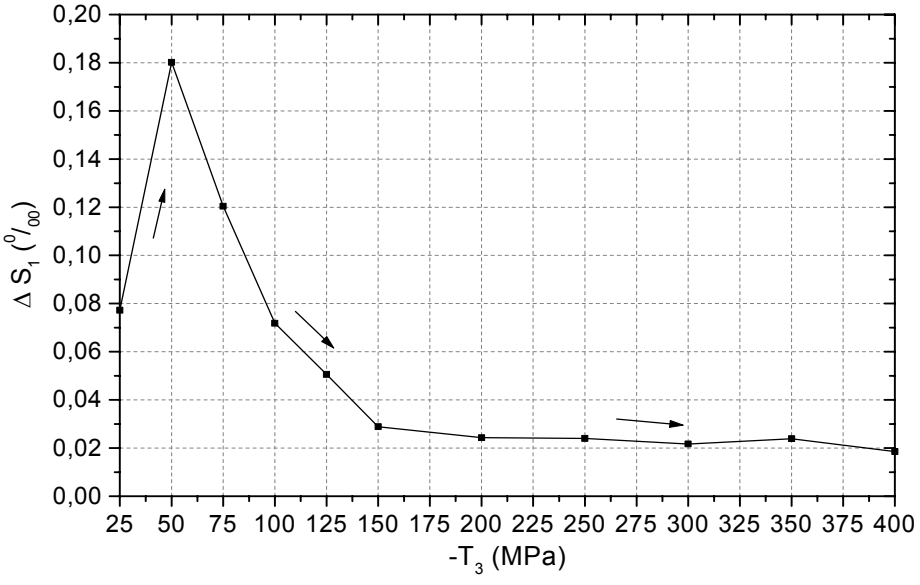

(b)

Figure 4.3.3. Longitudinal (a) and transverse (b) strains induced during the hold time as a function of stress magnitudes, where the stress was held constant during the loading period.

To evaluate the influence of stress magnitude on the time-dependent strain response during the loading period of stress increasing from zero to – 400 MPa, changes of strains induced by different constant compression loads at the end of the hold time are compared in Fig. 4.3.3.

We can see that the time-dependent effect significantly depends on the magnitude of the compressive stress. The strain increment (ΔS_3 and ΔS_1) induced during the hold time initially increases with stress magnitude increment. After achieving a maximum at – 50 MPa, the induced strain increment decreases quickly with increasing compression load. When the stress level is higher than – 150 MPa, the time-dependent effects tend to be saturated, only little strains can be further induced during the holding time. Recalling the discussion in section 4.1.2, we know that – 50 MPa approximately corresponds to the stress value at the inflection point of the continuous stress-strain curve.

The macroscopic time-dependent strain response can be interpreted by gradually induced additional microscopic non-180° domain switching during the hold time. As mentioned earlier, mechanical stresses mainly have two contributions to the total strain responses, i.e. elastic deformation and ferroelastic domain switching. In unit cells, a slight displacement of ions from their equilibrium positions will give rise to the elastic deformation. The strain induced by this *instantaneous* process is *reversible* and will be removed after the stress is reduced to zero.

The process of domain reorientation as close as possible to a plane perpendicular to the mechanical load is called ferroelastic switching. For unit cells, this switching process is also *instantaneous*. Whenever a critical stress level is reached, non-180° switching will occur. Such a threshold corresponds to the *microscopic coercive stress* for unit cells.

As discussed in Chapter 3 (section 3.3), the microstructure of a commercial piezoceramic material is very complicated, consisting of grains, grain boundaries, domains, domain walls, unit cells and defects. With application of an external stress, the complicated microstructure will give rise to fluctuation of the microscopic stress distribution inside the material. In some regions, the local stress may be higher than the switching threshold, and domain reorientation in these regions occurs instantaneously. While, in other regions, the local stress is lower than the coercive stress, and switching processes can not be initiated until a larger driving force is applied. One aspect of the driving force could be higher external stress loading. This argument can be confirmed by the observed non-linear stress-strain curves (see Fig. 4.1.1), in which the initially rapid strain increment is due to more and more domains switching induced

by continuously increased external stress, until the reservoir of this irreversible contribution is exhausted, the stress-strain behavior becomes linear elastic.

In case of holding the stress at a constant value, the creep-like strain increment indicates that there is gradually induced further domain switching during the hold time. Since the external load was kept constant, there must be some other kinds of mechanisms responsible for the time-dependent effects. A tentative explanation is the gradual changing of internal local electric fields through the time-dependent defects diffusion process.

In a piezoceramic material, uniform alignment of unit cells leads to strong local electric field existing around a domain structure. The initially unpoled material is polycrystalline. Due to the random distribution of grains and the isotropic domain orientation, the internal local electric fields cancel each other out and have no contribution to the domain switching process. An external mechanical load will activate the direct piezoeffect on the micro-scale for either switched or un-switched domains. As a consequence, it will disturb the internal electric field equilibrium. Local electric field intensifications may occur at some regions inside the material.

As discussed in Chapter 3 (section 3.3), there are a large number of microscopic defects existing inside a piezoceramic material and acting as pinning centers to stabilise the domain configuration by applying internal bias fields. Due to the disturbance of the internal E field equilibrium induced by compressive stress load, the high local E fields in some regions will cause the realignment of microscopic defects through the migration process of dopant ions or vacancies. As a result, the clamping effects of these defects on those unswitched domains are effectively reduced. When the local stress achieves the coercive stress level, ferroelasitic domain switching will occur and contribute to the macroscopic strain increment. The migration of defects is a time-dependent diffusion process, related to typical time constants by diffusion coefficients. With the passage of hold time, more defects will be aligned by the high local E fields, and this process results in the minimising of pinning effects for more unswitched domains. Consequently, the local stresses may achieve the coercive stress at various locations and give rise to more ferroelastic domain switching. The gradually induced microscopic switching processes will cause the macroscopic time-dependent strain behavior.

On the other hand, due to the local E field intensification and continuous reducing of pinning effects of defects on the unswitched domains, when the coercive field is reached in some regions, ferroelectric switching will also be induced. This process will further change the

local E field and stress distribution, and result in subsequent correlated defects diffusion and domain switching processes.

So far, the time-dependent effects under mechanical load have been interpreted by the mechanism of changing of local E field strength through the transient diffusion process of defects. A similar explanation has been used for the time-dependent effects under electric field loading. Such a qualitative interpretation still needs to be proved experimentally or theoretically.

The most pronounced time-dependent effect is observed at – 50 MPa and this indicates that the material possesses the maximum domain switching ability around the stress level near the inflection point of the non-linear stress-strain curve. According to the experimental results under pure electric field loading conditions (see Chapter 3, section 3.3), we know that this material also exhibits most pronounced time-dependent effects as a constant electric field close to the coercive field (E_c). The coercive field also corresponds to the inflection point of polarisation *vs*. E field hysteresis loop. Consequently, it seems to be somewhat reasonable that the stress value at the inflection point of the non-linear stress-strain curve can be analogously defined as *coercive stress*. Whereas, here, we should notice that this coercive stress is only meaningful for the macroscopic stress-strain behavior and can't be considered as the threshold stress for unit cell switching.

As seen in Fig. 4.3.3, with stress magnitudes beyond – 50 MPa, the creep strain decreases quickly. After about – 150 MPa, the stress-strain responses are dominated by linear elastic behavior. Since the reservoir of switchable domains is nearly exhausted, we can see the time-dependent effects become very weak with further increasing stress magnitudes.

In contrast to loading process, strains induced at constant stress levels during the unloading period exhibit creep-like *decreasing* or *recovery* behavior. In Fig. 4.3.4, changes of strains with hold time at constant stress levels of – 50 and 0 MPa are shown as two examples of the strain recovery phenomenon. Clearly, the absolute values of strains are observed to decrease with time. The strain recovery behavior is most pronounced at the beginning of the hold time, and then, the recovery rate slows down and gradually becomes saturated.

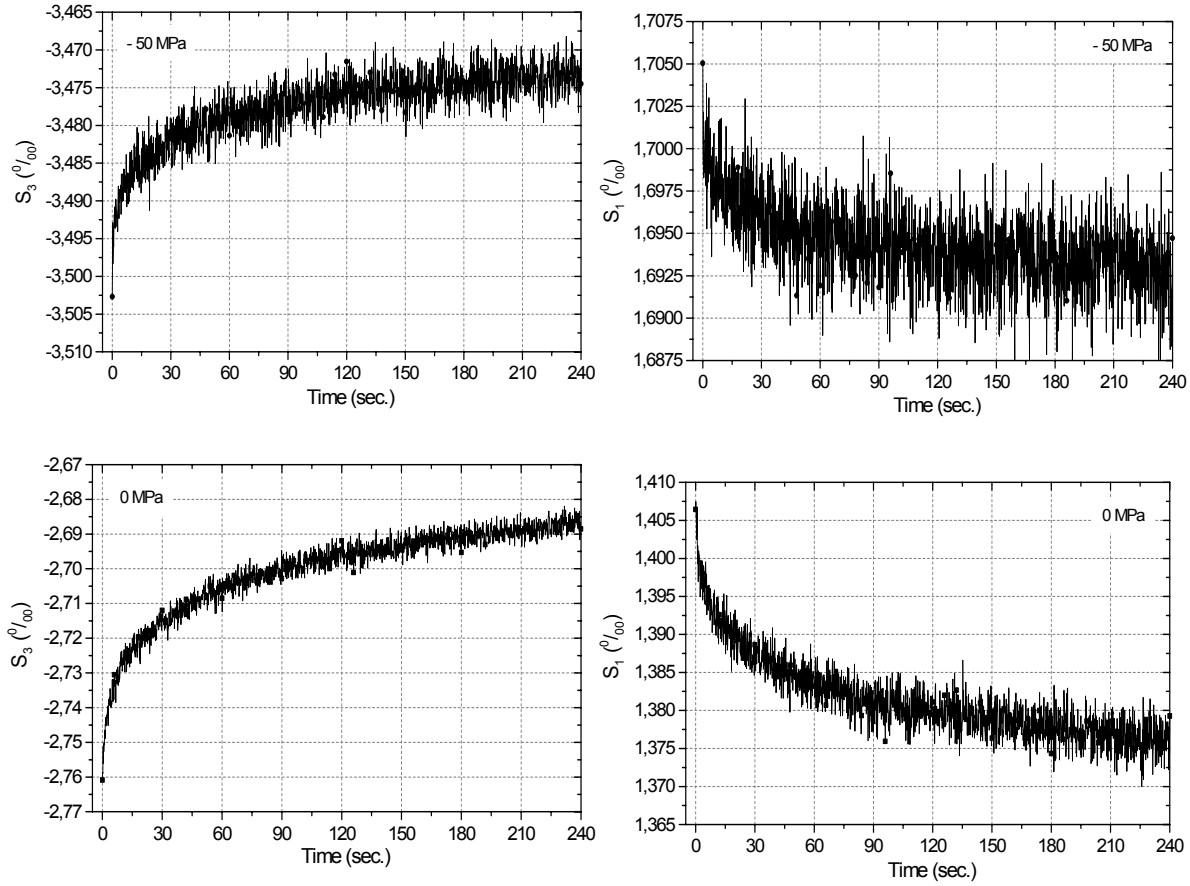

Figure 4.3.4. Changes of strains versus hold time at – 50 and 0 MPa, respectively. The compression load was held constant during the stress decrease unloading process. Left panel is corresponding to the longitudinal strain, and right panel is the response of transverse strain.

For the unloading period of stress decreasing from – 400 MPa to zero, recovered strain (ΔS_3 and ΔS_1) during the hold time at different constant stress magnitudes are compared in Fig. 4.3.5.

We find that the time-dependent strain recovery effects are very weak as holding at higher stress levels (e.g., from – 300 to – 150 MPa). After unloading from – 150 MPa, strains recovered during the hold time become significant and increase quickly with decreasing stress magnitudes. In Fig. 4.1.1, we can see that the corresponding continuous stress-strain curves during the unloading process also mainly exhibit linear elastic behavior at first. After the stress is lower than about – 150 MPa, a slight non-linearity can be observed. As discussed earlier, the strain recovery phenomenon might be due to some domains switching back to their original positions prior to the compression load. High internal stresses generated inside the material during the non-180° ferroelastic domain switching process can be the driving force for domains back switching.

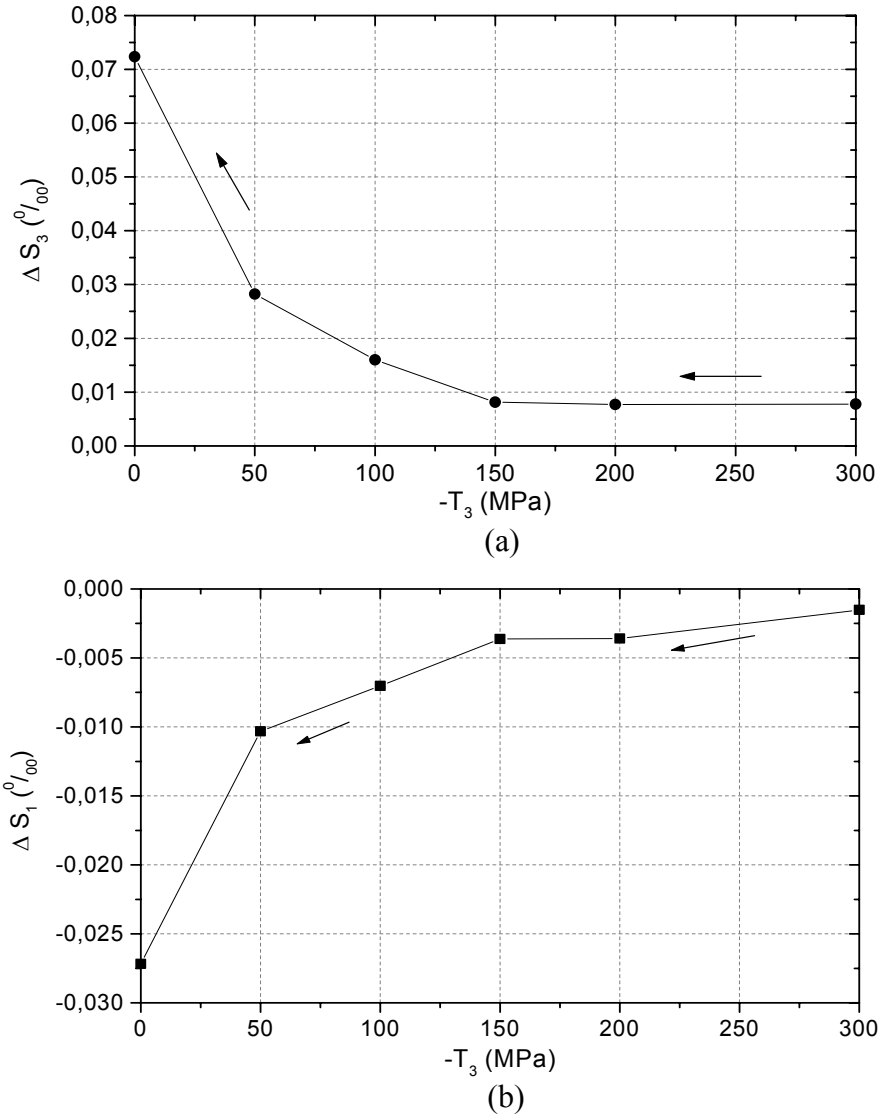

Figure 4.3.5. Longitudinal (a) and transverse (b) strains induced during the hold time as a function of stress magnitudes. During the unloading period, the stress was held constant for 240 seconds at different levels.

In Fig. 4.3.6, the first cycle of stress-strain curves of a continuous loading test and the stress hold experiment are plotted together in the same diagram for comparison. The stress-strain curves of these two experiments have a similar shape. The maximum strains induced at – 400 MPa and the remnant strain values after removal of the stress loading do not show too much difference. This indicates that the stress-strain behavior of this material is mainly determined by the stress amplitude.

By comparing the curves during the loading period, it is interesting to find that, for the stress hold experiment, the stress-strain curve right after holding at a constant stress level initially exhibits a segment of approximately linear elastic development. Then, it becomes coincident with the curve from the continuous test until the beginning of stress holding at a new level.

This observation together with the gradually saturated creep-like strain behavior during the hold time (see Fig. 4.3.2) give us further evidence that, for a given constant stress, the amount of switchable domains is limited. With the passage of the hold time, the reservoir of the transient irreversible contribution belonging to the current stress level will be gradually exhausted. Therefore, the stress-strain curve right after a hold time mainly exhibits linear elastic behavior. Until the stress achieves a higher level, which can initiate new domain switching process once more, the stress-strain plot will join the curve that was obtained without stress holding.

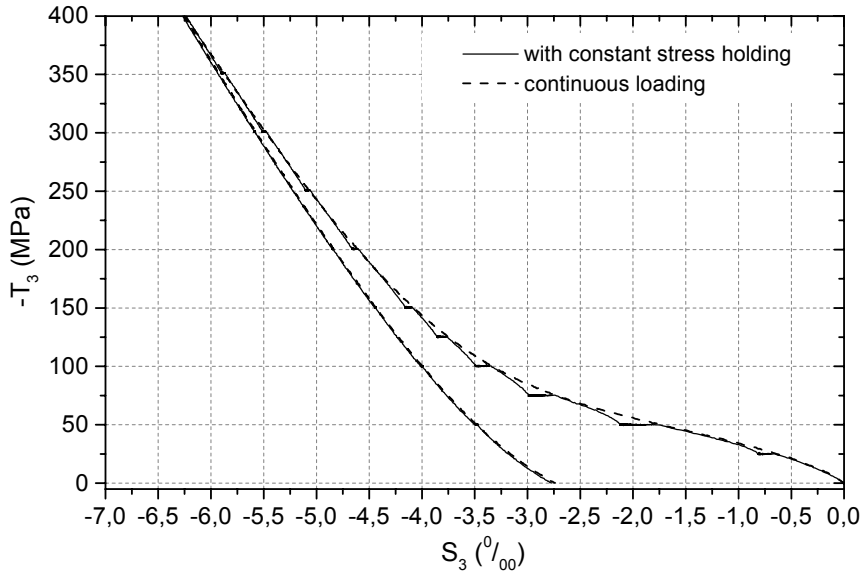

(a)

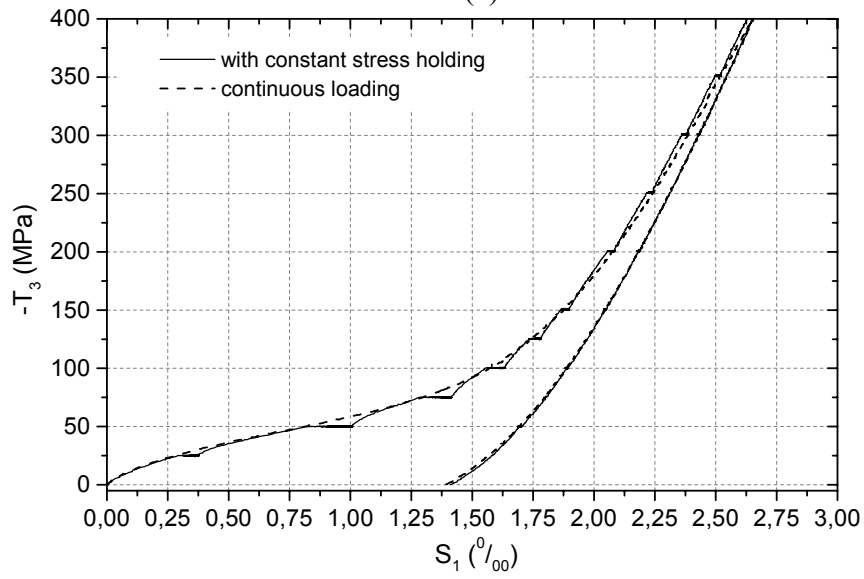

(b)

Figure 4.3.6. Comparison of stress-strain curves from continuous loading test and experiment for time-dependent effects investigation. The material is initially unpoled PIC151 soft PZT, same stress loading/ unloading rate of 4 MPa/sec. was used in these two experiments. (a) Longitudinal strain *vs.* stress; (b) Transverse strain *vs.* stress.

Chapter 5 Responses under Combined Electromechanical Loading

In contrast to the experimental investigations under a pure electric field or a pure mechanical stress loading, it is more important to understand the non-linear behavior of piezoelectric materials under combined electromechanical loading conditions.

This is because modern actuators tend to be utilized under severe conditions, i.e., high E field together with large mechanical load. For example, in the applications of sonar projectors, in order to prevent the ceramics from experiencing tension, the active materials are always placed under significant uni-axial stress, and the driving electric field is also very high [Viehland, et al., 2001]. As discussed earlier, under large signal E field and/or stress loading, the materials display significant hysteresis and non-linearity, which are caused by the irreversible domain switching. Therefore, the conventional linear constitutive formulas for small signal loading conditions become insufficient to represent the general behavior of piezoceramics. To characterise and model the material response under conditions simulating operating environments, the real responses of piezoceramics under large signal electromechanical coupling loading conditions must be experimentally investigated.

In this chapter, the response of PIC151 soft PZT under combined electromechanical loading is evaluated. The polarisation and strain versus electric field hysteresis loops under different superimposed compression loads will be introduced at first. To determine the optimum operating conditions of an actuator, the influence of a compressive stress preload on the dielectric and piezoelectric properties of the piezoceramic material has been investigated. The results indicate that the actuation capability of piezoceramics can be enhanced by a compressive stress preload within a small magnitude range. Finally, the depolarisation and strains versus stress curves in response to a bias electric field with different magnitudes and loading directions will be presented, and based on these curves, the influence of a bias E field on the value of coercive stress will be analysed.

5.1 Polarisation and strains versus full cycles of electric field hysteresis loops under uni-axial compressive stress preloads

In this section, the influence of uni-axial compressive stress preload on the polarisation and strains versus full cycles of electric field curves will be discussed.

The experiment was performed on initially unpoled PIC151 soft PZT, full cycles of a ramp-shaped electric field was applied to the specimen under different compressive stress preloads. The electric field and the superimposed stress were co-axial. The E field amplitude range was

selected between – 2 kV/mm and + 2 kV/mm, with a loading rate of 0.08 kV/mm per second (100 seconds per cycle). The superimposed stress levels were increased from 0 to – 400 MPa, with a loading rate of 5 MPa per second. Polarisation, longitudinal and transverse strains *vs*. electric field hysteresis loops were monitored simultaneously. Considering the time-dependent effects of depolarisation and strain responses under a constant mechanical stress load (for details, see section 4.3), when the preload stress was increased to a new level, there was a hold time of 150 seconds before starting the electric field cycling. A total of four cycles of the electric field was applied to the specimen at each constant preload stress level, and only the curves induced during the last loading cycle were plotted for illustration.

1. *P-E curves under different compressive stress preloads*

The polarisation *vs*. electric field (P-E) hysteresis loops under different compressive stress preload levels are shown in Fig. 5.1.1.

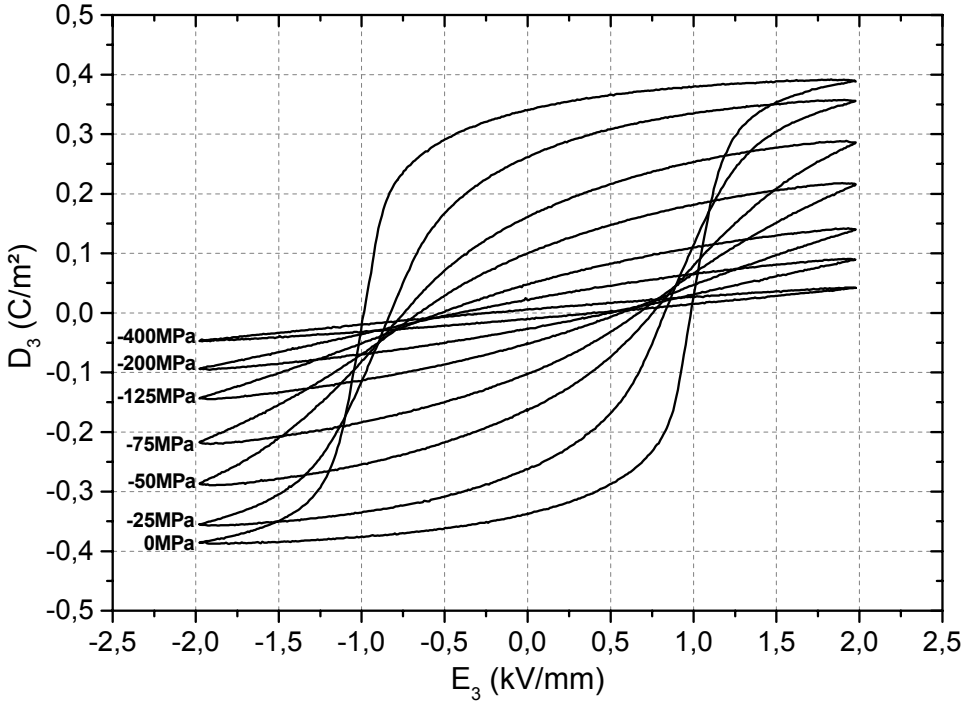

Figure 5.1.1. Polarisation *vs*. electric field (P-E) hysteresis loops under different preload compressive stresses.

From these P-E hysteresis loops, first we can notice that the loops area decreases with increasing preload stresses. We know that the polarisation *vs*. electric field hysteresis loop area represents the unit volume polarisation dissipation energy of a ferroelectric material subjected to one full electric field cycle loading [Lines and Glass, 1977]. The change of

polarisation dissipation energy with increasing preload stresses is plotted in Fig. 5.1.2. It is found that the dissipation energy decreases non-linearly with preload stress increment.

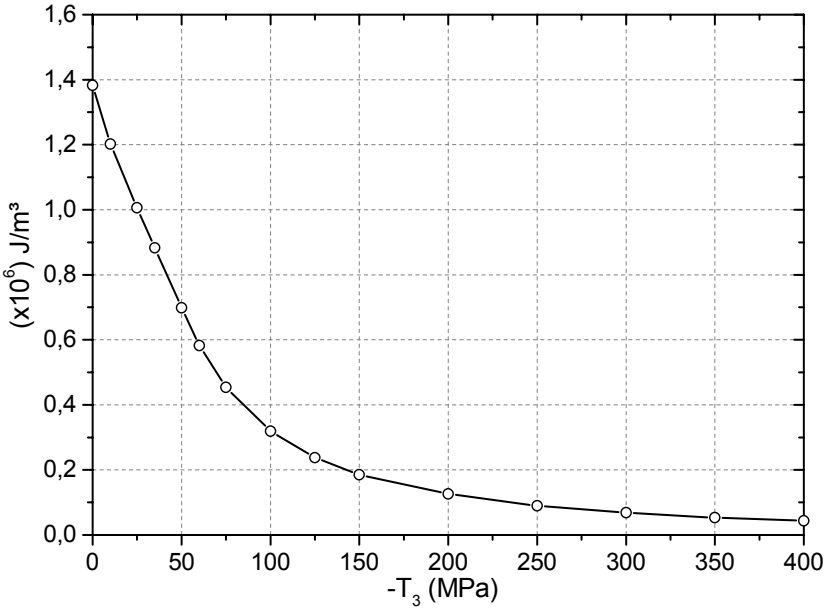

Figure 5.1.2. Change of polarisation dissipation energy with compression preload increment.

The dissipation energy is also named as energy loss, and it is directly related to the amount of domains, which could be reoriented by one cycle of electric field loading. From Fig. 5.1.2, it is clear that the amount of domains, which contribute to the polarisation reversal in one electric field loading cycle, non-linearly decreases with increasing prestress. At stress free state (T = 0 MPa), the dissipation energy is 1.382×10^6 J/m³; and at – 400 MPa, the dissipation energy decreases to 0.043×10^6 J/m³, which is nearly 30 times smaller than it at stress free state. As seen in Fig. 5.1.1, the corresponding P-E curve at – 400 MPa becomes a nearly straight line with very small hysteresis, which implies that there are rather few domains taking part in the polarisation reversal under such a high preload stress.

The resulting P-E hysteresis loops in Fig. 5.1.1 show a steady decrease of the remnant polarisation, saturation polarisation (at +/- 2 kV/mm) and coercive field as the compressive stress is increasing. The changes of the absolute values of remnant polarisation and coercive field with increasing prestresses are plotted in Fig. 5.1.3 and Fig. 5.1.4, respectively; where $+P_r$ and $-P_r$ symbolize positive and negative direction remnant polarisation, respectively; and $+E_c$ and $-E_c$ are defined as positive and negative direction coercive electric field, respectively.

Apparently, both of the remnant polarisation and coercive field non-linearly decrease with the increment of the superimposed compressive stress. For example, at the stress free state (T = 0 MPa), the $+P_r$ is 0.341 C/m², and it has the new value of 0.006 C/m² at – 400 MPa; whereas,

the - P_r is – 0.337 C/m² at 0 MPa, and it decreases to -0.010 C/m² at – 400 MPa. From Fig. 5.1.3, it can be seen that the changes of positive and negative remnant polarisation are approximately symmetric.

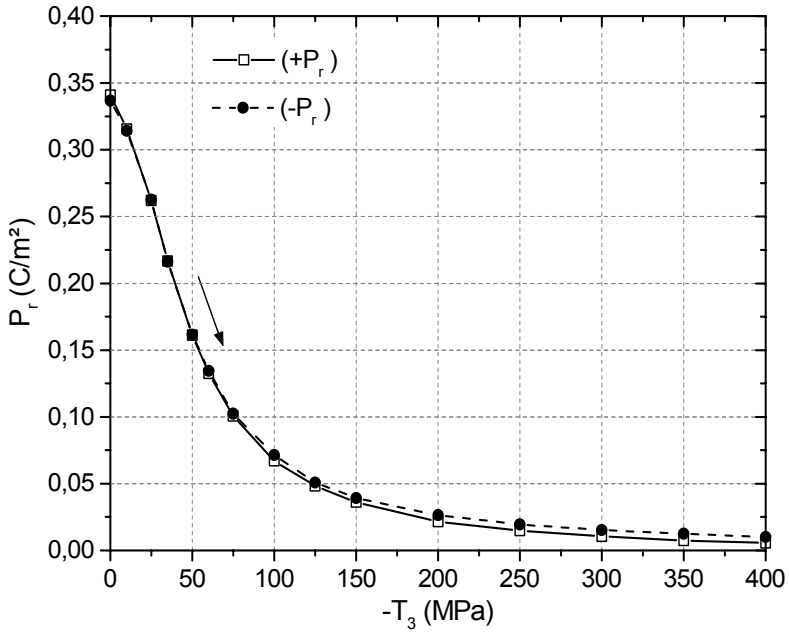

Figure.5.1.3. Changes of positive and negative direction remnant polarisation with increasing preload compressive stress.

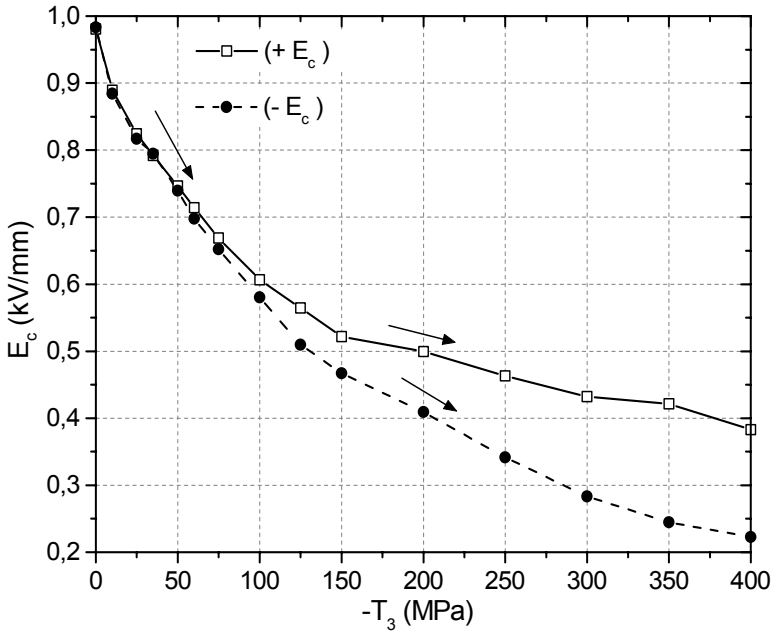

Figure.5.1.4. Changes of positive and negative direction coercive field with increasing preload compressive stress.

The positive direction coercive field (+ E_c) at stress free state is 0.981 kV/mm, and it decreases to 0.383 kV/mm at – 400 MPa. - E_c has the value of – 0.983 kV/mm at 0 MPa, and at – 400 MPa, it is – 0.223 kV/mm. The plots of +/- E_c in Fig. 5.1.4 indicate that the changes of positive and negative direction coercive field with increasing preload stress appear not to be symmetric. The negative direction coercive field (– E_c) decreases slightly significantly than + E_c. The same phenomenon has been observed in repeated experiments, while the reason is still not clear.

The experimental results of the changes of remnant polarisation and coercive field with increasing preloaded compressive stress are coincident with the work of Lynch for $(Pb,La)(Zr,Ti)O_3$ soft piezoceramic material [Lynch, 1996].

The decrease of the remnant polarisation with increasing preload stress is attributed to mechanical load induced depolarisation through non-180° ferroelastic domain switching processes, where domains are aligned orthogonal to the applied electric field. Summing up the plot of dissipation energy in Fig. 5.1.2, we can conclude that more and more domains are constrained with increasing preload compressive stress and can not be reoriented by the electric field to participate in polarisation reversal. Consequently, both of the remnant polarisation and the maximum polarisation at +/- 2 kV/mm become smaller and smaller with preload stress increasing.

At different prestress levels, the dielectric permittivity was approximately calculated by using Equation 5.1.1, which gives

$$\varepsilon_{33}(T) \approx \Delta D_3 / \Delta E_3 \tag{5.1.1}$$

where the electric field range was selected between – 0.1 kV/mm and + 0.1 kV/mm. Within such a small range, the calculated ε_{33} from Equation 5.1.1 is nearly equivalent to the slope of P-E curve as the electric field passes through zero. The calculated dielectric constant can be called a differential permittivity, which includes both of the reversible (intrinsic dielectric property) and irreversible (extrinsic domain switching related property) contributions of the material. Generally, the differential dielectric constant is significantly higher than the dielectric constant measured by a dynamic method, which is normally realized by measuring the response of material to a small AC signal superimposed on a substantial DC bias signal. The dynamic coefficients are mainly determined by the reversible effects [Yang et al., 2000]. The change of the differential dielectric constant with preload stress is illustrated in Fig. 5.1.5.

From Fig. 5.1.5, we can see that the magnitude of differential ε_{33} (slope of P - E curve at E = 0 kV/mm) depends on the preload stress levels. The relative dielectric constant at the stress free state is about 7400.

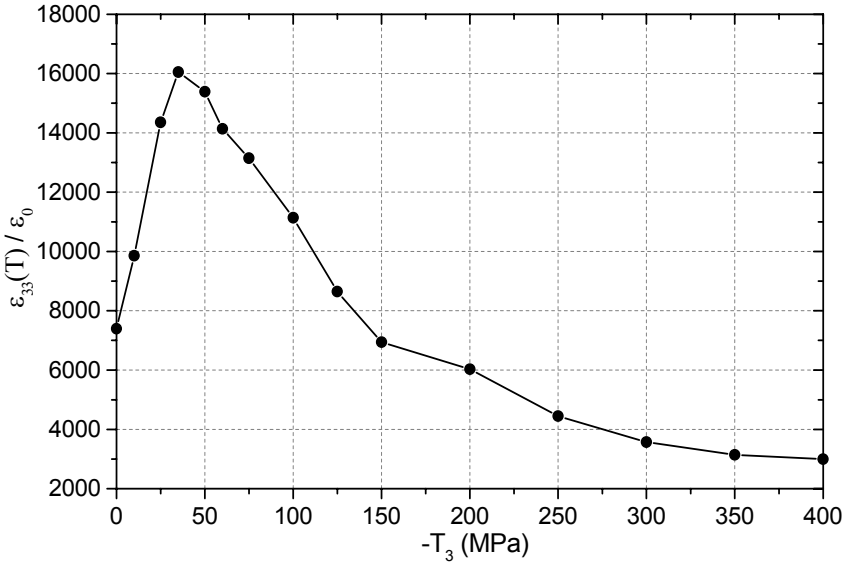

Figure 5.1.5. Change of relative dielectric constant (measured from the slope of P-E curves as E field passes through 0 kV/mm) with preload stresses.

Initially, it increases with increasing stress, until achieving a maximum value of $\varepsilon_{33}/\varepsilon_0 \approx 16000$ at – 35 MPa. Then, it steadily decreases with further prestress increments. At – 400 MPa, nearly all the domains have been aligned orthogonal to the electric field, and the corresponding relative permittivity is about 3000. The experimental results indicate that preload stress has significant influence on the dielectric property of ferroelectric materials.

2. *Strains vs. E field curves under different superimposed stresses*

The longitudinal strain (S_3) and the transverse strain (S_1) *vs*. electric field "butterfly" curves are measured simultaneously with the polarisation hysteresis loops at various prestress levels. The results are shown in Fig. 5.1.6 and Fig. 5.1.7, respectively.

One of the most notable features we can see from Fig. 5.1.6 and Fig. 5.1.7 is that, as the stress level is increased, the $S_3 - E_3$ curves are shifted to negative strain direction and the $S_1 - E_3$ curves are shifted to positive strain direction. We can also find that the downward/upward dips of the longitudinal/transverse strain *vs.* electric field curves become rounded and eventually flatten out. There are very little strains electrically induced at much higher stress

levels. In Fig. 5.1.8, non-linear changes of the remnant longitudinal and transverse strains (at E = 0 kV/mm) can be clearly observed with increasing stresses.

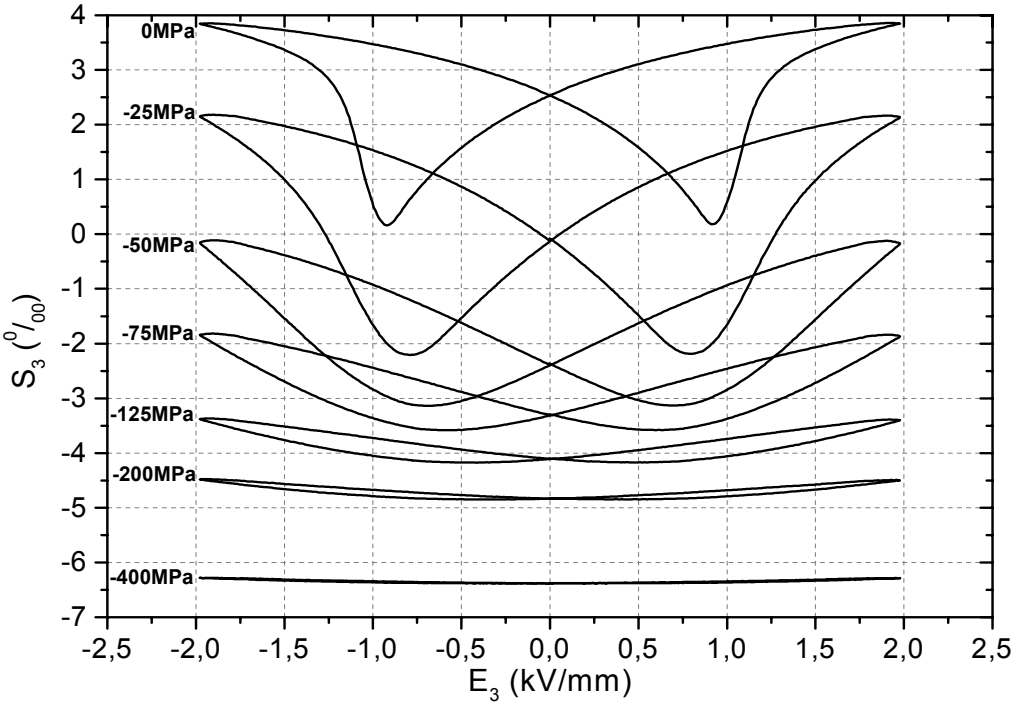

Figure 5.1.6. Longitudinal strain *vs.* electric field curves under different preload stresses.

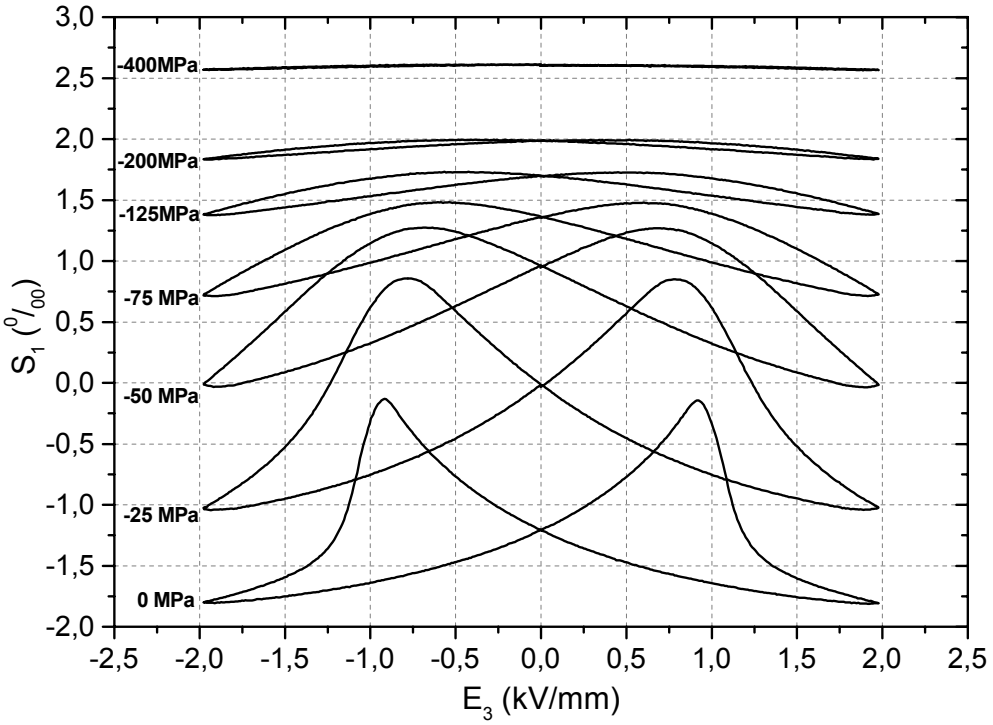

Figure 5.1.7. Transverse strain *vs.* electric field curves under different preload stresses.

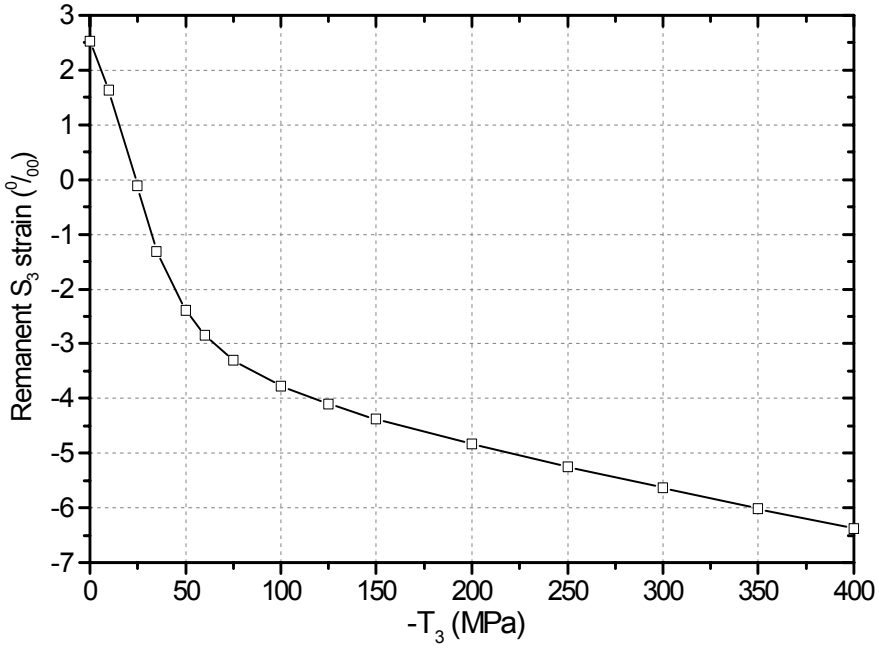

(a)

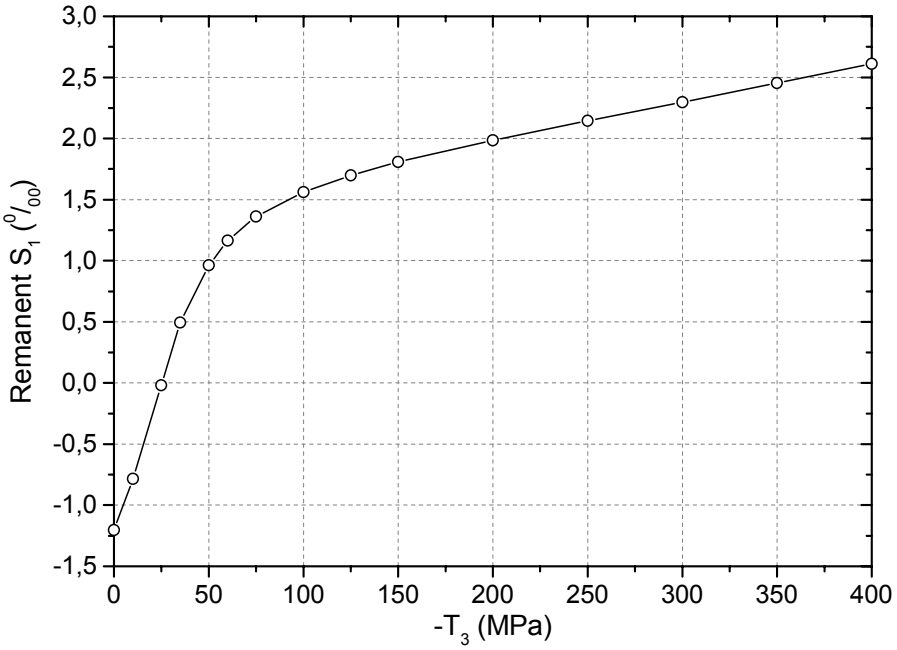

(b)

Figure 5.1.8. Changes of longitudinal (a) and transverse (b) remnant strains (the strain values at E = 0 kV/mm) with preload stresses.

As pointed out by Lynch, the superimposed compressive stress has two contributions to the total strain behavior. First, it induces elastic deformation, which will shift the entire longitudinal strain curves downward and move the transverse strain curves upward. The second contribution of preload stress is the ferroelastic non-180° domain switching. Besides

the effect of shifting the strain curves, the stress induced ferroelastic domain switching also has significant impact on the shapes of polarisation or strains *vs*. electric field hysteresis loops, dielectric permittivity and piezoelectric coefficients [Lynch, 1996].

The influence of the preload stress on the shapes of P-E and S-E curves can be clarified in terms of two successive non-180° domain switching processes. Chaplya and Carman have presented a similar explanation in one of their recent publications [Chaplya and Carman, 2001].

At the stress free state, when the E field is unloading from + 2 kV/mm to 0 kV/mm, most of the domains are preserved with their orientations parallel to the positive electric field loading direction (only a few unstable domains are switching back to their initial unpoled states). From 0 kV/mm, the first non-180° domain switching process starts in the material with a negative electric field application. When the negative coercive field (- E_c) is reached, the first non-180° switching process will be completed. The strain is found to achieve its minimum absolute value and the polarisation is zero. After - E_c, the second non-180° domain switching process begins, both polarisation and strain are observed to experience a "jump-like" increasing, and finally become saturated at higher electric field levels. (To simplify the discussion, here it is assumed that the polarisation and strain achieve their minimum values simultaneously. For a detailed discussion of this aspect, see section 3.1 in Chapter 3).

When a relatively small compressive stress is superimposed on the specimen (e.g., - 25 or - 50 MPa), the shapes of P - E and S - E curves are different from them at stress free state. Due to the compression load induced depolarisation, the resultant polarisation and strain at maximum E field (+/- 2 kV/mm) are apparently smaller than them at the stress free state. As discussed earlier, this is because some of the domains have been constrained orthogonal to the E field by the superimposed stress and can't be reoriented by the electric field with the maximum amplitude of +/- 2 kV/mm in this experiment. Unloading from + 2 kV/mm to 0 kV/mm, the preload stress will induce part of the first non-180° domain switching even before 0 kV/mm. As a result, we can see both of the polarisation and strain decrease more drastically than at stress free state. After 0 kV/mm, the negative E field acts together with the prestress to complete the residual first non-180° switching. Until the negative coercive field (- E_c) is reached, the polarisation and strain achieve their minimum values. The magnitude of coercive field with compressive stress preload is smaller than it at the stress free state. This is due to three reasons: (1) less amount of domains takes part in the polarisation reversal; (2) the preload stress destabilizes the poled state and leads to a part of the first non-180° domain

switching in the period of electric field unloading from +/- 2 kV/mm to 0 kV/mm; (3) the first non-180° switching process is completed by the combined action of E field and prestress. After E_c, the steadily increasing electric field load will act against the prestress to induce the second non-180° domain switching. Consequently, the polarisation and strain experience a more gradual development rather than a "jump" in the case of T = 0 MPa. With further preload stress increments, less and less domains take part in the polarisation reversal, and the resultant P-E and S-E curves become flat. For example, at – 400 MPa, the P-E curve is an approximately straight line and nearly no electrically induced strain change can be observed.

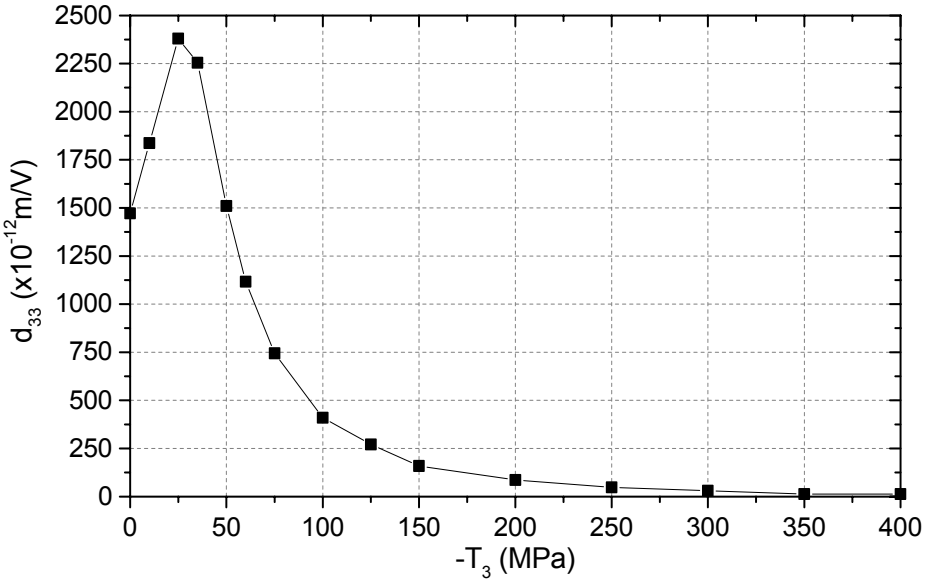

(a)

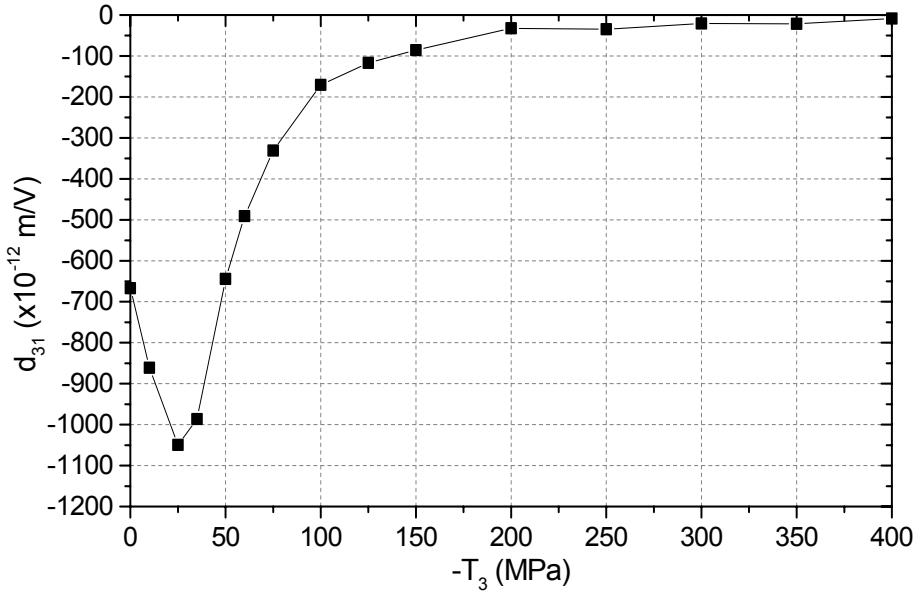

(b)

Figure 5.1.9. Changes of piezoelectric coefficients d_{33} (a) and d_{31} (b) with increasing superimposed compressive stress.

Similar to ε_{33}, two important piezoelectric constants d_{33} and d_{31} are calculated at different prestress levels by Equation 5.1.2, which gives

$$\begin{aligned} d_{33}(T) &\approx \Delta S_3 / \Delta E_3 \\ d_{31}(T) &\approx \Delta S_1 / \Delta E_3 \end{aligned} \tag{5.1.2}$$

Again, the electric field range was limited between – 0.1 kV/mm and + 0.1 kV/mm. Within this small range, the calculated d_{33} and d_{31} are nearly equal to the slopes of S_3-E_3 and S_1-E_3 curves as the electric field passes through zero.

The changes of d_{33} and d_{31} with various preload stress levels are plotted in Fig. 5.1.9. At the stress free state, the calculations give d_{33} = 1470 and d_{31} = - 670. Both d_{33} and d_{31} initially increase with increasing preload stress, and they achieve their maximum values at – 25 MPa with d_{33} = 2380 and d_{31} = - 1050. Afterwards, d_{33} and d_{31} non-linearly decrease with further preload increment and finally approach zero, which indicates that there is nearly no piezoelectric effect under such high compressive stress preload, e.g., from – 300 to – 400 MPa in this experiment.

So far, the influences of preload compressive stress on the polarisation and strain *vs*. electric field curves have been presented. From the plots of ε_{33}, d_{33} and d_{31} as a function of the preload stress, we can see that the superimposed stress has a significant impact on the piezoelectric and dielectric properties of a piezoceramic material. The general observation of all these plots is: the investigated coefficients initially increase with increasing preload stress, and after achieving a maximum value at a certain small stress level, then they steadily decrease with further stress increment. From the experimental results, we can imagine that the dielectric and piezoelectric properties can be enhanced by a preload stress within a small range, and the enhancement of the performance is attributed to the mechanical stress induced more extrinsic domain switching contributions.

More detailed experimental investigations and discussions of the enhanced high field dielectric and piezoelectric properties by small stress preload will be presented in the next section 5.2.

5.2 Uni-axial compressive stress dependence of high-field dielectric and piezoelectric properties of PZT ceramics

Modern actuators are tended to be used under severe conditions, i.e., high electric fields, low frequencies and large mechanical loads. Consequently, experimental investigations of the dielectric and piezoelectric properties of piezoceramics as a function of mechanical stress and/or electric field loading are necessary. The uni-axial stress dependence of the differential coefficients, i.e., ε_{33}, d_{33} and d_{31}, has been presented in the last section, where these coefficients were obtained from the slopes of P-E and S-E hysteresis loops in the neighbourhood of zero E field. In this section, the influence of a uni-axial compressive stress preload on the average coefficients of the material within a large electric field loading range will be outlined. These experiments are more important for the practical applications.

The measurements were performed on the initially unpoled PIC151 soft PZT ceramic material. With the help of the custom designed electromechanical coupling test fixture, the specimen was first poled by full electric field reversals (+/- 2 kV/mm, 0.08 kV/mm per second, 4 cycles). After poling, the sample possessed remnant polarisation and strains. Then, the specimen was preloaded to a specific constant compressive stress parallel to poling direction followed by the application of an alternating (ramp wave) E field. There were a total of five E field loading cycles under each constant stress level, and only the responses induced in the last cycle were used to plot the curves. The magnitude of the discretely preloaded constant stress was varied from 0 up to – 400 MPa, with a loading rate of 5 MPa/sec. between two steps. Electric field induced polarisation and strains were measured simultaneously to evaluate the dependence of the dielectric permittivity and the piezoelectric constants on the prestress values. Considering the time-dependence of the depolarisation and strains responses under a constant mechanical load, when the prestress was increased to a new magnitude, there was a hold time of 150 seconds before starting the electric field cycling. There were two sets of tests in this experiment: in the first set of tests, the electric field range was limited between 0 and + 2 kV/mm, which was exactly parallel to the pre-poling direction; and in the second set of tests, the electric field varied from – 0.4 kV/mm to + 2 kV/mm. This means that, from 0 to – 0.4 kV/mm or vice versa, the E field is anti-parallel to the pre-poling direction. However, since the coercive field of PIC151 soft PZT is about +/- 1 kV/mm, the second set of tests can be still considered in the range of piezoelectric response. The electric field loading rate was 0.08 kV/mm per second for all the measurements.

1. *Dielectric property in response to preload stress*

The polarisation *vs*. electric field curves under different compressive stress preloads are shown in Fig. 5.2.1.

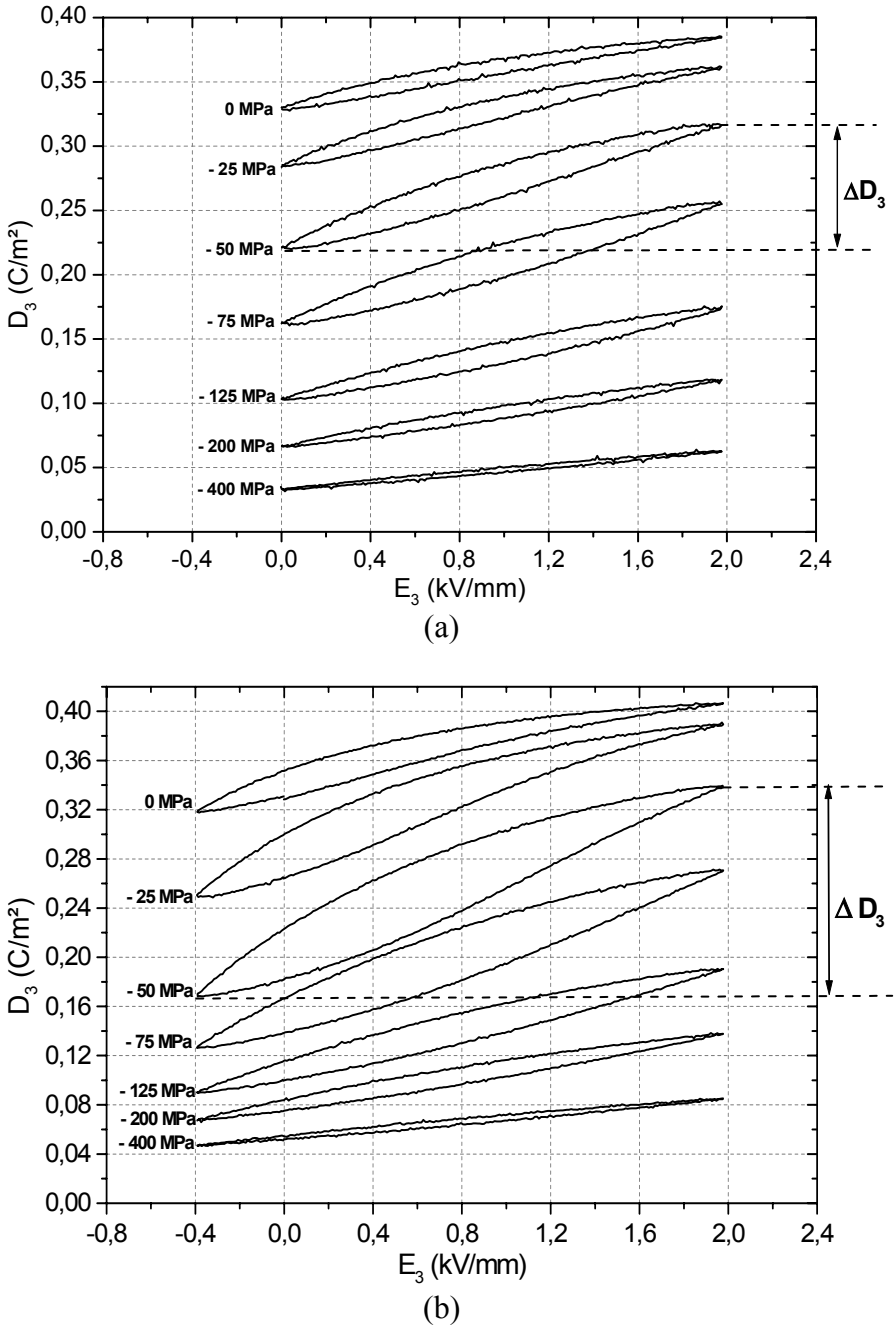

Figure 5.2.1. Polarisation versus electric field curves as a function of preload stress; (a) E field between 0 and + 2 kV/mm, and (b) E field between – 0.4 and + 2 kV/mm.

From Fig. 5.2.1, we can see that the maximum polarisation at + 2kV/mm as well as the minimum polarisation at 0 or – 0.4 kV/mm significantly decrease with increasing preload stress. This phenomenon should be attributed to the mechanical depolarisation, where non-

180° ferroelastic domain switching is induced by the preload stress. With the prestress level increasing, more and more domains are aligned orthogonal to the initial poling direction, leaving less and less domains available to contribute to the polarisation.

As shown in Fig. 5.2.1, the difference between the maximum polarisation at + 2 kV/mm and the minimum polarisation at 0 or – 0.4 kV/mm is defined as polarisation difference. The change of polarisation difference (ΔD_3) as a function of superimposed compressive stress is plotted in Fig. 5.2.2. For both of these two sets of tests, the ΔD_3 initially increases with increasing preload stress, and after achieving a maximum value at a specific stress level, the ΔD_3 will decrease with further prestress increment. In the first test ($0 \le E \le + 2$ kV/mm), ΔD_3 at the stress free state is 0.055 C/m², and it achieves its maximum at 60 MPa with the value of 0.096 C/m². In the second test (- 0.4 to + 2 kV/mm), the polarisation difference becomes prominently higher, e.g. ΔD_3 is about 0.088 C/m² at stress free state, and its maximum occurs at – 50 MPa with the value of 0.168 C/m². When the preload stress is higher than – 150 MPa, the polarisation difference becomes smaller than it at the stress free state.

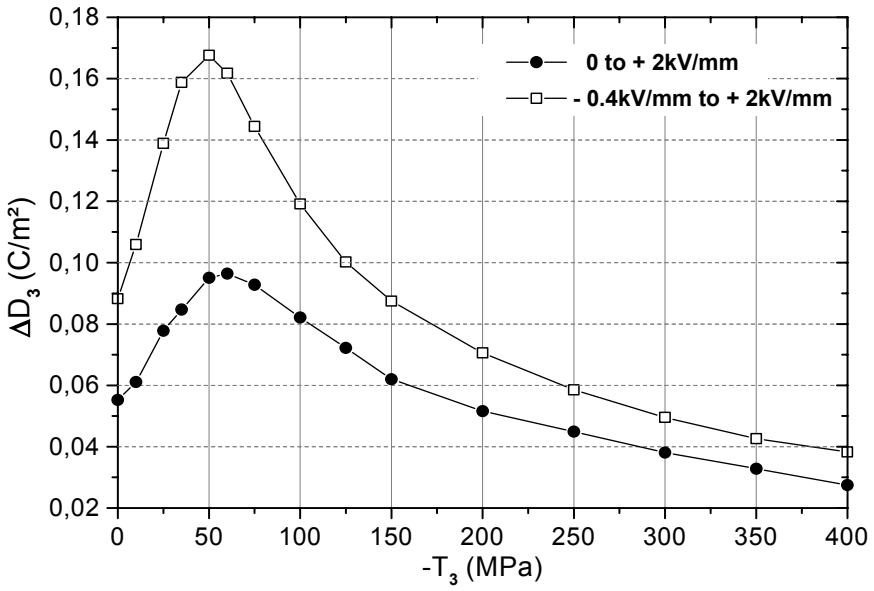

Figure 5.2.2. Polarisation difference between the maximum at + 2 kV/mm and the minimum at 0 or – 0.4 kV/mm as a function of preload compressive stress.

The high field dielectric permittivity can be calculated from the polarisation difference by a kind of linear approximation, which is given by

$$^{*H}\varepsilon_{33}(T) \approx \Delta D_3 / \Delta E_3 \qquad (5.2.1)$$

---

* superscript "H" for "high field"

where ΔE_3 is the electric field loading range, and T means different compressive stress preload conditions.

As pointed out by Viehland et al., such a kind of approximation has limitations, but is always used for materials performance estimation in transducer applications [Viehland, et al., 2001]. The variation of the dielectric permittivity as a function of the preload stress is plotted in Fig. 5.2.3.

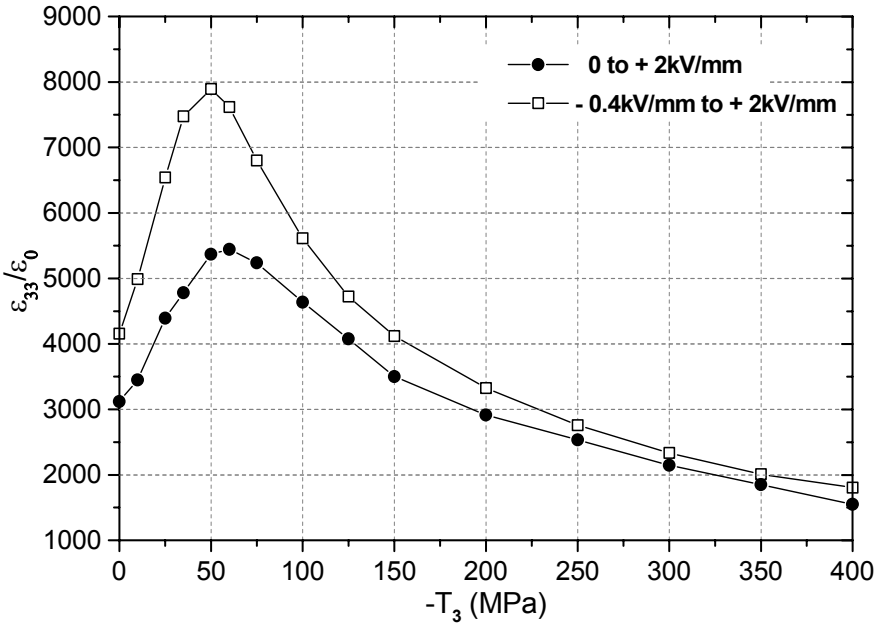

Figure 5.2.3. Relative dielectric constant calculated from the polarisation difference, in response to the preload compressive stress.

As seen in Fig. 5.2.3, similar to the behavior of ΔD_3, the superimposed constant compressive stress has a significant influence on the response of the high field dielectric constant. The value of relative dielectric constant $\varepsilon_{33}/\varepsilon_0$ first increases with increasing preloads; at a specific stress, the curves obtain a maximum value followed by a gradual decrease with further preload stress increments. For the first test, the relative dielectric constant at stress free state is about 3120, and it obtains its maximum at – 60 MPa with the value of about 5450. For the second test, the $\varepsilon_{33}/\varepsilon_0$ increases from about 4150 at 0 MPa to the maximum value of 7890 at – 50 MPa.

The experimental results from the polarisation measurement indicate that compressive stress preloads within a relatively small loading range can enhance the high field dielectric property of a piezoceramic material.

2. *Piezoelectric property in response to preload stress*

The longitudinal and transverse strains *vs*. electric field curves under different preload stresses are illustrated in Fig. 5.2.4 and Fig. 5.2.5, respectively. As discussed in the last section, the superimposed constant stress contributes to the strain response in two ways: one is the elastic deformation, and the other is ferroelastic non-180° domain switching. Due to these two effects, we can see that, with increasing of the preload stress, the longitudinal strain curves are shifted downward, whereas the transverse strain curves are moved upward.

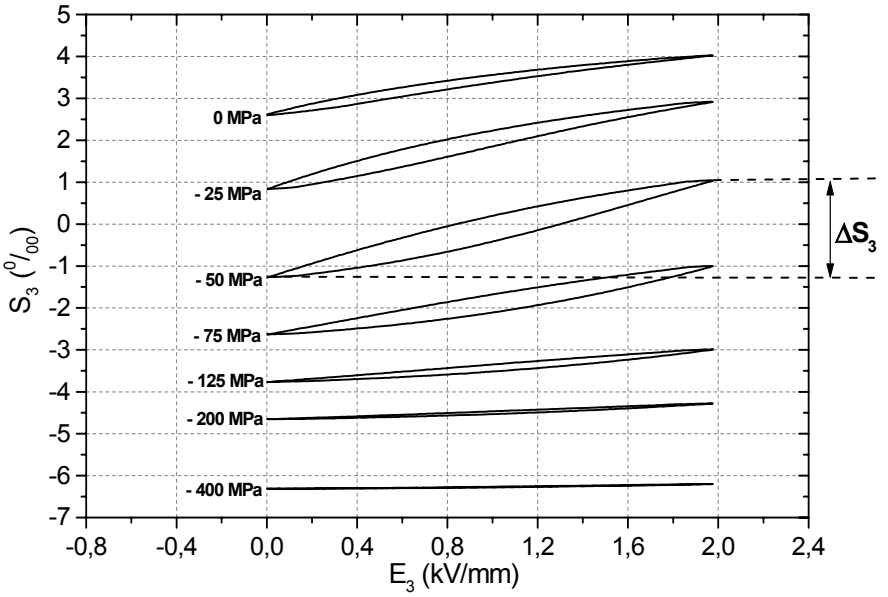

(a)

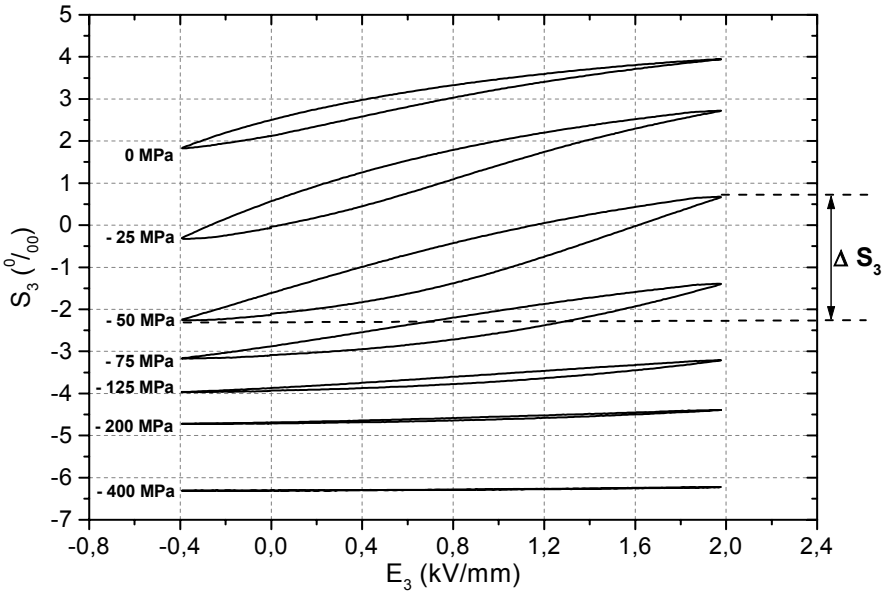

(b)

Figure 5.2.4. Longitudinal strain (S_3) versus electric field curves as a function of preload stress, (a) $0 \le E \le +2$ kV/mm, and (b) $-0.4 \le E \le +2$ kV/mm.

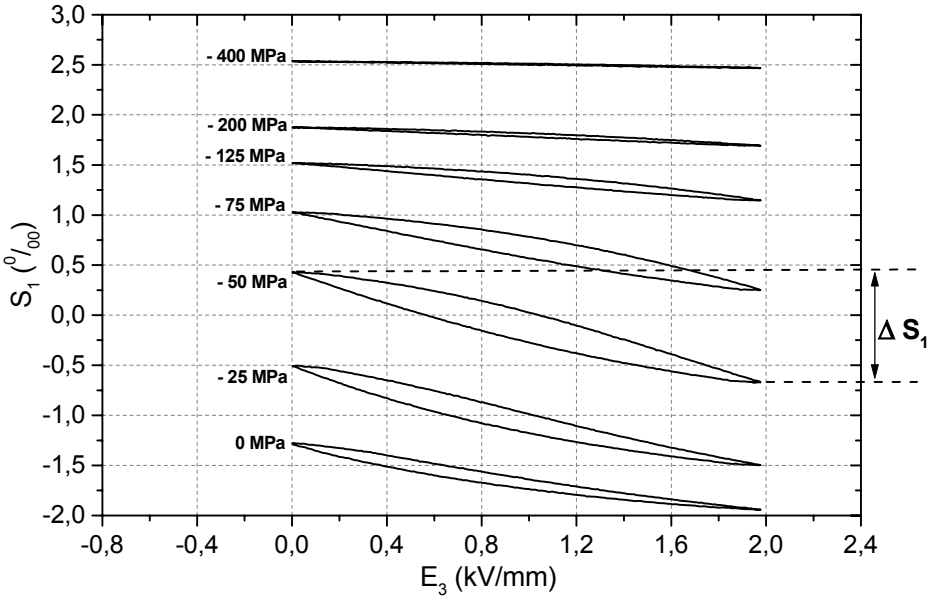

(a)

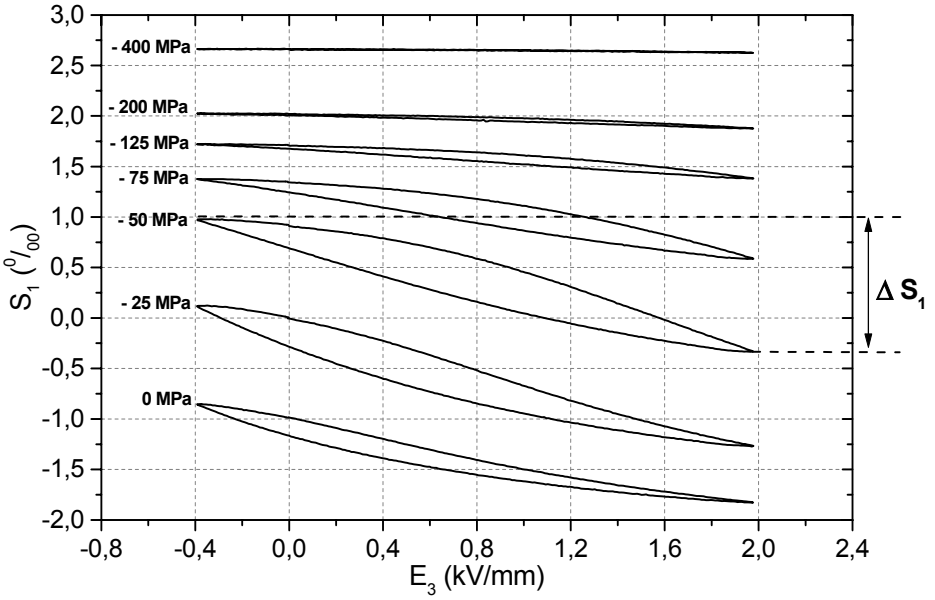

(b)

Figure 5.2.5. Transverse strain (S_1) versus electric field curves as a function of preload stress, (a) $0 \leq E \leq +2$ kV/mm, and (b) $-0.4 \leq E \leq +2$ kV/mm.

As illustrated in Fig. 5.2.4 and Fig. 5.2.5, the difference between the maximum strain at + 2 kV/mm and the minimum strain values at 0 or – 0.4 kV/mm is defined as high filed strain difference (ΔS), which is also called strain output in the literatures. The variation of the strain output is plotted in Fig. 5.2.6 as a function of the preload stress. Similar to the response of the polarisation difference (ΔD_3), both the longitudinal strain output (ΔS_3) and the transverse strain output (ΔS_1) initially increase with increasing stress, and after achieving their maximum

at a certain prestress value, both of them decrease with further stress increments. Within a small stress range, the strain output of the second test (- 0.4 ≤ E ≤ + 2 kV/mm) is evidently larger than it in the first test (0 ≤ E ≤ + 2 kV/mm). When the stress is higher than – 75 MPa, the strain outputs from these two tests become similar and decrease very quickly with increasing stress.

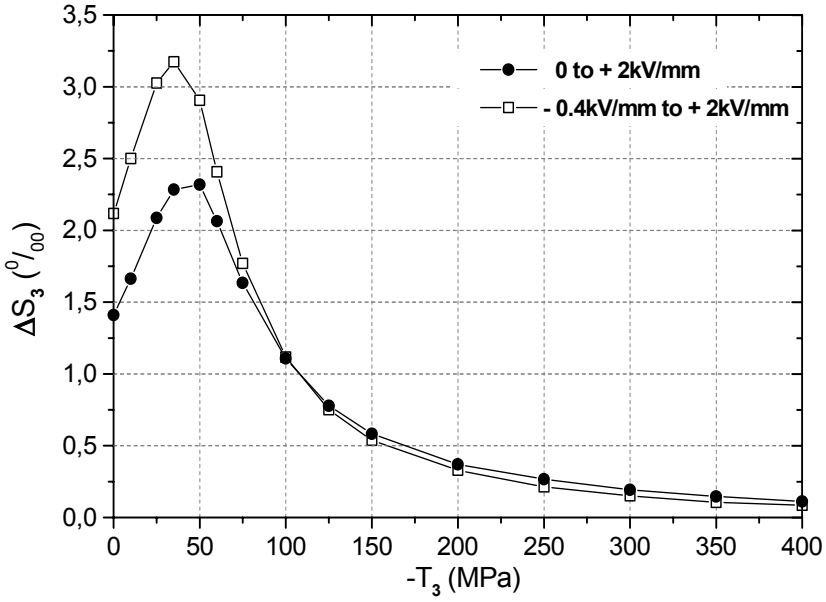

(a)

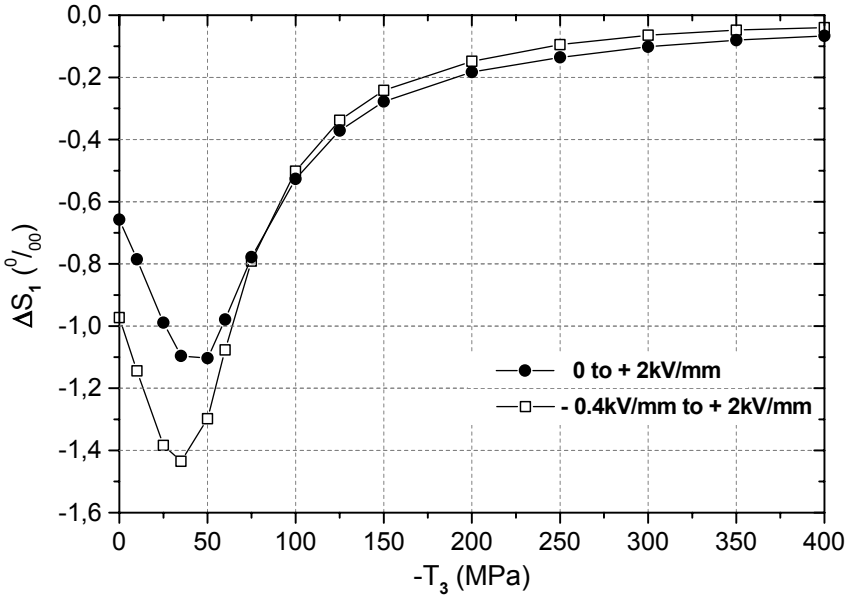

(b)

Figure 5.2.6. Strain difference between the maximum value at + 2 kV/mm and the minimum value at 0 or – 0.4 kV/mm as a function of preload compressive stress, (a) longitudinal strain difference, and (b) transverse strain difference.

Two piezoelectric coefficients, i.e. d_{33} and d_{31}, are calculated from the results of strain output by a linear approximation method:

$$^{H}d_{33}(T) \approx \Delta S_3 / \Delta E_3 \tag{5.2.2}$$

$$^{H}d_{31}(T) \approx \Delta S_1 / \Delta E_3 \tag{5.2.3}$$

Changes of d_{33} and d_{31} in response to preload stress are shown in Fig. 5.2.7.

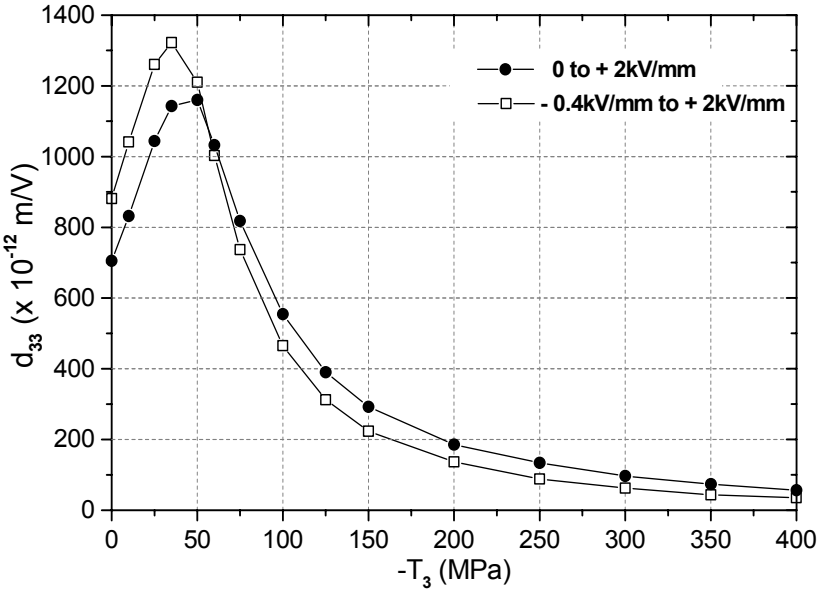

(a)

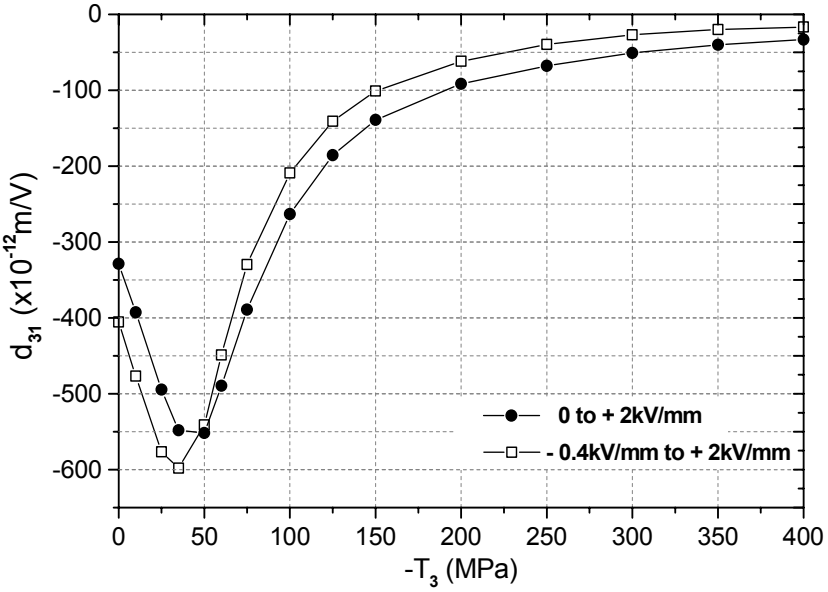

(b)

Figure 5.2.7. Piezoelectric charge constants d_{33} (a) and d_{31} (b) calculated from strain difference as a function of the superimposed compressive stresses.

The piezoelectric constants d_{33} and d_{31} are initially enhanced with an increase of mechanical preload, and after obtaining their maximum at a specific prestress, both of them decrease drastically with increasing stress. When the compressive stress is higher than – 200 MPa, as shown in Fig. 5.2.7, these two coefficients become very small, which indicates that there is nearly no piezoeffect present under such high stress preload conditions.

For the first test ($0 \leq E \leq + 2$ kV/mm), d_{33} and d_{31} at the stress free state are 705 and - 330, respectively. They obtain their maximum at - 50 MPa with the values of 1160 and - 550, respectively. For the second test ($- 0.4 \leq E \leq + 2$ kV/mm), at the stress free condition, d_{33} and d_{31} are 880 and - 405, respectively, and they achieve their maximum values of 1320 and - 600 at – 35 MPa, respectively.

Similar to the earlier presentation of the dielectric property, the experimental results of the strain measurements and the further evaluation of the piezoelectric coefficients (d_{33} and d_{31}) indicate that the high field piezoelectric properties of PZT ceramics can also be enhanced by small compressive stress preload.

3. *Discussion*

The results of enhancement of the high field dielectric and piezoelectric performance by small stress preload are consistent with several recently published experimental works, in which the response of PZT ceramics was evaluated by similar methods like this work [Viehland, et al., 2001; Chaplya and Carman, 2001; Mitrovic, et al., 2001]. In the work of Yang et al., a dynamic small stress was superimposed on the static constant compression load, and by measuring the change of polarisation *vs*. dynamic small stress at different preload stress levels, the influence of prestress on the piezoelectric coefficient d_{33} could be characterized. They also confirmed the phenomenon of small prestress enhanced piezoeffects for both soft and hard PZT ceramics [Yang et al, 2000]. These authors attributed this interesting phenomenon to larger extrinsic contribution, which is mainly derived from more non-180° domain switching induced by combined electromechanical loading.

Zhang et al. provided evidence that, at room temperature and stress free condition, the piezoelectric response of PZT ceramics included both intrinsic and extrinsic contributions. The intrinsic contribution corresponds to the response of a single domain crystal under appropriate conditions. All other contributions, which derive mainly from non-180° domain switching in a ceramic material, constitute the extrinsic part of the response. Extrinsic domain switching was found to make the major contribution to the dielectric and piezoelectric

responses of PZT ceramic materials, while the intrinsic dielectric and piezoelectric contributions are less than 25% and about 37% of the total response for soft PZT, and 30% and 33% for pure PZT at MPB [Zhang et al., 1988, 1994].

To understand the experimental results, a tentative explanation will be given in terms of non-180° domain switching processes induced by combined electromechanical loading. For convenience of the discussion, the corresponding domain configurations under different stress preloads are pictorially presented in Fig. 5.2.8, where the dashed line rectangle represents the original sample dimension at initially unpoled state.

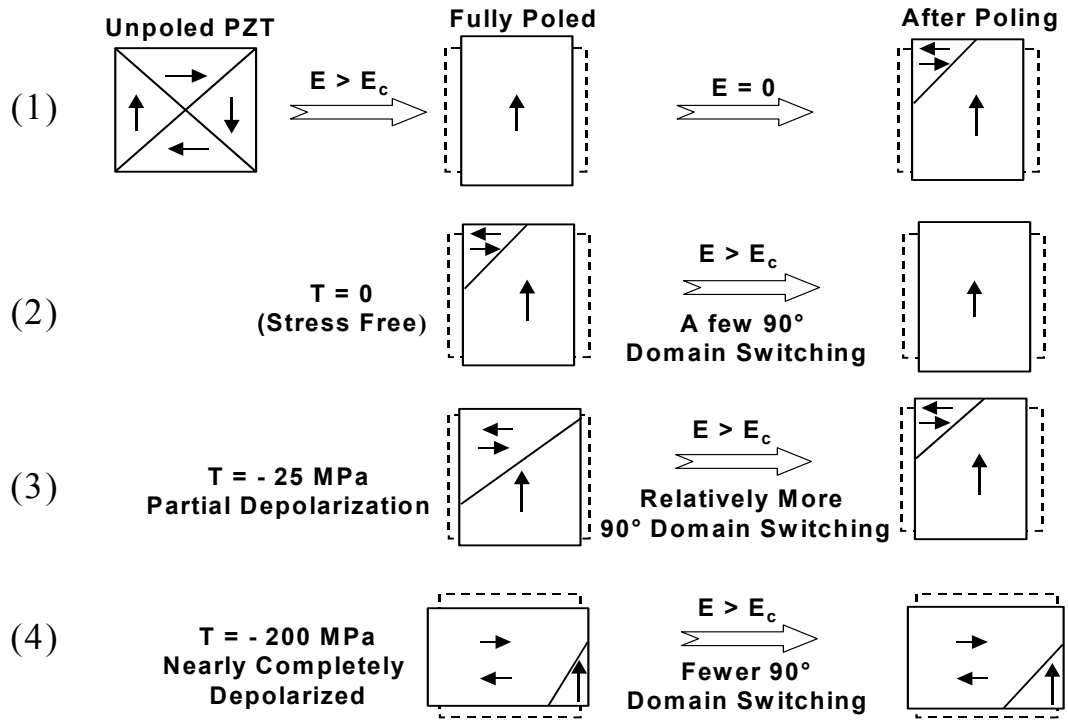

Figure 5.2.8. Domain switching processes corresponding to different compressive stress preload conditions.

As shown in Fig. 5.2.8, at the stress free state (T = 0 MPa), the initially unploed PZT ceramic material can be fully poled through the application of a sufficiently high electric field. Ideally, all the domains can be considered being aligned parallel to the poling direction (state ①). After poling, due to internal stresses, there will be some unstable domains switching back to their initially unpoled states. Further cyclic electric field loading will repeatedly realign these domains to the poling direction (state ②). Therefore, the resultant P-E and S-E curves do not really show a linear response, rather exhibit a slight hysteresis and non-linearity (see Fig. 5.2.1, 5.2.4 and 5.2.5). In case of the second set of E field cyclic loading tests ($-0.4 \le E \le +2$ kV/mm), the hysteresis of the curves is more pronounced than it in the first set of tests ($0 \le E \le +2$ kV/mm). This is due to

some electric depolarisation induced by the anti-parallel negative E field loading from 0 to – 0.4 kV/mm, where some domains are orientated orthogonal to the poling direction.

With a small compressive stress superimposed on the specimen (e.g., - 25 MPa at state ③), the stress will induce mechanical depolarisation. In contrast to the stress free condition, more domains are aligned orthogonal to the applied load. The following applied high E field will reorient most of the domains again parallel to the poling direction. Apparently, with a small stress preload, there are more repeated non-180° domains switching during the cyclic E field loading process, resulting in larger polarisation difference and strain output. The dielectric and piezoelectric performances are consequently enhanced. At the same time, the larger amount of non-180° domain switching also leads to more significant non-linearity and hysteresis in the corresponding polarisation and strain curves. In the second set of tests, the negative electric field and prestress orient the domains in the same way to increase the amount of domains orthogonal to the load. As a result, more non-180° domains are available for switching under cyclic E field loading than in the first set of tests, and consequently, the enhanced performance and the hysteresis of the curves also become more pronounced. We can see that the calculated dielectric constant (ε_{33}) and piezoelectric coefficients (d_{33} and d_{31}) in the second set of tests are evidently higher than the values obtained from the first set of tests at the same prestress level.

When the preload stress becomes much higher (e.g., - 200 MPa at state ④), the mechanical depolarisation becomes prominent, most of the domains are aligned perpendicular to the applied load and constrained by the high compressive stress. Subsequent electric field loading with the maximum amplitude of + 2 kV/mm in this experiment is insufficient to overcome the stress. Consequently, fewer domains can be reoriented to contribute to polarisation and strain. The resultant piezoelectric responses become neglectable, and at the same time, the corresponding P - E and S - E curves display quite slight hysteresis.

So far, the reason of the enhancement of the high field dielectric and piezoelectric properties by small stress preload has been clarified. For piezoelectric actuators utilized under stringent conditions, i.e. high mechanical stress and high AC electric field, the enhanced electromechanical performance must be considered to model the real response of devices and to optimise the operating conditions.

However, as seen in the polarisation and strain *vs*. electric field curves, the enhanced material responses are found to be accompanied by relatively significant hysteresis and non-linearity. The larger hysteresis of polarisation *vs*. electric field curves corresponds to higher energy losses

(dissipation energy). The energy loss in one electric field loading cycle can be determined by integrating the area of P - E hysteresis loops. For the second set of tests (- 0.4 ≤ E ≤ + 2 kV/mm), the calculated energy loss is plotted in Fig. 5.2.9 as a function of preload stress.

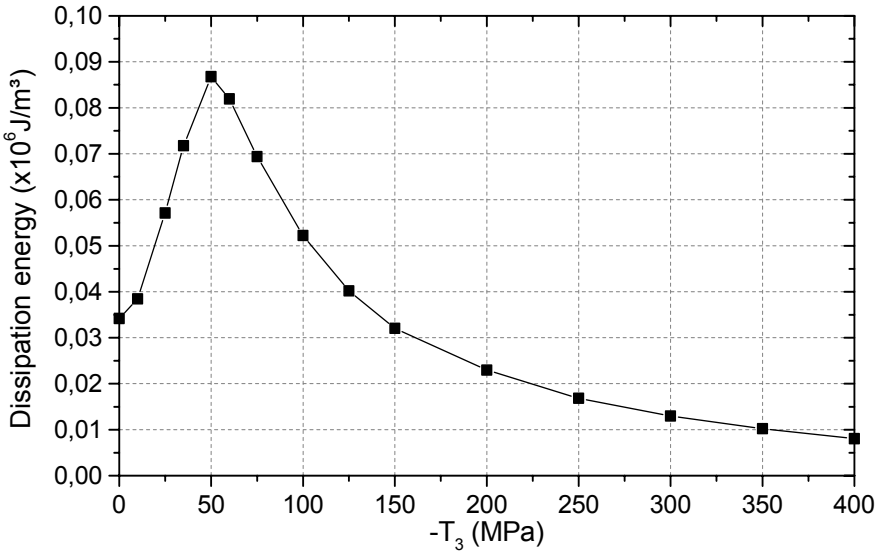

Figure 5.2.9. Energy loss obtained from the P - E curves in the second set of tests (- 0.4 ≤ E ≤ + 2 kV/mm) as a function of preload stress.

In Fig. 5.2.9, we can see the dissipation energy (energy loss) initially increases with increasing preload stress, after achieving maximum at – 50 MPa with the value of 0.087×10^6 J/m³, then decreases with further stress increments. The results of this investigation demonstrate that the maximum dielectric and piezoelectric performances are associated with the maximum energy loss. As pointed out by Viehland et al., this energy loss is so high such that in fact it may not be acceptable for current thermal management technologies in transducer design. In addition, the significant non-linearity will also introduce harmonic distortion into the electrical and acoustic signals, reducing the effective coupling realizable in transducer devices [Viehland, et al., 2001].

The enhanced performance achieved by small stress preloads is due to the contribution of more extrinsic non-180° domain switching. When the materials are used to achieve large displacement through domains switching, one of the important features that needs to be addressed is the long-term fatigue. The electromechanical fatigue from domain switching can degrade the electromechanical properties of PZT materials [Mitrovic, et al., 2001].

Therefore, for practical actuator design and applications, the thermal stability and long-term reliability should be cautiously considered in the context of enhanced electromechanical performance.

5.3 Effects of bias electric field on the non-linear stress-depolarisation and stress-strain responses of PZT ceramics

The response of piezoelectric ceramics under purely mechanical stress loading has been investigated by several researchers. At high stress levels, the materials display large non-linearities with distinct irreversible strain and depolarisation (if the material is polarized) present after unloading. The observed non-linear behavior was explained in terms of mechanical stress induced ferroelastic domain switching processes (for more details see Chapter 4). However, direct measurement of stress-strain/depolarisation behavior with high bias electric field is still rare.

In this section, the experimental results for the effects of constant preload electric field on the non-linear stress-strain/depolarisation responses of PIC151 soft PZT ceramic material will be presented. This comprehensive experimental investigation will provide more information to study the non-linear behavior of piezoceramics, and also give helps to select appropriate working conditions of multilayer actuators.

An initially unpoled PIC151 soft PZT specimen was first subjected to four full cycles of electric field loading (+/- 2 kV/mm, 0.08 kV/mm per second). After poling, the material possessed remnant polarisation and strain. Then three subsequent ramp-shaped loading-unloading cycles by a compressive stress were applied to the sample under short-circuit condition, with the amplitude of – 400 MPa and a loading rate of 5 MPa/sec.. The changes of polarisation and longitudinal/transverse strains were monitored simultaneously. After the end of stress loading, the specimen was repoled again by four full cycles of electric field loading to remove the mechanical load induced strain and to recover the material to original poling configuration. After repoling, a bias electric field was applied to the specimen followed by three cycles of stress loading again. The same procedure was repeated for the measurement under each new bias E field loading. Due to the time-dependence of polarisation and strain responses under a constant electric field, when the superimposed E field achieved a new level, there was a hold time of 150 seconds before starting the stress load.

In this experiment, the polarisation state after poling is negative. Therefore, a bias E field with negative value indicates that it acts in the same direction of the initial poling state, whereas a positive field is acting oppositely to the poling direction. The maximum magnitude of the positive bias E field was chosen as + 0.50 kV/mm. This is about half of the material's coercive field ($E_c \approx$ +/- 1 kV/mm for PIC151 soft PZT), such that domain switching processes induced by bias electric field alone (electric depolarisation) are neglectable.

1. *Response of stress-depolarisation behavior to bias electric field*

Fig. 5.3.1 shows a series of plots of compressive stress versus depolarisation curves obtained at different bias electric field conditions. In order to get a better illustration, the loading and unloading curves were plotted separately and only the results of the first stress cycle are presented.

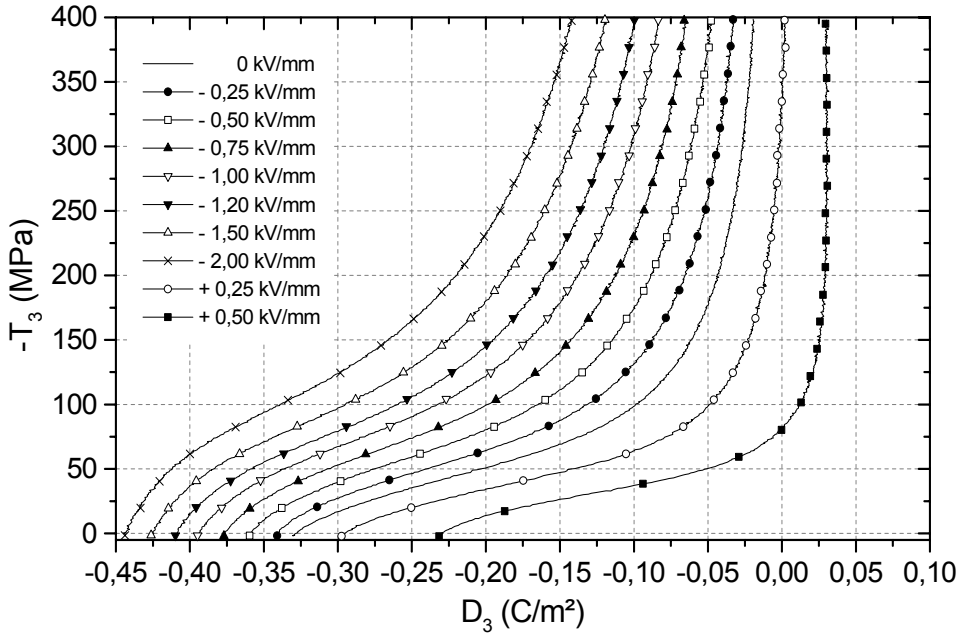

(a)

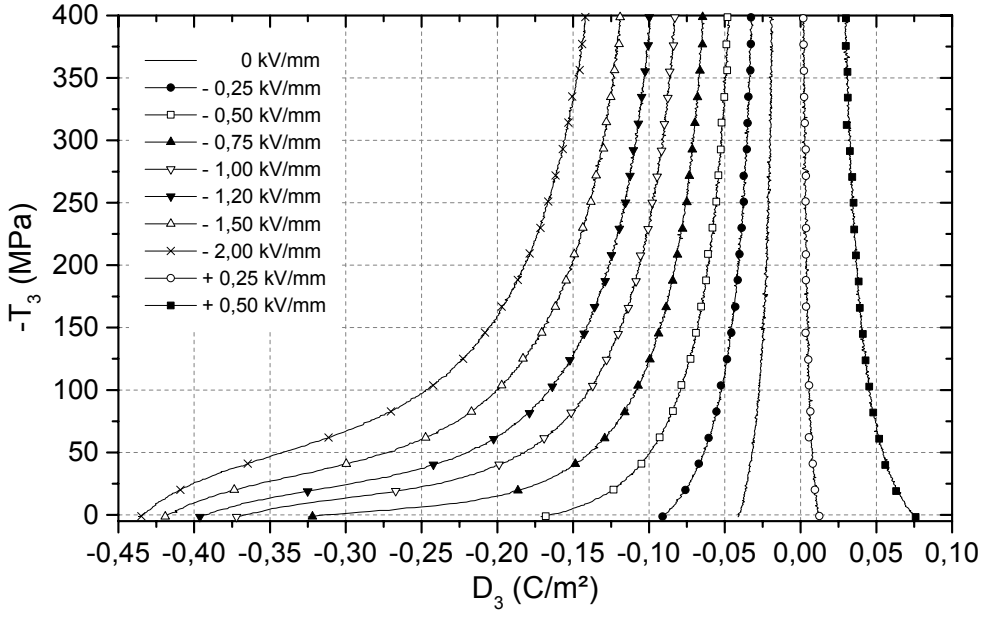

(b)

Figure 5.3.1. Compressive stress induced depolarisation of PIC151 soft PZT under different bias electric fields. (a) stress increasing from zero to – 400 MPa, and (b) stress decreasing from – 400 MPa to zero.

At short-circuit condition (E_{bias} = 0 kV/mm), the initial remnant polarisation before stress loading is – 0.330 C/m². With stress loading increment, we observe a non-linear depolarisation curve, which is due to the compressive stress induced non-180° domain switching orthogonal to the original poling direction. The final remnant polarisation at – 400 MPa is – 0.019 C/m², i.e. nearly 94% of the polarisation is removed. During the stress unloading process from – 400 MPa to zero, at first we can observe a vertical straight line; when the stress is lower than – 250 MPa, the curve becomes slightly non-linear, and some of the polarisation is recovered. The final polarisation at T = 0 MPa is – 0.041 C/m².

With a negative constant electric field bias on the specimen (same direction to the initial poling), the beginning polarisation before stress loading increases with preload E field magnitude increment, e.g., the beginning polarisation with – 2 kV/mm electric field bias is about – 0.444 C/m², which is significantly higher than the value at short-circuit condition (E_{bias} = 0 kV/mm). The total polarisation in this experiment can be expressed as:

$$D_3 = \varepsilon_{33} E_3 + P_r + d_{33} T_3 \tag{5.3.1}$$

Where $\varepsilon_{33}E_3$ represents the linear dielectric contribution, P_r corresponds to the domain switching related polarisation, and $d_{33}T_3$ is the direct piezoeffect.

The increment of initial polarisation with increasing negative bias E field is attributed to: (1) a larger dielectric contribution ($\varepsilon_{33}E_3$), (2) time-dependence of polarisation (P_r) under the constant electric field preload, more domains are aligned to the poling direction.

From the tendency of the curves in Fig. 5.3.1 (a), we can find that the development of depolarisation induced by a compressive stress becomes gradually more and more difficult with the negative bias E field increasing. At – 2 kV/mm, as the stress increases up to – 400 MPa, the remnant polarisation is still as high as – 0.142 C/m², only about 68% polarisation is removed by the stress.

As pointed out by Kamlah in his review article, an electric field acting in the direction of previous poling has the trend to support the existing domain state. Therefore, higher stresses are needed to initiate and forward mechanically caused domain switching processes [Kamlah, 2001].

As illustrated in Fig. 5.3.1 (b), during the stress unloading process from – 400 MPa to 0, the negative bias E field will try to restore the original domain configuration prior to stress loading. As a result, part of the polarisation is recovered after the stress reduced to zero, and this polarisation recovery phenomenon becomes more and more pronounced with negative bias E field increment. For example, at constant bias E = - 2 kV/mm, the final polarisation

after one stress loading cycle is about – 0.435 C/m². Comparing this value with the initial polarisation before stress loading (- 0.444 C/m²), we can see that nearly all the polarisation is recovered by such a high superimposed E field.

An electric field acting opposite to the initial poling direction (i.e. positive superimposed E field in this work) will work together with the compressive stress to destabilize the domain state. Consequently, compressive stress induced switching processes become easier than at zero-bias electric field.

As shown in Fig. 5.3.1 (a), with application of a positive bias electric field, the beginning remnant polarisation prior to stress loading becomes smaller than at zero-bias E field. From Equation 5.3.1, this smaller initial polarisation is due to: (1) the dielectric contribution ($\varepsilon_{33}E_3$) and P_r have opposite signs, (2) a long time positive E field load induces some non-180° domain switching orthogonal to the prepoling direction. The initial polarisation at E_{bias} = + 0.50 kV/mm is about – 0.232 C/m². A non-linear depolarisation curve is observed with loading stress increment. When the stress is increased up to about – 80 MPa, the polarisation passes through zero and then becomes positive with increasing stress. After – 200 MPa, the variation of the curve is saturated, and no more polarisation changes with further stress increment. In this case, we can imagine that the stress-induced domain switching processes are nearly completed and the corresponding polarisation is mainly from the dielectric contribution ($\varepsilon_{33}E_3$). The polarisation at – 400 MPa is + 0.030 C/m². As the compressive stress unloading from – 400 MPa to zero, some domains will be oriented to positive direction with the help of positive bias E field. Consequently, we observe the polarisation becomes slightly higher during the unloading process. The final polarisation after one stress loading cycle is about + 0.076 C/m².

Full cycle stress-depolarisation curves at several selected bias E field levels are shown in Fig. 5.3.2. As discussed earlier, with the increase of negative bias electric field, more and more depolarisation is recovered during the stress unloading process. Consequently, the depolarisation curves are effectively closed. At – 2 kV/mm, a nearly completely closed stress-depolarisation hysteresis loop is obtained.

Recovery of the remnant polarisation after one stress loading cycle is significantly depending on the bias electric field magnitude. The polarisation difference between the initial values prior to stress loading and the final values right after one cycle stress loading is plotted versus bias E field in Fig. 5.3.3. Apparently, when the bias electric field is higher than the coercive

field of this material ($E_c \approx$ +/- 1 kV/mm), most of the stress-induced depolarisation can be restored after removal of the stress.

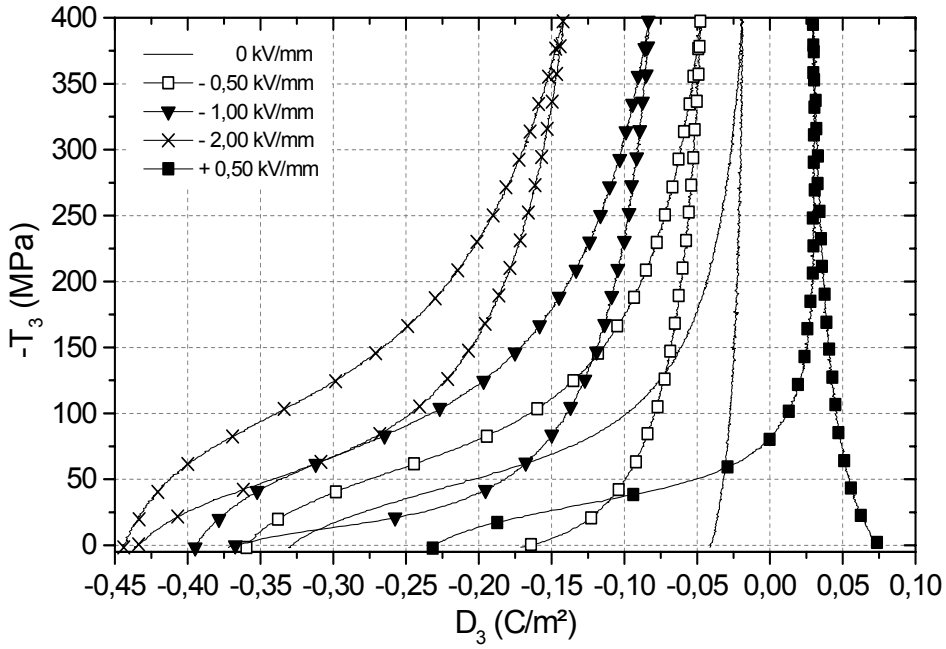

Figure 5.3.2. Compressive stress induced depolarisation curves of the first stress loading-unloading cycle, bias electric fields of 0, - 0.50, - 1.00, - 2.00 and + 0.50 kV/mm are selected for comparison.

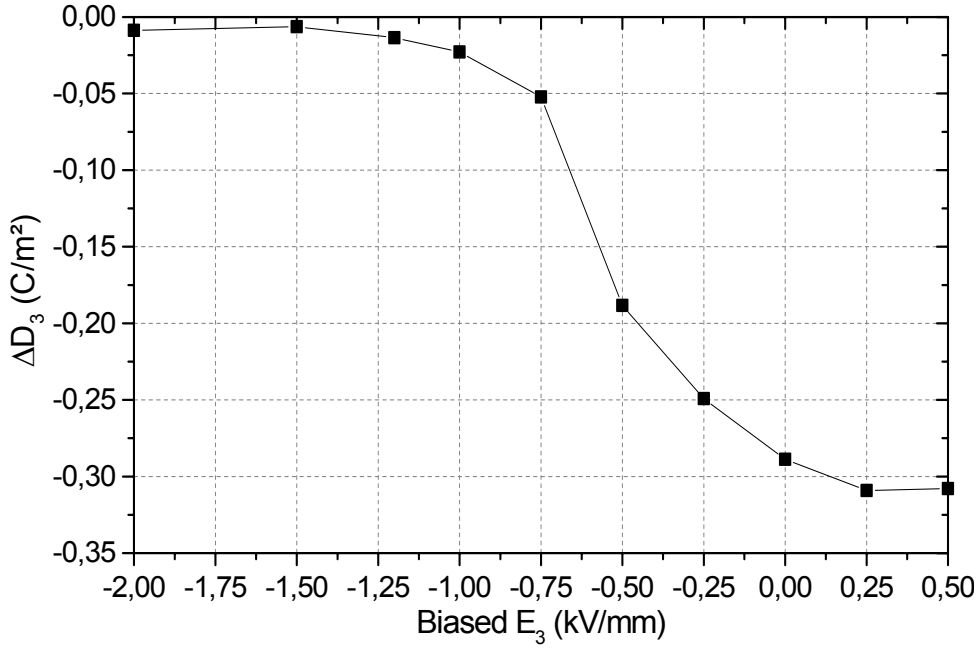

Figure 5.3.3. Difference of polarisation prior to mechanical stress loading and right after one cycle stress loading, in response to bias electric field.

2. *Response of stress-strain behavior to bias electric field*

A series of plots of stress-longitudinal strain and stress-transverse strain curves at different constant bias electric field levels are given in Fig. 5.3.4 and Fig. 5.3.5, respectively. The loading and unloading sections are plotted separately again for the reason of better illustration.

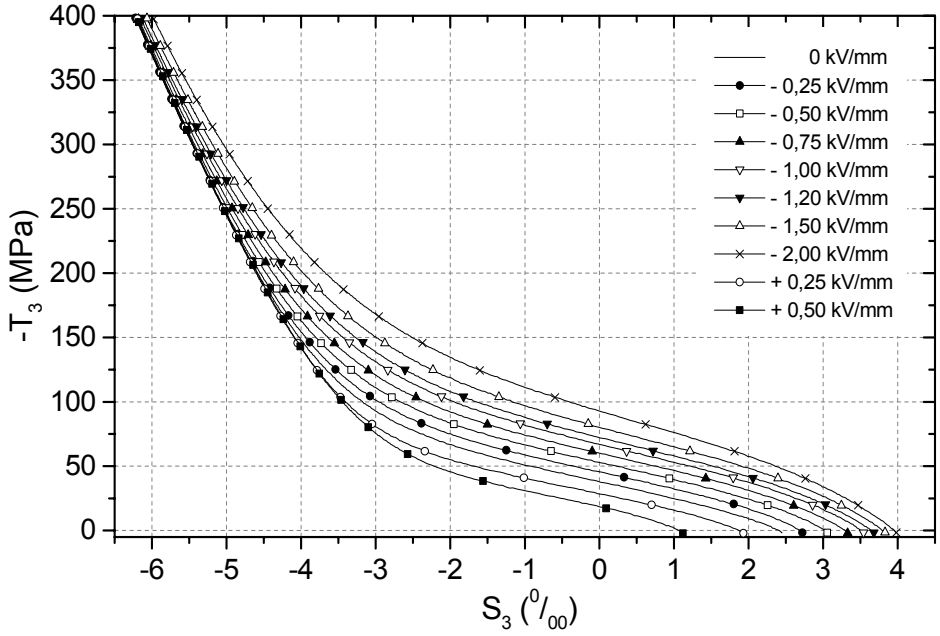

(a)

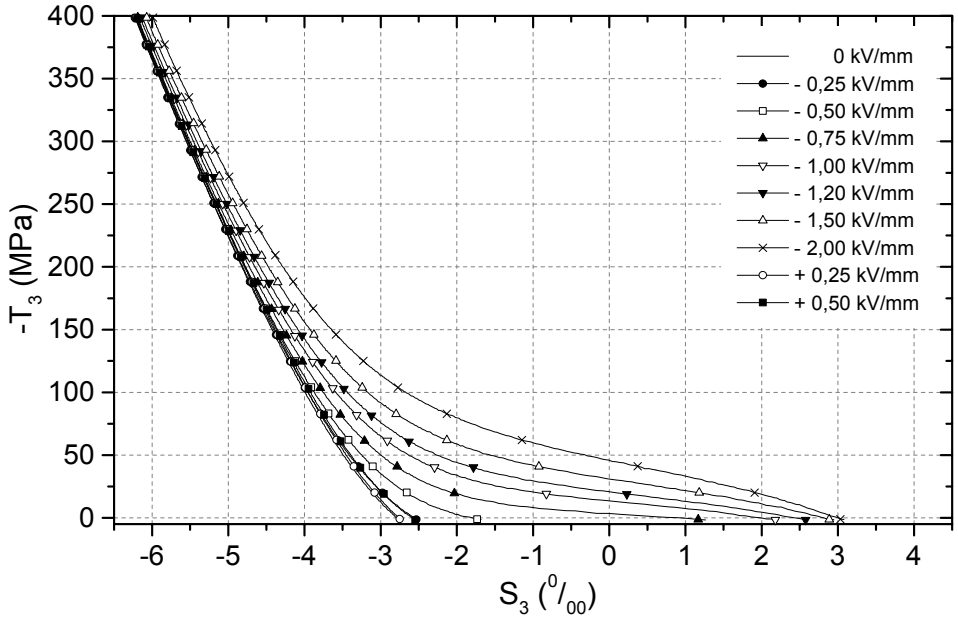

(b)

Figure 5.3.4. Longitudinal strain (S_3) in response to the first cycle of compressive stress (T_3) loading with different constant electric fields superimposed. (a) Stress loading from zero to - 400 MPa, and (b) Stress unloading from – 400 MPa to zero.

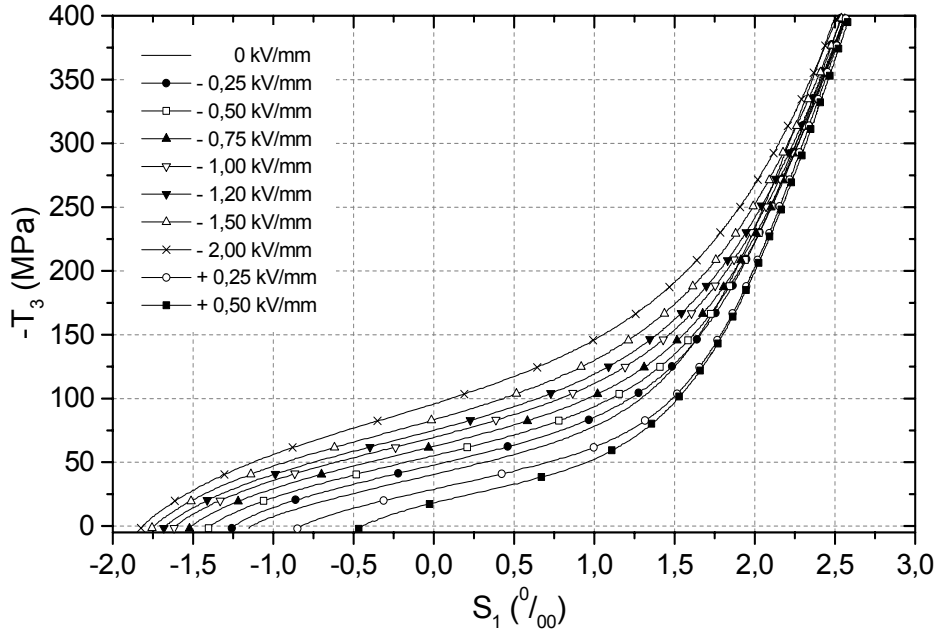

(a)

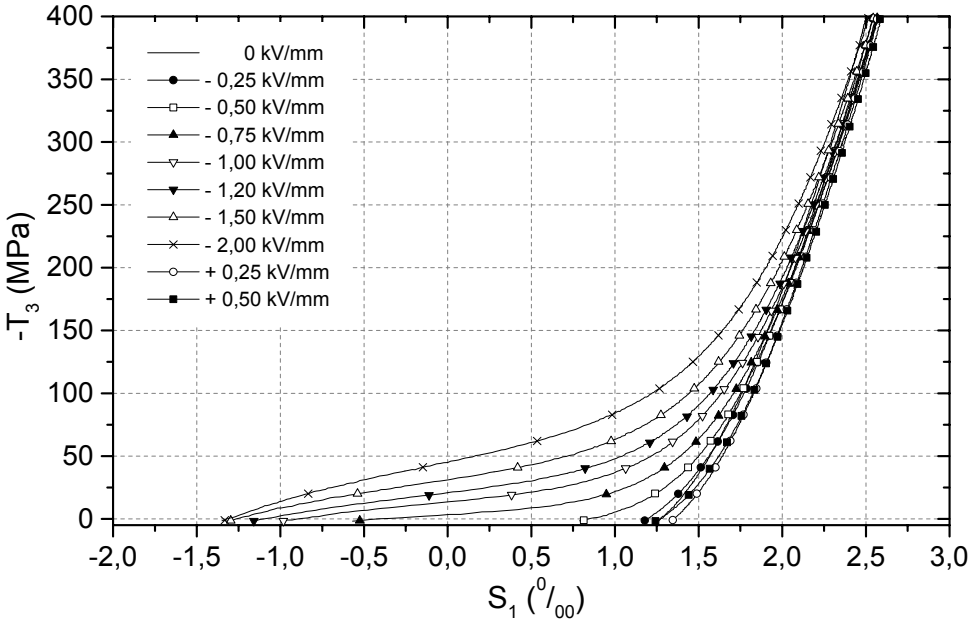

(b)

Figure 5.3.5. Transverse strain (S_1) in response to the first cycle of compressive stress (T_3) loading with different bias electric fields superimposed; (a) Stress loading from zero to – 400 MPa, and (b) Stress unloading from – 400 MPa to zero.

At short-circuit state (E_{bias} = 0 kV/mm), the electric field induced remnant strain S_3 and S_1 prior to stress loading are $2.45^0/_{00}$ and $-\ 1.15^0/_{00}$, respectively. With compressive stress increasing, we can observe a non-linear stress-strain curve. When the material is compressed

up to – 400 MPa stress magnitude, S_3 is - $6.22^0/_{00}$, and S_1 is + $2.49^0/_{00}$. After one loading cycle, the stress induced remnant strain S_3 is -$2.76^0/_{00}$, and S_1 is + $1.26^0/_{00}$.

The total strains obtained in this experiment can be expressed as

$$S_3 = s_{33}T_3 + S_{3(r)} + d_{33}E_3 \tag{5.3.2}$$

$$S_1 = s_{13}T_3 + S_{1(r)} + d_{31}E_3 \tag{5.3.3}$$

where $s_{33}T_3$ and $s_{13}T_3$ represent the elastic strains (s_{33} for longitudinal strain and s_{13} for transverse strain), $S_{3(r)}$ and $S_{1(r)}$ are the electric field and mechanical load induced irreversible strains due to domain switching, and $d_{33}E_3$ and $d_{31}E_3$ are the contributions from inverse piezoelectric effects (d_{33} for longitudinal strain and d_{31} corresponding to transverse strain).

As shown in Fig. 5.3.4 (a) and Fig. 5.3.5 (a), when a negative bias electric field is applied to the specimen, the initial remnant strains before stress loading increase with the increment of superposed E field, whereas, in case of a positive bias electric field superposition, the beginning strains prior to stress loading are smaller than at zero-bias E field.

The initial strain difference prior to stress loading is due to: (1) the contribution of the inverse piezoelectric effects ($d_{33}E_3$ and $d_{31}E_3$) from the bias E field, (2) time-dependence of domain switching related irreversible strain under a constant electric field loading.

With a bias electric field of E_{bias} = - 2 kV/mm, the E field induced remnant longitudinal strain S_3 prior to stress loading is + $3.98^0/_{00}$, and the remnant S_1 is – $1.82^0/_{00}$. Both of them are apparently higher than at zero-bias E field. In case of + 0.50 kV/mm bias electric field, the beginning longitudinal strain S_3 is + $1.12^0/_{00}$ and S_1 is about – $0.467^0/_{00}$. They are obviously smaller than at short-circuit condition (E_{bias} = 0 kV/mm).

Another notable feature which can be observed from Fig. 5.3.4 and Fig. 5.3.5 is that the stress induced maximum strains at T_3 = - 400 MPa do not exhibit such a pronounced difference as seen in the response of polarisation at different bias E field levels (see Fig. 5.3.1). At – 2 kV/mm, the longitudinal and transverse strains at T_3 = – 400 MPa are – $5.99^0/_{00}$ and + $2.51^0/_{00}$, respectively. At + 0.50 kV/mm, the stress induced maximum S_3 is – $6.19^0/_{00}$, and S_1 is equal to + $2.58^0/_{00}$.

From Fig. 5.3.1, we can see that, as the compression load approaching – 400 MPa, approximately vertical stress-depolarisation curves are observed at various bias electric field levels. The electric displacement (D_3) is nearly independent to the change of mechanical load. This result indicates that the piezoelectric constants d_{33} and d_{31} become very small under such a high compressive stress load. Consequently, the contribution of inverse piezoeffects to the total strain response is neglectable. This argument can also be confirmed from the

experimental results shown in last section (section 5.2). At T_3 = - 400 MPa, most of the domains have been oriented orthogonal to the prepoling direction, and the mechanical elastic strains $s_{33}T_3$ and $s_{13}T_3$ can be considered equal at different bias electric field conditions. Consequently, according to Equations 5.3.2 and 5.3.3, the maximum stress induced strains at – 400 MPa do not display too much difference.

During the stress unloading process from – 400 MPa to zero, the negative bias E field has the tendency to restore the material to its original poling state, such that the initial remnant strains induced by E field poling process will be partially recovered. For example, at E_{bias} = - 2 kV/mm, the final longitudinal strain S_3 after one stress cycle is + $3.08^0/_{00}$, and S_1 is – $1.35^0/_{00}$. Comparing to the initial strain values prior to stress loading ($S_3 = 3.98^0/_{00}$, and S_1 = - $1.82^0/_{00}$), we can see about 77% of the longitudinal strain and 74% of the transverse strain are recovered by such a high bias electric field.

In case of a positive bias electric field, e.g. + 0.50 kV/mm, the longitudinal strain S_3 after one stress cycle is – $2.53^0/_{00}$ and S_1 is + $1.24^0/_{00}$. The absolute values of these two strains are slightly smaller than them at zero-bias electric field (at E_{bias} = 0 kV/mm, after one stress loading cycle, S_3 = - $2.76^0/_{00}$, and S_1 = + $1.26^0/_{00}$). In Fig. 5.3.1 (b), we can find that, at E_{bias} = + 0.50 kV/mm, slight positive polarisation is induced during the stress unloading process from – 400 MPa to zero. These phenomena can be interpreted by time-dependent effects of polarisation and strain under a constant bias E field load. (For details of the time-dependent effects, see Chapter 3). Since the experiment was performed under "quasi-static" regime, during the relatively long time stress unloading process, some domains will be oriented to positive direction by the positive bias electric field. Therefore, some positive polarisation is observed and the mechanical load induced remnant strains are also smaller than at zero-bias E field.

The first full cycle stress-strain curves at several selected bias electric fields are plotted in Fig. 5.3.6. Clearly, the stress-strain curves are effectively closed by superposition of a high negative E field, which is analogical to the stress-depolarisation curves.

From Fig. 5.3.6, we can also find that the stress-strain curve area at + 0.50 kV/mm is apparently smaller than that at zero-bias E field. The area of the stress-strain curve represents the strain energy absorbed in a compressive work cycle [Chaplya and Carman, 2002]. The smaller stress-strain curve area at + 0.50 kV/mm provides further evidence that, for a pre-poled specimen with negative remnant polarisation, the positive bias E field and the compression load induce domain switching in the same direction. With the assistance of

positive bias E field, the amount of domains which is needed to be oriented by stress loading is less than at short-circuit condition. As a result, non-linear stress-strain curve with smaller area is observed.

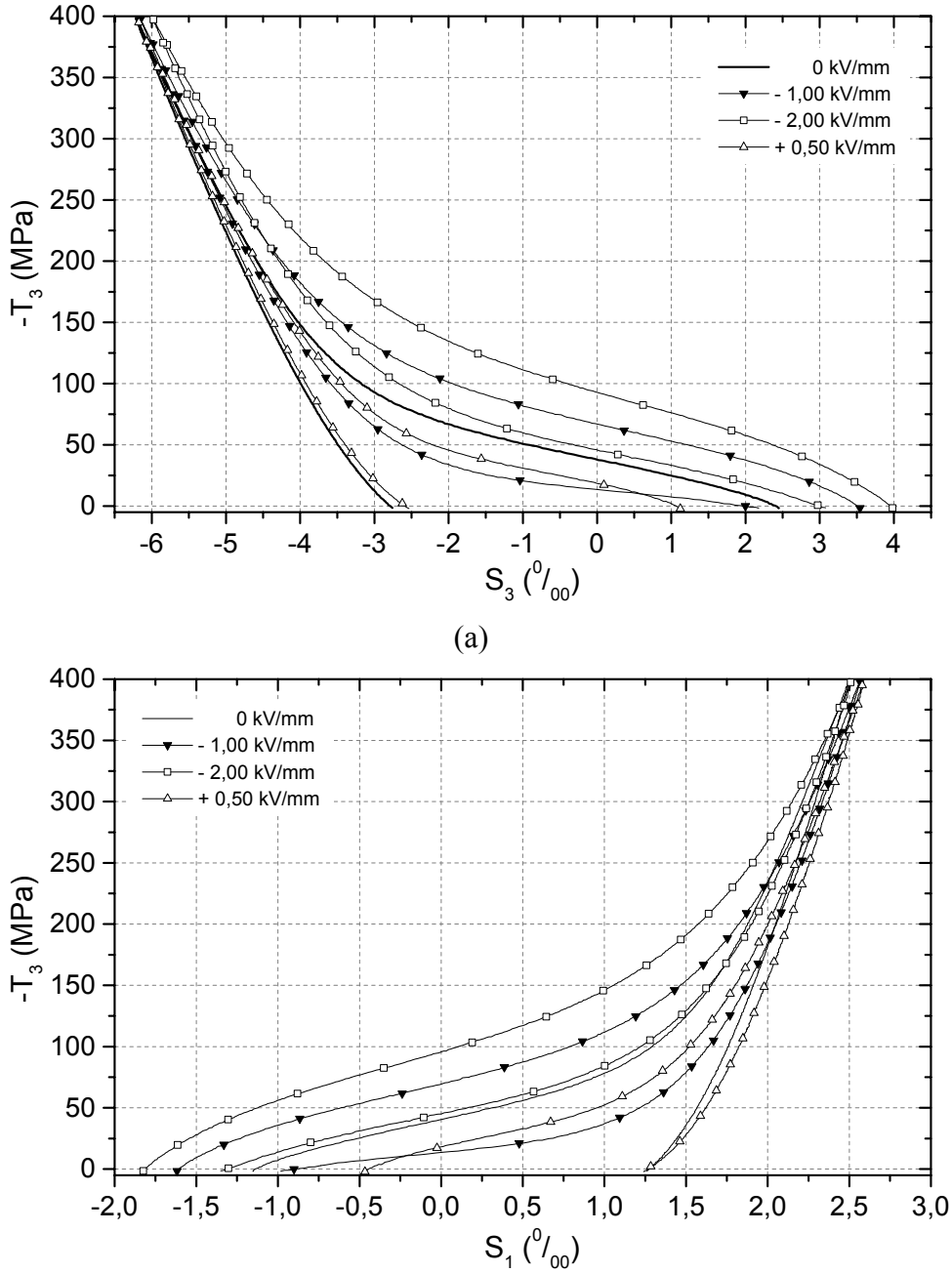

Figure 5.3.6. Stress-strain curves in the first stress loading-unloading cycle with 0, -1.00, -2.00 and +0.50 kV/mm bias electric fields. (a) longitudinal strain, and (b) transverse strain.

3. *Coercive stress in response to bias E field*

To understand the effects of bias electric field on the non-linear stress - depolarisation and stress - strain behavior, it is useful to examine the change of coercive stress in this experiment.

For the meaning in microscopic scale, the coercive stress (T_c) corresponds to a threshold stress value to initiate non-180° switching of unit cells. Before and after this critical value, the stress – strain behavior is linear elastic. For a pre-poled material, the mechanical load induced linear change of polarisation prior to the coercive stress is attributed to the direct piezoeffect. Ferroelastic non-180° switching processes will give rise to a rapid increase of the irreversible strain and mechanical depolarisation for a pre-poled specimen. Detailed discussion of this concept can be found in Chapter 4 (section 4.1).

Recently, Chaplya and Carman published their experimental investigation of the stress – strain behavior of PZT ceramics under bias electric field loading conditions. Two coercive stress values were identified in their work: one for the beginning and the other one for the ending of domain switching. These two coercive stresses were manually measured by the authors from the stress-strain curves with different electric fields superposition. Their results show that if the bias electric field is parallel to the prepoling direction, the coercive stress values monotonically increase with the bias E field magnitude until signs of saturation appear, while with an anti-parallel bias E field application, the coercive stress values decrease approaching zero near the coercive E field [Chaplya and Carman, 2002].

In Chapter 4 (section 4.1), for a non-linear stress – strain curve, the derivative of S_3 with respect to T_3 ($\partial S_3/\partial T_3$) was plotted versus compressive stress during the loading period from zero to – 400MPa. The results indicate that PIC151 soft PZT is very sensitive to the compression load. The derivative ($\partial S_3/\partial T_3$) is found to start to decrease as soon as the stress is applied, nearly no linear elastic response can be detected even within a quite small stress range. The macroscopic coercive stress for the beginning of domain switching can hardly be determined. After reaching its minimum value, which is corresponding to the inflection point of the non-linear stress – strain curve, the derivative ($\partial S_3/\partial T_3$) increases with compressive stress increment and finally tends to be saturated at much higher stress levels. However, it is still very difficult to determine the exact stress value corresponding to the end of the non-linearity. So far, we can know that it is hard to exactly determine the stress values for the beginning and ending of domain switching processes from the macroscopic stress – strain

measurement. The experimental result given by Chaplya and Carman is a kind of graphically constructed approximation [private communication with Chaplya and Carman].

From the plot of the derivative ($\partial S_3/\partial T_3$) versus compressive stress curve, it is relatively easier to determine the stress value corresponding to the inflection point of the non-linear stress – strain curve. From the discussion in Chapter 4 (section 4.3), we know that, since the material possesses maximum domain switching mobility, most pronounced time-dependent effects can be observed at the stress level approaching this inflection point. This specific stress value at the inflection point will be defined as coercive stress in the following discussion. The same definition was used in the in the work of Schäufele and Härdtl [Schäufele and Härdtl, 1996].

Based on the non-linear longitudinal strain *vs*. compressive stress curves under different bias electric fields loading in Fig. 5.3.4 (a), the derivative ($\partial S_3/\partial T_3$) versus compressive stress curves were plotted for the stress loading period from zero to – 400 MPa. Two examples are shown in Fig. 5.3.7 for the measurements with zero-bias E field and E_{bias} = - 2 kV/mm, respectively.

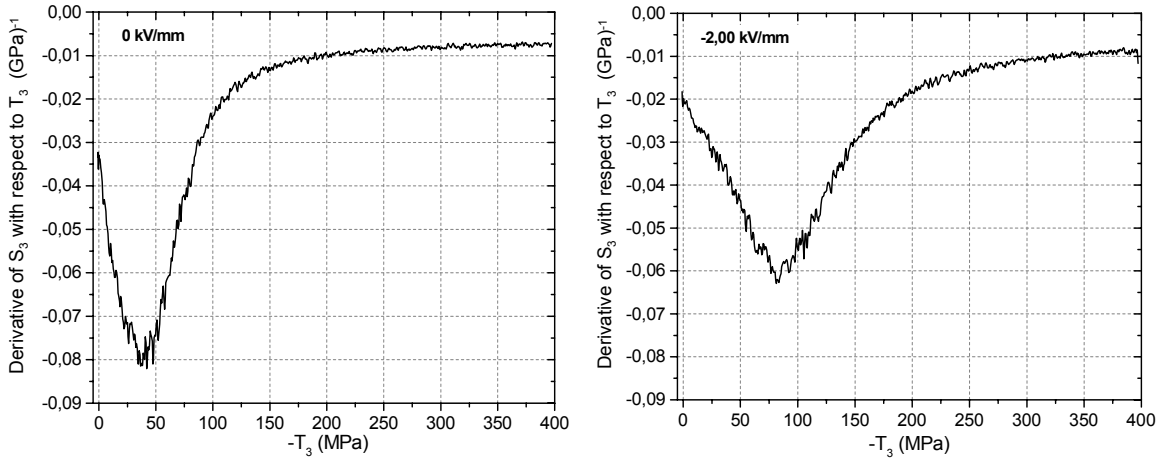

Figure 5.3.7. Derivative of S_3 with respect to T_3 ($\partial S_3/\partial T_3$) versus compressive stress curves during the loading period from zero to – 400 MPa. (a) short-circuit condition (E_{bias} = 0 kV/mm), and (b) with - 2 kV/mm bias electric field.

According to the plots of derivative ($\partial S_3/\partial T_3$) *vs.* compressive stress curves, the coercive stress is determined as the stress value corresponding to the minimum of the derivative. Change of coercive stress with bias electric field is plotted in Fig. 5.3.8.

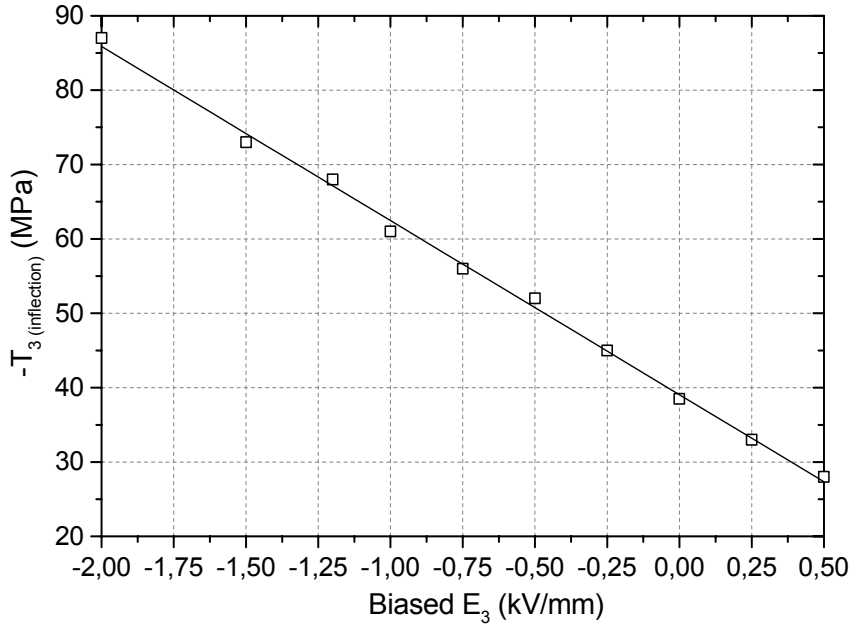

Figure 5.3.8. Stresses corresponding to the inflection points of the non-linear stress - longitudinal strain curves (coercive stress), in response to different bias electric field levels.

It is clear that the coercive stress is linearly depending on the bias electric field. At short-circuit state, this stress value is about – 38 MPa, and it decreases to – 28 MPa at + 0.50 kV/mm. With a bias electric field of – 2 kV/mm, the coercive stress value is – 87 MPa.

The experimental result of the coercive stress in response to a bias electric field further confirms the arguments that with a bias electric field in the poling direction, the domains are fixed in their poling orientations against the action of a compressive stress. Therefore, higher stresses are needed to induce domain switching. Conversely, an electric field anti-parallel to the poling direction supports the mechanically induced domain switching, and lower stresses are needed to initiate and forward domain switching in this case.

The linear dependence of coercive stress on the bias electric field was also found in the work of Schäufele and Härdtl for soft and hard PZT ceramic materials, and the experimental result was explained by considering the changes in energy densities during the domain switching process [Schäufele and Härdtl].

Chapter 6 Summary

The primary objective of this thesis is to present experimental data for constitutive modeling of piezoceramics. The research motivation is generated from the continuously increasing need of piezoceramic materials for modern sensing and actuation applications.

As the design of active devices becomes increasingly more complex and the actuators are intended to be utilized under severe conditions (e.g. high electric field and / or mechanical load), the conventional linear assumption under small signal loading conditions is inappropriate for representing the practical response accurately. Domain switching related nonlinear behavior must be taken into consideration for devices design, electromechanical coupling calculation and service reliability evaluation.

The large signal nonlinear behavior of PIC 151, an important commercially available soft PZT ceramic material (PI Ceramic, Lederhose, Germany), was systematically investigated under a pure electric field, a pure compressive stress, and combined electromechanical loading conditions, respectively. PIC 151 soft PZT is characterised by its prominent electromechanical coupling performance. The manufacturer recommends it to be exploited for ultrasonic transducers, micro-positioning components, and so on. Therefore, all the experimental results presented in this thesis have a direct relevance to the development of practical devices.

A special method of specimen preparation and an improved experimental setup were developed to realize the measurements under combined electromechanical load securely and correctly.

As a consequence of the ferroelectric domain switching, nonlinear polarisation and butterfly strain hysteresis loops were observed under a pure cyclic electric field load. The corresponding strain versus polarisation (S - P) curves were found to exhibit significant hysteresis at the same time, which could be qualitatively interpreted by two successive 90° domain switching processes. The material responses were found to depend on the loading rate and the amplitude of the E field. The loading rate dependence was most pronounced when the E field magnitude was approaching the coercive field (E_c), where the residual polarisation and strain decreased significantly with the increment of loading rate. When the amplitude was about two times than the coercive field, typical P – E and S – E curves were observed with various loading rates. In particular, the coercive field (E_c) was found to increase with the increasing of loading rate. After removing the E field application, remnant polarisation and

remnant strain were found to decrease with the passage of time. This phenomenon was attributed to the ageing effect. A lower loading rate resulted in a lowered ageing rate, and larger remnant polarisation and remnant strain.

Nonlinear stress-strain behavior was observed under a pure compressive stress load. In addition, nonlinear mechanical depolarisation curves were obtained for the pre-poled samples. Systematic analysis of the strain – depolarisation (S - ΔP) curves further confirmed that the nonlinear changes of the strain and the polarisation originated from the same ferroelastic non-180° domain switching process.

Piezoelectric ceramics have memory abilities with respect to their polar state and shape. Permanent changes of polarisation and strain induced by the mechanical load could be brought back to their initial values by a subsequent application of an electric field to repolarise the material.

The nonlinear stress-strain behavior was also found to be loading rate dependent. To achieve the same strain value, a slightly higher stress was needed in the case of higher loading rate. Similar to the ageing effect under E field load, after removal of the stress loading, the remnant strain was also found to decrease with the passage of time.

There is an inflection point in the nonlinear stress - strain curve. Before this inflection point, the tangent modulus of the nonlinear curve decreases with increasing stress. However, after passing this point, the tangent modulus increases with stress increment, the material shows enhancive hardening behavior.

When being subjected to a constant external load, time-dependent effects were found for this material. Polarisation and strain exhibited creep-like behavior with the passage of the external load hold time. In the case of a pure E field load, the time-dependence was most pronounced for a holding of E field close to the coercive field. While under a pure mechanical loading, the most distinct time-dependent effect occurred at the stress level corresponding to the inflection point of the nonlinear stress - strain curve. It was considered that the macroscopic time-dependent polarisation and strain responses were caused by further microscopic domain switching process, which was gradually induced during the hold time of the external load. A proposed explanation for the time-dependent effects is the variation of local E field strength through the diffusion process of microscopic defects.

Besides the normally used polarisation and strain measurements, the relative change of a specimen volume (defined as volumetric strain) was evaluated simultaneously in this work. A butterfly-shaped volumetric strain versus E field curve was observed under a pure cyclic

electric field loading, and a significant positive remnant volumetric strain was induced after the removal of the E field. A nonlinear volumetric strain curve was obtained under a pure compression load, and after unloading the remnant volumetric strain was found to be negative.

Phase transition induced by the external load was suggested to explain the apparently remnant volumetric strain. Electric field loading would induce phase transition from the rhombohedral phase to the tetragonal phase, and consequently result in a positive remnant volumetric strain. A reversed phase transition could be induced by a uni-axial compressive stress load, which gave rise to a negative remnant volumetric strain.

The response of a piezoceramic material under combined electromechanical loading is the focus of this thesis. Full cycles of polarisation and strain *vs*. E field hysteresis loops were investigated under various compressive stress preloads. It turned out that with increasing mechanical load, the dielectric and butterfly hysteresis became less and less pronounced, as the compressive stress prevented the full alignment of the domains and induced mechanical depolarisation. The experimental results revealed that the superimposed compression load reduced the remnant polarisation, decreased the coercive field, and also had a significant impact on the dielectric and piezoelectric properties. The slopes of P – E and S – E curves at zero E field and various preload stress levels were referred to as differential dielectric and piezoelectric constants, respectively. The dielectric permittivity and piezoelectric coefficients were a function of the applied stress. They were found to initially increase with the increasing prestress, after achieving a maximum at a certain small stress level, they decreased with further stress increment. At much higher preload stress levels, the P-E curves became a nearly straight line, and nearly no electrically induced strain change could be observed.

High field dielectric permittivity and piezoelectric coefficients were found to be enhanced with the application of a small compressive prestress. This was attributed to larger extrinsic contribution due to more non-180° domain switching. However, it was also found that the enhanced performance achieved by small stress preload was accompanied by larger hysteresis and nonlinearity arising from more domain switching. Therefore, the thermal stability and long-term reliability must be addressed to design the practical actuators, and to determine the optimum operating conditions.

The effects of a bias electric field on the nonlinear stress – strain and stress – depolarisation responses were also experimentally investigated. A bias E field acting in the direction of previous poling had the tendency to support the existing domain state. Therefore, higher

compressive stresses were needed to initiate and forward the mechanically induced ferroelastic domain switching processes. In the duration of stress unloading, the bias E field would try to restore the original domain configuration prior to stress loading. As a result, part of the polarisation and strain were recovered after the stress decreased to zero. When the bias E field was higher than the coercive field, the stress – strain and stress – depolarisation curves were effectively closed. On the other hand, an E field acting opposite to the initial poling direction would work together with the compressive stress to destabilize the domain state. Consequently, relatively lower stresses were needed to induce ferroelastic domain switching. The stress value at the inflection point of the nonlinear stress – strain curve (defined as the coercive stress) was linearly dependent on the bias E field, increased with increasing bias E field which was parallel to the pre-poling direction.

Through the systematically experimental work presented in this thesis, nonlinear behavior of piezoceramics under large signal uni-axial loading conditions was clearly outlined. Such a kind of knowledge is needed for the simple design of piezoelectric transducers and basic modeling of the constitutive behavior. In order to further the understanding of the response of components with complex geometries or with field intensifiers such as cracks or embedded electrodes, experimental investigations under multi-axial electromechanical loading should be carried out in the future.

Acknowledgements

Appreciation is expressed to those who have made contributions to this thesis. First I would like to thank my supervisor, Prof. D. Munz, for giving me the opportunity to perform this work, and for his continuous support and encouragement. I gratefully acknowledge my tutor, Dr. M. Kamlah, who has introduced me to such an exciting area of ferroelectricity, shown great patience with all my questions and been attentive to the development of this work all the time. Prof. M. J. Hoffmann is acknowledged for reading and appraising the thesis and making meaningful comments.

Dr. T. Fett is especially thanked for his valuable advice to the experiments and many fruitful discussions we have had. In addition, helpful ideas and suggestions have been provided by Prof. K. H. Härdtl (Uni. Karlsruhe), Dr. A. Fröhlich, and Dr. Z. Wang, whom I also wish to appreciate.

All the technical assistance and other contributions offered by the following personnel: G. Thun, M. Weber, M. Klotz, S. Knaak-Dojan, E. Ernst and D. Papazoglou are sincerely thanked. D. Schröder from ESA Messtechnik GmbH and Dr. A. Weber at IWE, Uni. Karlsruhe are further acknowledged for their great help of solving difficulties during the experimental work.

Furthermore I wish to thank Dr. N. Huber, Dr. E. Diegele, Dr. V. Licht, Dr. Y. Yang, V. Hegadekatte, K. Heiermann, and E. Tioulioukovski for their help and supports during this work.

I also deeply appreciate my family and friends, especially my wife J. Xu, for their continual encouragement and supports during all these years.

This work was financially supported by the Deutsche Forschungsgemeinschaft.

References

1. Abraham, T., "Applications, Markets Expand for Piezoelectric Ceramics", *The American Ceramic Society Bulletin*, pp. 45-47, September 2000.
2. Akhras, G., "Smart materials and smart systems for the future", *Canadian Military Journal*, pp. 25-32, Autumn 2000.
3. Alatsathianos, S., *Experimentelle Untersuchung des Materialverhaltens von piezoelektrischen Werkstoffen*, Dissertation Thesis, Universität Karlsruhe, Institut für Zuverlässigkeit und Schadenskunde im Maschinenbau, Karlsruhe, 2000.
4. Al-Shareef, H. N., Dimos, D., Warren, W. L., and Tuttle, B. A., "A model for optical and electrical polarization fatigue in $SrBi_2Ta_2O_9$ and $Pb(Zr,Ti)O_3$", *Integrated Ferroelectrics*, vol. 15, pp. 53-67 (1997).
5. Arlt, G., Dederichs, H. and Herbiet, R., "90°-domain wall relaxation in tetragonally distorted ferroelectric ceramics", *Ferroelectrics*, vol.74, pp.37-53 (1987).
6. Berlicourt, D., "Piezoelectric Ceramic Compositional Development", *J. Acoust. Soc. Am*., vol. 91, No. 5, pp. 3034-3040 (1992).
7. Cady, W. G., *Piezoelectricity*, McGraw-Hill, New York, 1946.
8. Calderon-Moreno, J. M., Guiu, F., et al., "Anisotropic and Cyclic Mechanical Properties of Piezoelectrics-Compression Testing*", J. Eur. Ceram. Soc.*, vol. 19**,** pp. 1321-1324 (1999).
9. Calderon-Moreno, J. M., "Stress induced domain switching of PZT in compression tests", *Materials Science and Engineering A,* vol. 315, pp. 227-230 (2001).
10. Cao, Hengchu and Evans, A. G., "Nonlinear Deformation of ferroelectric Ceramics", *J. Am. Ceram. Soc.*, vol. 76, No. 4, pp. 890-896 (1993).
11. Carl, K. and Härdtl, K. H., "Electrical after-effects in $Pb(Ti,Zr)O_3$ ceramics", *Ferroelectrics*, vol. 17, pp. 473-486 (1978).
12. Chaplya, P. M. and Carman, G. P., "Dielectric and piezoelectric response of lead zirconate-lead titanate at high electric and mechanical loads in terms of non-180° domain wall motion", *J. Appl. Phys.*, vol. 90, No. 10, pp. 5278-5286 (2001).
13. Chaplya, P. M. and Carman, G. P., "Compression of piezoelectric ceramic at constant electric field: Energy absorption through non-180° domain-wall motion", *J. Appl. Phys.*, vol. 92, No. 3, pp. 1504-1510 (2002).

14. Chen, Wei and Lynch, C. S., "Multiaxial Constitutive Behavior of Ferroelectric Materials", *Journal of Engineering Materials and Technology*, vol. 123, pp. 169-175 (2001).
15. Chen, Yun-Han and Viehland, D., "Relaxational polarisation dynamics in soft ferroelectrics", *Appl. Phys. Lett.*, vol. 77, No.1, pp.133-135 (2000).
16. Cross, L. E., "Relaxor Ferroelectrics", *Ferroelectrics*, vol. 76, pp. 241-267 (1987).
17. Cross, L.E., "Ferroelectric Ceramics: Tailoring Properties for Specific Applications", *Ferroelectrics ceramics: tutorial reviews, theory, processing and applications*, Berlin: Birkhäuser, 1993.
18. Damjanovic, D., "Ferroelectric, dielectric and piezoelectric properties of ferroelectric thin films and ceramics", *Rep. Prog. Phys*., vol. 61, pp. 1267-1324 (1998).
19. Endriss, A., Hammer, M., Hoffmann, M. J., Kolleck, A. and Schneider, G., "Microscopic and macroscopic ferroelectric-ferroelastic and piezoelectric behavior of PZT ceramics", *J. Eur. Ceram. Soc.*, vol. 19, pp. 1229-1231 (1999).
20. Fan, Huiqing and Kim, Hyoun-Ee, "Perovskite stabilization and electromechanical properties of polycrystalline lead zinc niobate-lead zirconate titanate", *J. Appl. Phys.*, vol.91, No.1, pp.317-322 (2002).
21. Fett, T. and Thun, G., "Determination of room-temperature tensile creep of PZT", *Journal of Materials Science Letters*, vol. 17, pp. 1929-1931 (1998).
22. Fett, T., Munz, D., and Thun, G., "Tensile and bending strength of piezoelectric ceramics", *Journal of Materials Science Letters*, vol. 18, pp. 1899-1902 (1999).
23. Fett, T., Munz, D., and Thun, G., "Polarisation measurements on PZT under transverse tensile loading", *Ferroelectrics*, vol. 247, No. 4, pp. 321-332 (2000).
24. Fett, T., Munz, D., and Thun, G., "Young's modulus of soft PZT from partial unloading tests", *Ferroelectrics*, vol. 274, pp. 67-81 (2002).
25. Fröhlich, A., *Mikromechanisches Modell zur Ermittlung effektiver Materialeigenschaften von piezoelektrischen Polykristallen*, Forschungszentrum Karlsruhe GmbH, wissenschaftliche Berichte, vol. FZKA 6628, Karlsruhe, 2001.
26. Gerthsen, P. and Krueger, G., "Coercive field in fine-grained PLZT ceramics", *Ferroelectrics*, vol.11, pp.489-492 (1976).
27. Haertling, G. H., "Ferroelectric Ceramics: History and Technology", *J. Am. Ceram. Soc.*, vol. 82, No. 4, pp. 797-818 (1999).

28. Hoffmann, K., *An Introduction to Measurements Using Strain Gages*, published by Hottinger Baldwin Messtechnik GmbH, Darmstadt, Germany, 1989.
29. Hoffmann, M. J., Hammer, M., Endriss, A., and Lupascu, D. C., "Correlation between microstructure, strain behavior, and acoustic emission of soft PZT ceramics", *Acta Mater.*, vol.49, pp. 1301-1310 (2001).
30. Huber, J. E. and Fleck, N. A., "Multiaxial models and experiments with ferroelectrics", in Smart Structures and Materials 2000: Active Materials: Behaviour and Mechanics, Christopher S. Lynch, Editor, *Proceeding of SPIE*, vol. 3992 (2000).
31. Huber, J. E., Shieh, J. and Fleck, N. A., "Multiaxial response of hard and soft ferroelectrics under stress and electric field", in Smart Structures and Materials 2002: Active Materials: Behaviour and Mechanics, Christopher S. Lynch, Editor, *Proceeding of SPIE*, vol. 4699 (2002).
32. Intellmat: *www.intellimat.com*
33. Jaffe, B., Cook, W. R. and Jaffe, H., *Piezoelectric Ceramics*, Academic Press, New York, pp. 117-142, 1971.
34. Kamlah, M., "Review Article: Ferroelectric and ferroelastic piezoceramics-modeling of electromechanical hysteresis phenomena", *Continuum Mech Thermodyn*, vol. 13, No. 4, pp. 219-268 (2001).
35. Krueger, G.,"Domain wall motion concept to describe ferroelectric rhombohedral PLZT ceramics", *Ferroelectrics*, vol.11, pp.417-422 (1976).
36. Krueger, H. H. A., "Stress Sensitivity of Piezoelectric Ceramics. Part 1: Sensitivity to Compressive Stress Parallel to the Polar Axis", *J. Acoust. Soc. Am.*, vol. 42, No. 3, pp. 636-645 (1967).
37. Krueger, H. H. A., "Stress Sensitivity of Piezoelectric Ceramics. Part 3: Sensitivity to Compressive Stress Perpendicular to the Polar Axis", *J. Acoust. Soc. Am.*, vol. 43, No. 3, pp. 385-91 (1968).
38. Kuwata, J., Uchino, K., and Nomura, S., "Electrostrictive Coefficients of $Pb(Mg_{1/3}Nb_{2/3})O_3$ Ceramics", *Jpn. J. Appl. Phys*., vol.19, pp.2099-2103 (1980).
39. Lines, M. E. and Glass, A. M., *Principles and Applications of Ferroelectrics and Related Materials*, Oxford, 1977.
40. Lohkämper, R., Neumann, H., and Arlt, G., "Internal Bias in Acceptor Doped $BaTiO_3$ Ceramics: Numerical Evaluation of Increase and Decrease", *J. Appl. Phys.*, vol. 68, pp. 4220-4224 (1990).

41. Lynch, C. S., "The effect of uniaxial stress on the electro-mechanical response of 8/65/35 PLZT", *Acta mater*, vol. 44, No.10, pp.4137-4148 (1996).
42. Mitrovic, M., Carman, G. P., and Straub F. K., "Response of piezoelectric stack actuators under combined electro-mechanical loading", *International Journal of Solids and Structures*, vol. 38, pp. 4357-4374 (2001).
43. Munz, D. and Fett, T., *Ceramics-Mechanical Properties, Failure Behaviour, Materials Selection*, Chapter 13, pp. 275-277, Springer series in materials science, v.36, ISSN 0933-033X, 1999.
44. Newnham, R. E. and Ruschau, G. R., "Smart Electroceramics", *J. Am. Ceram. Soc.,* vol. 74, No. 3, pp. 463-480 (1991).
45. Newnham, R. E., "Molecular Mechanisms in Smart Materials", *MRS Bull.,* vol. 22, No. 5, pp. 20-34 (1997).
46. Nuffer, J., Lupascu, D. C., and Rödel, J., "Damage evolution in ferroelectric PZT induced by bipolar electric cycling", *Acta Mater.*, vol. 48, pp. 3783-3794 (2000).
47. Pan, W. Y., Zhang, Q. M., Jiang, Q. Y. and Cross, L. E., "Electric field induced strain in (Pb,La)(Ti,Zr)O_3 ferroelectric ceramics near the tetragonal-rhombohedral morphotropic phase boundary", *Ferroelectrics*, vol.88, pp.1-15 (1988).
48. Robels, U. and Arlt, G., "Domain-wall clamping in ferroelectrics by orientation of defects", *J. Appl. Phys.*, vol. 73, pp. 3454-3460 (1993).
49. Schäufele, A. B. and Härdtl, K. H., "Ferroelastic Properties of Lead Zirconate Titanate Ceramics", *J. Am. Ceram. Soc.*, vol. 79, No. 10, pp. 2637-2640 (1996).
50. Schmidt, N. A., "Coercive force and 90° domain wall motion in ferroelectric PLZT ceramics with square hysteresis loops", *Ferroelectrics*, vol.31, pp.105-112 (1981).
51. Schnell, A., "Nonlinear charge release of piezoelectric ceramics under uniaxial pressure", *Ferroelectrics*, vol. 28, pp. 351-353 (1980).
52. Shirane, G., and Suzuki, K., "Crystal Structure of Pb(Zr, Ti)O_3", *J. Phys. Soc. Jpn.*, vol. 7, pp. 333-336 (1952).
53. Soares, M. R., Senos, A. M. R. and Mantas, P. Q., "Phase coexistence region and dielectric properties of PZT ceramics", *J. Eur. Ceram. Soc.*, vol.20, pp.321-334 (2000).
54. Stotz, S., "Shift of the morphotropic phase bourdary in the PZT system under the influence of electric fields and uni-axial stresses", *Ferroelectrics*, vol.76, pp. 123-132 (1987).

55. Trease, B. P., *A Survey and Comparison of Smart Material Linear Actuators*, Master's degree thesis, Dept. of Mechanical Engineering, University of Michigan, 2002.
56. Tsurumi, T., Kumano, Y., Ohashi, N., Takenaka, T., and Fukunaga, O., "90° Domain Reorientation and Electric-Field-Induced Strain of Tetragonal Lead Zirconate Titanate Ceramics", *Jpn. J. Appl. Phys*., vol.36, pp.5970-5975 (1997).
57. Viehland, D. and Chen, Yun-Han, "Random-field model for ferroelectric domain dynamics and polarisation reversal", *J. Appl. Phys.*, vol.88, pp. 6696-6707 (2000).
58. Viehland, D., Tito, F., McLaughlin, E., Robinson, H., Janus, R., Ewart, L. and Powers, J., "Enhancement of electromechanical coupling coefficient and acoustic power density in conventional "hard" $Pb(Zr_{1-x}Ti_x)O_3$ ceramics by application of uniaxial stress", *J. Appl. Phys.*, vol.90, No.3, pp. 1496-1500 (2001).
59. Weber, M.A., Kamlah, M., and Munz, D., *Experimente zum Zeitverhalten von Piezokeramiken*, Forschungszentrum Karlsruhe GmbH, wissenschaftliche Berichte, vol. FZKA 6465, Karlsruhe, 2000.
60. Xu, Y., *Ferroelectric Materials and Their Applications*, North Holland, 1991.
61. Yang, G., Liu, S.-F., Ren, W., and Mukherjee, B. K. "Uniaxial stress dependence of the piezoelectric properties of Lead Zirconate Titanate ceramics", in Smart Structure and Materials 2000: Active Materials: Behaviour and Mechanics, Christopher S. Lynch, Editor, *Proceeding of SPIE*, vol. 3992 (2000).
62. Zhang, Q. M., Pan, W. Y., Jang, S. J. and Cross, L. E. "Domain wall excitations and their contributions to the weak-signal response of doped lead zirconate titanate ceramics", *J. Appl. Phys.*, vol. 64, No. 11, pp. 6445-6451 (1988).
63. Zhang, Q. M., Wang, H., Kim, N., and Cross, L. E. "Direct evaluation of domain-wall and intrinsic contributions to the dielectric and piezoelectric response and their temperature dependence on lead zirconate-titanate ceramics", *J. Appl. Phys.*, vol. 75, No. 1, pp. 454-459 (1994).